Polymer Chemistry

REVIEW

View Article Online
View Journal | View Issue

Cite this: *Polym. Chem.*, 2015, **6**, 2580

Supramolecular anticancer drug delivery systems based on linear–dendritic copolymers

Homa Gheybi[a] and Mohsen Adeli*[a,b]

Received 22nd October 2014,
Accepted 20th February 2015

DOI: 10.1039/c4py01437e

www.rsc.org/polymers

Current cancer chemotherapy often suffers severe side-effects of the administered cancer drugs on the normal tissues. In addition, poor bioavailability, due to the low water solubility of the anticancer drugs, limits their applications in chemotherapy. New delivery technologies could help overcome this challenge by improving the water solubility and achieving the targeted delivery of the anticancer drugs. Linear–dendritic hybrid nanomaterials, which combine the highly branched architectures and multifunctionality of dendrimers with the processability of traditional linear–linear block copolymers, have been introduced as ideal carriers in anticancer drug delivery applications. This review presents recent advances in the investigational aspects of linear–dendritic copolymers to be applied as anticancer drug delivery vehicles. We highlight the structures, synthesis of linear–dendritic block copolymers, interaction mechanisms between linear–dendritic copolymers and anticancer drug molecules, and findings on their drug release behavior and anticancer efficacies *in vitro* and *in vivo*.

1. Introduction

Cancer is one of the leading causes of morbidity and accounts for approximately 20% of all deaths world-wide (World Health Organization). When a cell acquires enough mutations to become cancerous, it will be replicated at a higher rate than normal cells. After tumor mass formation, it is not possible for the normal cells to compete with the cancerous ones for an adequate supply of nutrients from the blood vessels.[1–4] Clinical surgery to remove a cancerous tumor is considered to be the primary method for fighting cancer. However, surgery may have undesirable side effects, such as changing the growth rate of the remaining cancer cells by triggering a faster metastatic process. Following surgical resection, radiotherapy, chemotherapy and immunotherapy are the most common methods currently employed in the clinical management of cancer.[5,6] One of the major problems facing cancer chemotherapy is the lack of mandatory selectivity of chemotherapeutic

[a]*Department of Chemistry, Faculty of Science, Lorestan University, Khorramabad, Iran. E-mail: mohadeli@yahoo.comor, m.aadeli@fu-berlin.de*
[b]*Institut für Chemie und Biochemie, Freie Universität Berlin, Germany*

Homa Gheybi

Homa Gheybi received her BS, MS, and PhD degrees from University of Tabriz (Iran) in 2003, 2007, and 2013, respectively. Then she continued her study in a postdoctoral research program at Lorestan University (Iran) supported by Iran Nano Council in 2014. Her research interests are nanotechnology, conducting polymers, and biodegradable drug delivery systems.

Mohsen Adeli

Mohsen Adeli received his undergraduate degree from Lorestan University (Iran) in 1996. He obtained his MS and PhD degrees from Tabriz University. After joining Lorestan University in 2005, he added a postdoctoral stage from the Institute for Nanoscience and Nanotechnology of Sharif University of Technology in 2007. He was promoted to the rank of associate and full professor in 2010 and 2013, respectively. He joined Freie Universität Berlin as a guest professor in 2014.

drugs to direct the cytotoxicity to tumor cells, leading to undesirable side effects.[7,8] A promising approach to overcome this problem is the application of nanomaterial based drug delivery systems[9] including inorganic or other solid nanoparticles (gold,[10,11] iron oxide,[12,13] quantum dots[14,15] and carbon nanotubes[16–18]), polymeric micelles,[19–21] dendrimers,[22–24] and liposomes.[25,26] The advantages of such nanocarriers include the ability to improve drug solubility and slow down the metabolism of the drug, prolonging the circulation time, tumor specific delivery, and higher accumulation in tumors *via* the enhanced permeability and retention (EPR) effect, resulting in enhanced efficacy and reducing side effects.[27–29] Use of nanomaterial based drug delivery systems for biomedical applications is one of the constituents of an emerging field called nanomedicine, which has shown great promise for the development of novel diagnostic, imaging, and therapeutic agents for a variety of diseases, including cancer.[30–35] Among the nanomaterials, linear–dendritic hybrid materials are a growing class of nanoscopic carriers, which combine the highly branched architecture and multifunctionality of dendrimers with the processability of traditional linear–linear block copolymers.[36,37] The concept of the linear–dendritic block copolymer was announced by the Fréchet group in the early 1990s for the first time; it included a polystyrene and a dendritic poly(benzyl ether) block,[38] and later on a PEG block and a hydrophobic dendritic poly(benzyl ether) block.[39] Because of their unique self-assembly properties, linear–dendritic systems have received increasing attention to use as a versatile platform for drug delivery applications.[40–42] Dendrimers offer plenty of advantages compared to other architectural forms of polymers that have been used in drug-delivery systems. Unique characteristics, such as highly branched globular architecture, narrow polydispersity, nanometer size range, periphery groups, physicochemical, and self-assembly properties make dendrimers promising candidates in nanomedicine. The main successes of dendrimers in nanomedicine resulted in their appropriate, reproducible and optimized design parameters, addressing the physicochemical limitations of classical drugs (*e.g.* solubility, specificity, stability, biodistribution and therapeutic efficiency) and their ability to overcome biological issues to reach the right target(s) (*e.g.* first-pass effect, immune clearance, cell penetration, off-target interactions, *etc.*).[43–47] However, several drawbacks limit the transportation of small guest molecules by perfect dendrimers. Perfect dendrimers have a relatively rigid molecular structure with interior cavities, which are not flexible, and have certain dimensions for accepting guest molecules with a certain and defined size. For the encapsulation and release of guest molecules from perfect dendrimers, a protection and deprotection reaction series is necessary. In contrast to the drawbacks of perfect dendrimers, linear–dendritic copolymers have flexible interiors and can encapsulate a variety of small guest molecules.[48–51] Recently, it has been shown that the transport capacity of some of linear–dendritic copolymers is much more than that of perfect dendrimers.[52,53] These advantages and interesting properties of linear–dendritic polymers have stimulated investigation in this area.

Three strategies have been reported for the synthesis of linear–dendritic copolymers[54]: (a) "coupling" method: coupling of a dendron with a functionalized linear polymer;[39] (b) "chain-first" method: growth of a dendritic segment from the terminal group of a linear polymer;[55] (c) "dendron-first" method: polymerization of a linear segment from the dendron macroinitiator by controlled/"living" radical routes.[56] These synthetic strategies lead to low polydispersity and a great deal of control over the molecular architecture of obtained linear–dendritic copolymers.[43,57–59]

Gitsov has described detailed architectures of linear–dendritic hybrids in a valuable review.[41] The building blocks of the linear–dendritic copolymers can be positioned in several distinct configurations, due to the presence of multiple anchoring points in blocks. According to Gitsov's classification, the first general group contains a single monodendron or dendrimer (D) and one (A), two (B), or multiple (C) linear segments (L), attached at the "focal" point or at the peripheral functional groups in the D fragments, Fig. 1.

The characteristic feature of the second group is the attachment of two monodendrons to the extremities of a single linear chain (E) or the incorporation of dendrimers into the main linear chain (F), Fig. 2.

The third group unifies the structures, where monodendrons are attached like "pendants" to a main linear chain through short (G) or long spacers (H). When the linear chain is "shrunk" (H), it is transformed into a star-like macromolecule, with the monodendrons anchored at the extremities of the star arms (K), Fig. 3. A special case of K arises when the core of the star is not a small multifunctional unit, but a dendrimer.

A network constructed by dendrimers as the crosslinking moieties and linear blocks as the interjunction fragments constitutes a special case of "infinite" linear–dendritic copolymer, Fig. 4.

Finally, the dendritic–linear–dendritic super dendrimer shown in Fig. 5 represents the ultimate challenge in synthetic organic and polymer chemistry.

Besides improving the water solubility of the hydrophobic drugs, encapsulated by the hydrophobic interior of dendritic segments,[60–62] the reactive surface end groups of dendritic

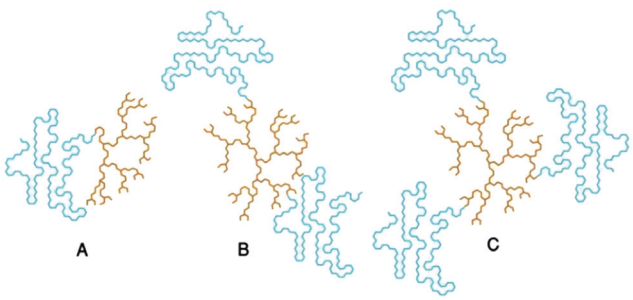

Fig. 1 Linear–dendritic architectures; first group: A, B and C. Structures were first published in ref. 41.

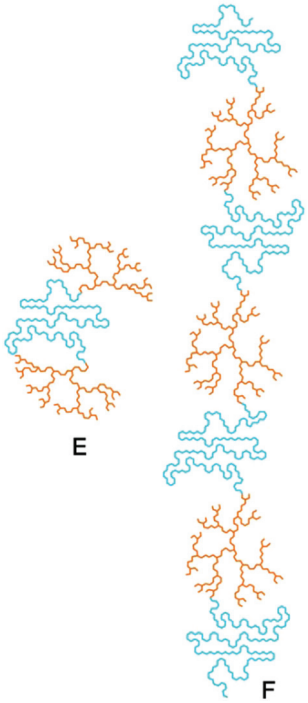

Fig. 2 Linear–dendritic architectures; second group: E and F. Structures were first published in ref. 41.

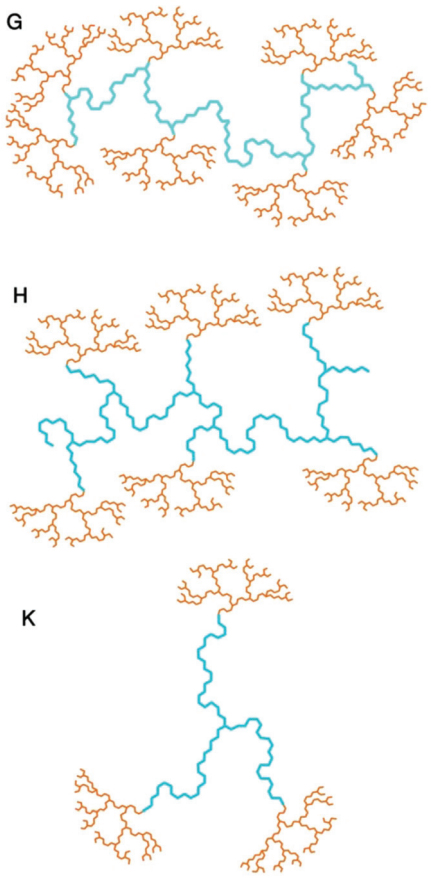

Fig. 3 Linear–dendritic architectures; third group: G, H and K. Structures were first published in ref. 41.

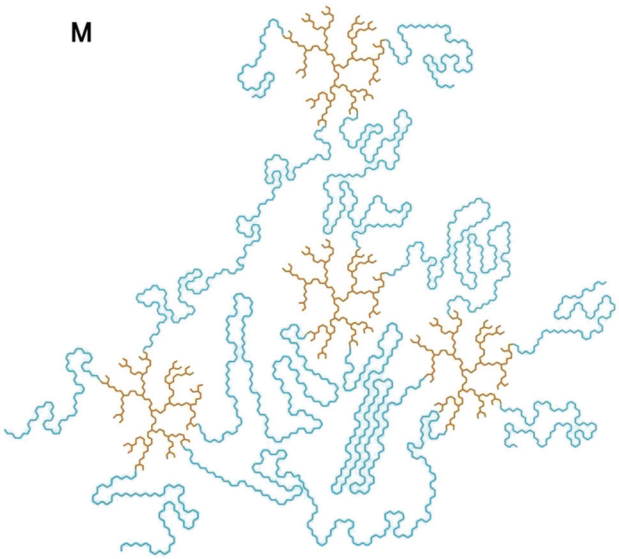

Fig. 4 Linear–dendritic architectures; fourth group: M. Structures were first published in ref. 41.

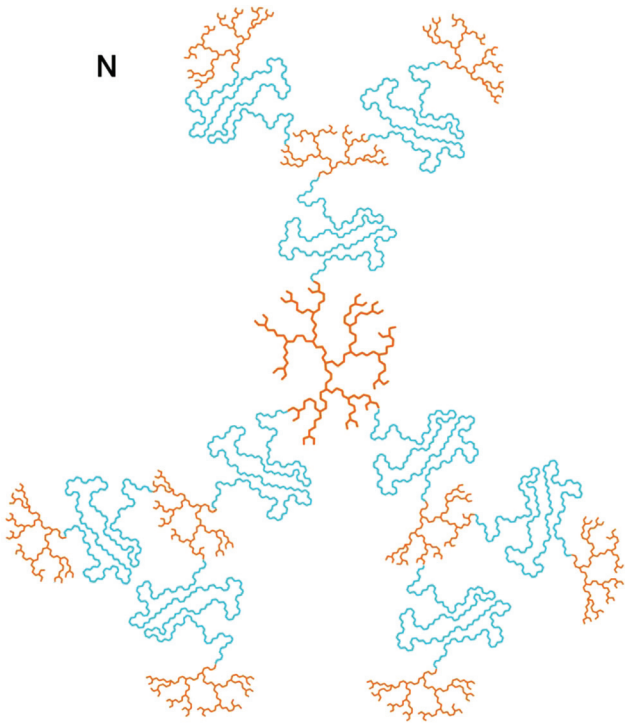

Fig. 5 Linear–dendritic architectures; fifth group: N. Structures were first published in ref. 41.

blocks can be covalently attached to a variety of drugs and therapeutic agents,[63,64] targeting and imaging moieties,[65–67] and bioactive molecules,[68] to achieve targeting, imaging, and therapeutic treatment of cancer. Several articles reviewed the research activities generated on linear–dendritic hybrids from

different points of view, such as discovery and synthetic strategies, PEG–dendritic block copolymer applications, and DNA–protein–dendritic biohybrids in nanobiotechnology.[41,43,58,69,70] This review will focus on the potential of several (A), (E), and (K) type linear–dendritic hybrids as nanosized carriers for anticancer drug delivery systems. Specifically, we will describe the synthesis methods of related linear–dendritic hybrids, loading/conjugating of anticancer agents onto linear–dendritic carriers, and the associated *in vitro* and *in vivo* anticancer activity.

2. Strategies employed to load anticancer drugs onto linear–dendritic vehicles

Currently used cancer chemotherapeutics are often inadequate to cure tumors because of the nonselectivity of these drugs, resulting in dose-limiting side effects. Strategies for reducing the toxicity and side effects without sacrificing efficacy could greatly improve treatment and quality of life for patients. Drug delivery systems that are specific to tumor cells offer both an increased therapeutic index and a reduction in harmful side effects.[71–73] Several attempts have been made to design linear–dendritic copolymers as drug carriers. Drug molecules can be transferred either as conjugated to the functional groups on the dendritic structure or encapsulated by the hydrophobic interior of the dendritic blocks. These two approaches have been developed substantially, although each approach has its own advantages and drawbacks.[74–78]

2.1. Linear–dendritic copolymers/drug conjugates produce vehicles

By conjugating appropriate targeting moieties, drugs, and imaging agents to linear–dendritic polymers, 'smart' drug-delivery nanodevices can be developed that can target, deliver, and monitor the progress of therapy.[8,79] However, the conjugation generally requires multi-step organic reactions and the covalent conjugation chemistry has to be optimized in order for the drug molecules to be cleaved and released under specific biological conditions.[75]

Drugs can be conjugated to linear–dendritic polymers, either directly or *via* a linker/spacer including:

- acid-labile hydrazone linkages, which are stable at physiological pH but readily cleaved under mildly acidic conditions, *e.g.*, inside endosomes and lysosomes;[78]

- ester linkages, which are hydrolyzed inside the cell by esterase enzymes;[8]

- disulfide bonds, which are reduced by glutathione inside the cytosol;[80]

- amide bond, but this bond is known to be very stable chemically in a biological environment;[81]

- acid sensitive acetal bonds, which are stable at pH >7, can be an interesting option. At mildly acidic pH, hydrolysis of the acetals is expected to occur, generating hydroxyl groups.[82]

2.2. Linear–dendritic copolymers produce vehicles upon encapsulation of drugs

In the physical encapsulated or complex form, the drugs can be loaded onto the dendritic blocks by non-covalent interactions such as van der Waals forces, hydrophobic interactions, hydrogen bonding and electrostatic interactions between oppositely charged fragments of drug molecule and dendritic blocks.[42,74,83] The latter approach is relatively simple; however, in spite of significantly improving the water solubility and bioavailability of the drugs, the *in vivo* stability of the copolymer/drug complexes could be a challenging issue.[75,84]

3. Classification based on the loaded drug

The present review focus on the application of linear–dendritic vehicles for the delivery of four anticancer drugs: paclitaxel, doxorubicin, cisplatin, and camptothecin. The following listing of drugs associated with carriers composed of linear–dendritic copolymers provides an overview of the potential of the linear–dendritic platform to serve as anticancer drug carriers (Fig. 6).

4. Paclitaxel

Paclitaxel (PTX), also known as Taxol (trade mark of Bristol–Myers–Squibb), is one of the most effective anticancer agents against a wide spectrum of cancers including ovarian, breast, and colon cancer. It exerts its antitumor effect by binding to microtubules and interfering with the normal growth of microtubules during cell division, which especially affects fast growing cancer cells.[61,85–89] However, systemically administered PTX causes serious side effects, such as neutropenia and peripheral sensory neuropathy. On the other hand, to overcome its limited solubility in water, paclitaxel (Taxol) is formulated in an oily solution of Cremophor EL (polyethoxylated castor oil) and absolute ethanol (1 : 1 v/v). This is known to

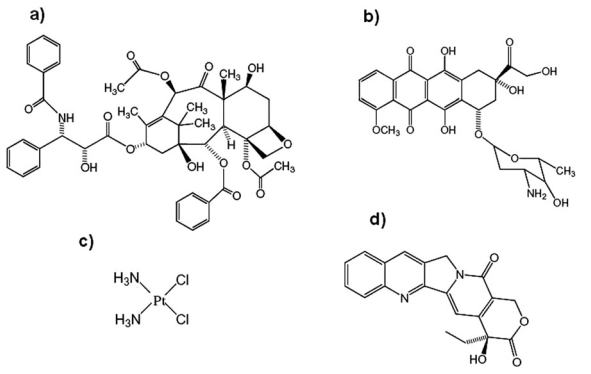

Fig. 6 Structures of (a) paclitaxel, (b) doxorubicin, (c) cis-platin, and (d) camptothecin.

create such effects as anaphylaxis and other severe hypersensitivity reactions attributable to Cremophor EL and ethanol.[85,86,90]

4.1. Paclitaxel-encapsulated linear–dendritic block copolymers

4.1.1. Physicochemical properties. In an attempt to overcome the mentioned limitations, paclitaxel has been encapsulated into micelle-based formulations. An interesting study has reported a micellar linear–dendritic block copolymer composed of polyethylene glycol (PEG, M_w = 5 KDa) and third generation polylysine terminated with 8 units of cholic acid (CA), named PEG^{5K}–CA$_8$ telodendrimer (Fig. 7), for delivery of PTX in the treatment of nude mice bearing ovarian cancer xenografts (Compound **1**).[84]

Physical entrapment of paclitaxel in linear–dendritic micelles has been carried out utilizing the hydrophobic interactions between PTX and the dendritic cholic acid cluster, resulting in high loading capacity (7.3 mg PTX mL^{-1}) through the evaporation method. The particle size of PEG^{5k}–CA$_8$ nanoparticles loaded with PTX was 56 nm, as measured by the dynamic light scattering (DLS) method. Cryo-TEM images showed that the particles were spherical *in situ*, and the sizes were 50–60 nm, which was consistent with the results obtained by DLS. PTX–PEG^{5k}–CA$_8$ NPs have also been found to be very stable at 4 °C, showing no significant changes in average particle size over 6 months. On the other hand, Abraxane® (the FDA-approved Albumin nanoparticle-bound Paclitaxel), was unstable and started to form larger aggregates and precipitate 4 days after dissolving the white powder of Abraxane with saline. The obtained PTX–PEG^{5k}–CA$_8$ NPs exhibited sustained drug release into surrounding the PBS, rapid release of 20% of the drug in the first 2 h, cumulative release of 35% of the drug by 12 h, and a slow linear release of 75% of the drug by 156 h.[84] In order to better define the relationship between the structures of the PEG^{mk}–CA$_n$ telodendrimers and their physicochemical properties for drug delivery, this group prepared a series of stable micelle systems with tuneable particle sizes by varying the PEG chain length and the number of cholic acids in the dendritic core.[90] Other natural lipophilic molecules such as cholesterol formate (CF), lithocholic acid (LA) (both with planar steroid scaffold), and heptadecanoic acid (HA) (linear fatty acid) have also been substituted for cholic acid in the PEG^{5k}–CA$_8$ linear–dendritic structure). The resulting micelles, with low critical micelle concentrations (CMC) at approximately 1 μM, tended to form precipitate in aqueous solution, and their PTX loading capacities were rather low,[90] indicating the essential role of facial amphiphilic cholic acid for stabilizing telodendrimer micelles. Also by varying the PEG chain length and the number of cholic acids in the dendritic core, it has been determined that larger numbers of cholic acids lead to low CMC, larger micelles with a heterogeneous size distribution, and significant precipitation after PTX loading. PEG^{5k}–CA$_8$ with a medium particle size of 61 nm and the highest PTX loading capacity (7.3 mg PTX loaded in 20 mg PEG^{5k}–CA$_8$ mL^{-1}, 36.5% (w/w) of drug/polymer ratio) has been found to be the optimized structure for carrying the drug.[90] The stability of the PTX-loaded PEG^{5k}–CA$_8$ micelles was followed by the DLS particle sizer. The particle size of these PTX-loaded micelles in aqueous solution was found to be highly stable at 4 °C for over 6 months, no further aggregations and no needle crystals of PTX were observed. As mentioned before, Abraxane tends to precipitate 24 h after being reconstituted with saline. Upon dilution with PBS to 125-fold, to mimic the dilution by the blood pool through intravenous (iv) injection, needle-like crystals of PTX were observed in the diluted Taxol (Cremophor formulation of PTX) but they were not observed in PTX-loaded PEG^{5k}–CA$_8$ micelle solutions even after 12 months, indicating that the PTX complex inside these micelles is very stable.

Later Li *et al.*[80] introduced a cross-linked micelle system for specific delivery of paclitaxel to tumor sites, composed of a dendritic oligomer of cholic acids attached to one terminus of the linear PEG through a poly(lysine-cysteine-Ebes) backbone (Compound **2**). Cysteine has been inserted into the linear–dendritic structure to achieve a self assembling disulfide-cross-linking system, so that micelles can be further stabilized to avoid premature release of the loaded drugs during circulation. At the tumor sites, the intracellular reductive agents such as glutathione cleaved the intra-micellar disulfide bonds and drug release occurred. PTX loading onto the micelles was carried out by the solvent evaporation method. PTX and the polymeric structure were first dissolved in chloroform. Then, the chloroform was evaporated under vacuum to form a thin film. PBS buffer (1 mL) was added to re-hydrate the thin film, followed by 30 min sonication. The PTX-loaded micelles were

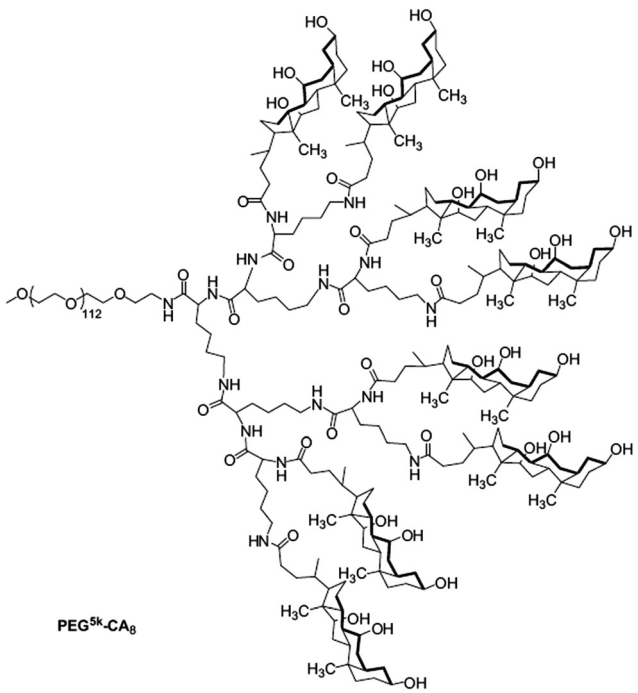

Fig. 7 The chemical structure of PEG^{5K}–CA$_8$ (Compound **1**). Reprinted with permission from ref. 84. Copyright (2009) Elsevier Ltd.

then cross-linked *via* O_2-mediated oxidization. The CMC value of 0.67 μM was determined for PTX loaded cross-linked micelles. The morphology of the PTX loaded cross-linked micelles was observed to be spherical with uniform sizes under a TEM. The size of the micelles observed under TEM was consistent with those measured by DLS (27 nm).[80] The loading capacity of PTX in the cross-linked system was 7.1 mg mL^{-1}, which was equivalent to a drug/micelle ratio of 35.5% (w/w). PTX loaded disulfide cross-linked micelles have been found to be very stable at 4 °C, showing no significant changes in average particle size and drug content over 8 months. The stability of the micelles in physiological conditions including blood was demonstrated by monitoring the particle sizes of micelles over time. The PTX loaded DCM micelles retained an average particle size around 30 nm, with uniform and narrow size distribution, in human plasma for 24 h. Drug release studies indicated that the PTX release was gradually facilitated as the GSH concentration increased from its extracellular level (2 mM) up to the intracellular level (10 mM). This drug release strategy indicated that premature drug release can be minimized during circulation *in vivo*, and accelerated release occurred upon internalization of the micelles into cancer cells.[80]

There is one interesting study employing biodegradable amphiphilic linear–dendritic block copolymers that present folate in clusters for cell targeting, as a means of selectively targeting drug-loaded nanocarriers for chemotherapeutics.[91] PTX has been loaded into the polymeric micelles noncovalently *via* self-assembly of amphiphilic linear–dendritic copolymers (LDP) composed of the hydrophobic linear polypeptide block [poly(β-benzyl-L-aspartate)] (M_w = 3000 Da) and the hydrophilic dendritic polyester-PEG block (M_w = 12 000 Da) (Fig. 8) (Compound **3**). Folate occupied approximately 10% of the surface (~4–5 wt% of micelle), leaving the other 90% exposed as PEG. During assembly, hydrophobic PTX is entrapped within the micelle core and the polyester-PEG dendron forms a dense antifouling shell around the micelle. The PTX-loaded micelles have a hydrodynamic diameter of ~90 nm and a negative surface charge of −20 mV. It was shown that PTX remained within the LDP carrier for at least 2 hours following systemic injection, which is sufficient time to allow their distribution to tumors in significant quantity *via* EPR. The longer stability observed can be attributed to the low micelle CMC (CMC of $\sim 10^{-8}$ M) for LDP micelles, making the system more resistant to dilution effects and destabilization by *in vivo* conditions. Increased effective solubility of PTX was achieved by PTX loading into the linear–dendritic micellar system with drug-loading weight efficiencies up to 40 wt%. Drug release studies showed enhanced release at lower pH, caused by breakdown and destabilization of the micelle structure.[91]

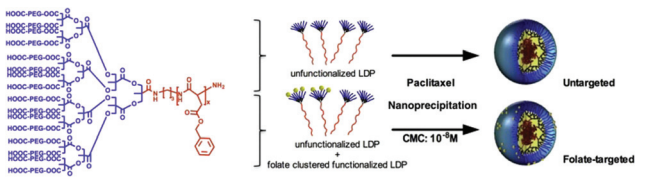

Fig. 8 Chemical structure of the linear dendritic polymer (LDP) made from biocompatible and degradable elements (linear polypeptide-[poly-(β-benzyl-L-aspartate)] block and dendritic polyester–PEG block) (X_n = 12–15). Blue, hydrophilic; red, hydrophobic. Schematic showing the preparation of paclitaxel (PTX)-encapsulated LDP micelles that do not present folate or folate clusters for enhanced cell targeting (compound **3**). Reprinted with permission from ref. 91. Copyright (2011) Elsevier Inc.

Qiao *et al.* have reported a novel linear–dendritic block copolymer micelle semi-polyamidoamine-*b*-poly(D,L-lactic acid) encapsulating hydrophobic docetaxel, a semisynthetic structural analogue of paclitaxel (Compound **4**).[92] Hydroxyl-tailed semi-polyamidoamine dendron (sPA-OH) was synthesized by a divergent method, in which the growth of a dendron has originated from a core site. Then, ring-opening polymerization (ROP) of D,L-lactide was carried out using hydroxyl-tailed sPA-OH G4.5 (or G3.5) and a catalytic amount of $Sn(Oct)_2$. DTX has been encapsulated to obtain a linear–dendritic copolymer by a co-solvent evaporation method. The hydrophobic linear PLA block formed a micelle inner core that acted as a container for insoluble drug DTX, which was subsequently stabilized by the hydrophilic capped polyamidoamine shell. The highest DTX loading efficacy (80.4%) was achieved for the copolymer with molecular weight of 11 500 g mol^{-1} bearing semi-PAMAM G4.5. CMC of 5.01 mg L^{-1} and a particle size of 87.4 nm was determined for these DTX loaded micelles. Based on drug release experiments, it was determined that approximately 100% of encapsulated DTX was released at pH 5.0, however this value was about 75% at pHs 6.8 and 7.4, indicating a facilitated DTX release under acidic conditions, which can be beneficial to specific drug targeting *in vivo* (Fig. 9). This pH dependence was described by the protonation of tertiary amine groups of semi-PAMAM dendritic block, which leads to conformational changes and triggers the drug release.[92]

4.1.2. *In vitro* evaluations. Investigations of *in vitro* anticancer activity of the PTX–PEG^{5k}–CA_8 NPs (Compound **1**), performed on SKOV3-luc-D3 ovarian cancer cells, demonstrated similar cytotoxic activity against cancer cells as the free drug.[84] *In vitro* cytotoxicity studies of PTX-loaded linear–dendritic micelles including PEG^{5k}–CA_8, PEG^{3k}–CA_4, and PEG^{3k}–CA_8 and the two clinical formulations of PTX (Taxol and Abraxane) on SKOV-3 cells demonstrated the IC_{50} in the range 4.3 to 6.2 ng mL^{-1} (Fig. 10).[90]

Investigation of *in vitro* antitumor effect of PTX loaded PEG–poly(lysine-cysteine-Ebes)–cholic acid crosslinked system (Compound **2**), evaluated on SKOV-3 cells, showed less cytotoxicity than Taxol.[80] This was attributed to the slower release of PTX within the cell culture media. However, enhanced cytotoxicity was achieved through studies on SKOV-3 cells with an enriched GSH level, which facilitates intracellular drug release by the cleavage of intra-micellar disulfide bridges.[80]

Cytotoxicity studies of docetaxel encapsulated semi-polyamidoamine-*b*-poly(D,L-lactic acid) (Compound **4**) on human breast cancer cell lines (MCF-7)[92] showed no inhibition of

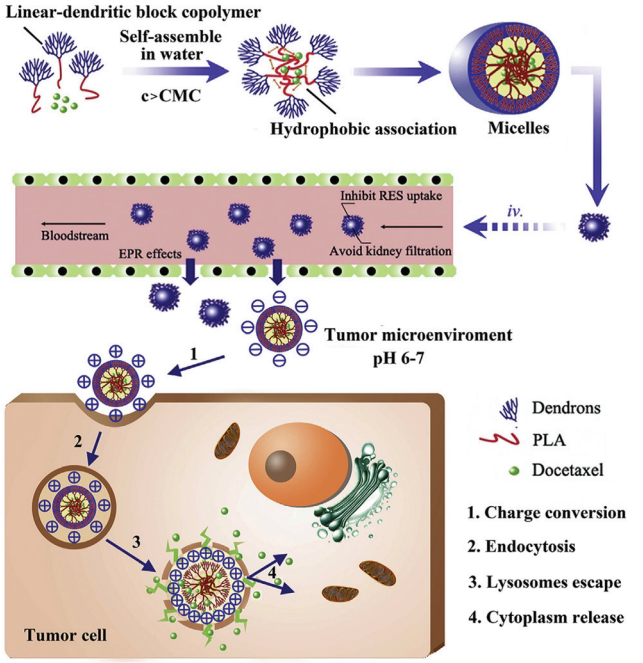

Fig. 9 Self-assembly and multifunctional target delivery of DTX-loaded polyamidoamine-*b*-poly(D,L-lactic acid) micelles (Compound **4**). Reprinted with permission from ref. 92. Copyright (2013) Elsevier B.V.

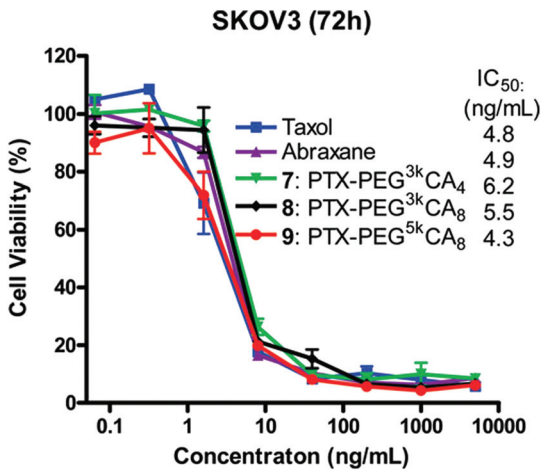

Fig. 10 Tumor cell killing of the PTX-loaded PEG^{mK}-CA$_n$ micelles in the SKOV-3 ovarian cancer cells; very similar IC$_{50}$ values were observed for all the formulations in *in vitro* tumor cell killing. Reprinted with permission from ref. 90. Copyright (2010) American Chemical Society.

cellular growth for blank micelles, attributed to reduction/shielding of the positive charge on the dendrimer surface by the terminal ester, while DTX-loaded micelles showed equipotent anticancer efficacy as control Taxotere® (IC$_{50}$ 2.23 ± 0.15 *vs.* 1.58 ± 0.11 μg mL^{-1}) (incubation time: 72 h) confirming semi-PAMAM-*b*-poly(D,L-lactic acid) as a promising anticancer drug carrier.[92]

4.1.3. *In vivo* evaluations. Evaluation of the anti-tumor effects of PTX–PEG^{5k}–CA$_8$ NPs (Compound **1**) after intravenous injection in subcutaneous SKOV3-luc tumor bearing mice showed inhibition of tumor growth for all PTX formulations, with inhibition being the greatest for PTX–PEG^{5k}–CA$_8$ NPs at 30 mg PTX kg^{-1}.[84] However, a second treatment cycle was initiated on day 38 because of noted tumor progression. A decreased tumor growth rate was demonstrated after the intravenous administration of PTX–PEG^{5K}–CA$_8$ NPs and free drug. PTX–PEG^{5k}–CA$_8$ exhibited superior anti-tumor activity as compared with Taxol. Based on near infrared fluorescence (NIRF) imaging, it was found that PTX–PEG^{5k}–CA$_8$ nanoparticles post i.v. injected into cancer bearing mice had a prolonged blood circulation time, and preferentially accumulated in tumors, possibly as a result of EPR effects.[84] *In vivo* biodistribution (evaluated in nude mice bearing the SKOV-3 ovarian cancer xenografts) was greatly influenced by the size of the micelles.[90] Demonstrated by NIRF images, PTX-loaded PEG^{3k}–CA$_4$ micelles with larger sizes (154 nm) had a very high uptake in the liver and lungs, but a low uptake in the tumor. On the other hand, PEG^{2k}–CA$_4$, PEG^{5k}–CA$_8$ micelles with smaller particle sizes (17 and 64 nm) showed a better ability to carry the loaded drug to the tumor sites, which was attributed to EPR effects. *In vivo* antitumor effects for PTX-loaded PEG^{5k}–CA$_8$ was found to be superior to those of Abraxane and Taxol, and cure of the disease was achieved in the group treated with PTX-loaded PEG^{5k}–CA$_8$ at its MTD dosage (45 mg kg^{-1}). No weight loss was observed in mice treated with this nanoformulation, while consistent weight loss was observed in those treated with Taxol.[90] This system has some significant advantages, such as nontoxicity of carrier in contrast to the commercial vehicle of PTX, high drug loading capacity, relatively small sustained drug release profile, superior stability, preferential accumulation in tumors, similar *in vitro* cytotoxic activity with Taxol, and superior *in vivo* anti-tumor activity as compared with Taxol.[84,90] Enhanced efficacy of PTX encapsulated PEG^{5k}–CA$_8$ NPs after intravenous injection can be explained as follows: First, the PEG^{5k}–CA$_8$ nanocarrier may improve the pharmacokinetic profile of PTX, prolonging its circulation time, thus resulting in a higher accumulation in tumors due to EPR effects. Secondly, since PTX encapsulated PEG^{5k}–CA$_8$ NPs accumulate in the tumor, PTX is released in a sustained manner so that tumor cells can be exposed to PTX for a longer time period. Thirdly, PTX encapsulated PEG^{5k}–CA$_8$ NPs have a relatively small size (50 nm) compared to Abraxane (130 nm), which may result in deeper penetration into tumor nodules. This is important as although some larger nanoparticles, such as liposomes, can be delivered effectively to a solid tumor *via* the EPR effect, they would not be distributed sufficiently to cancer cells distant from tumor vessels.[93] These promising features make PTX encapsulated PEG^{5k}–CA$_8$ NPs suitable for more investigations.[84,90]

For the PTX encapsulated PEG–poly(lysine-cysteine-Ebes)–cholic acid crosslinked system (Compound **2**),[80] according to noninvasive NIRF optical images, a significant contrast of the fluorescence signal has been observed between the tumor and

the background at 4 h after administration and was sustained up to 72 h (Fig. 11, top). *Ex vivo* imaging at 72 h post injection further confirmed the preferential uptake of crosslinked micelles in the tumor compared to normal organs (Fig. 11, bottom). This is due to the prolonged *in vivo* circulation time of the micelles and the size mediated EPR effect. A relatively high uptake in the liver was observed compared to other organs, which is likely attributed to the nonspecific clearance of nanoparticles by the reticuloendothelial system (RES). Similar biodistribution and tumor uptake of PTX loaded crosslinked micelles were observed *via* EPR effects (Table 1).[80]

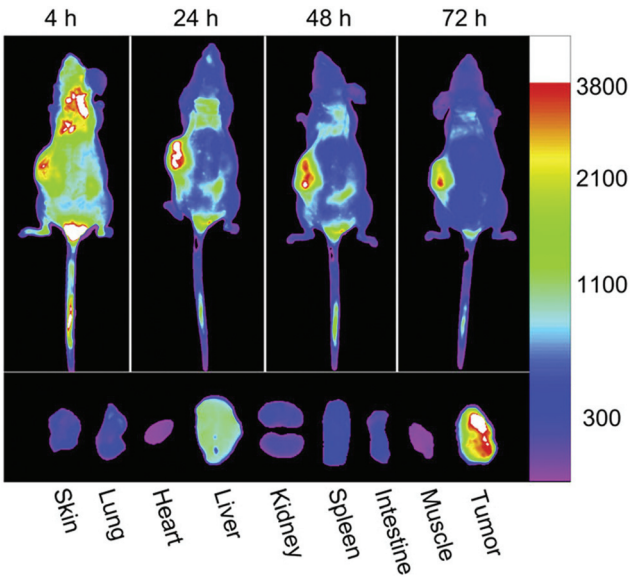

Fig. 11 *In vivo* and *ex vivo* near infra-red fluorescence (NIRF) optical imaging. Top: *In vivo* NIRF optical images of a SKOV-3 xenograft bearing mouse were obtained with a Kodak imaging system at different time points after i.v. injection of PEG–poly(lysine-cysteine-Ebes)–Cholic acid co-loaded with PTX and DiD; bottom: *ex vivo* NIR image of dissected organs and tumor was obtained at 72 h after injection. Reprinted with permission from ref. 80. Copyright (2011) Elsevier Ltd.

Based on *in vivo* studies evaluated in the subcutaneous SKOV-3 tumor bearing mice, increased *in vivo* therapeutic efficacy has been shown for PTX-loaded crosslinked micelles compared to the equivalent dose of free drug. This has been corresponded to the higher amount of PTX that reached the tumor site *via* their prolonged circulation time. In addition, the high glutathione level of the tumor site and particularly inside the tumor cells facilitated drug release and increased cytotoxicity.[80] Uniform size around of 27 nm for PTX encapsulated the PEG–poly(lysine-cysteine-Ebes)–cholic acid crosslinked system enables these PTX loaded micelles to take full advantage of the EPR effect and accumulate at tumor sites. In addition, the system has the characteristics of superior drug loading capacity, enhanced micellar stability, prolonged *in vivo* circulation time, preferential tumor targeting, and superior *in vivo* anti-tumor activity as compared with Taxol. However, a relatively high uptake in the liver was observed compared to other organs, which is likely attributed to the nonspecific clearance of nanoparticles by the reticuloendothelial system (RES).[80]

In the case of polymeric vehicle composed of hydrophobic linear polypeptide block [poly(β-benzyl-L-aspartate)] and hydro-

Table 1 Paclitaxel-encapsulated linear–dendritic block copolymers

Carrier	Size (nm)	CMC	*In vitro* activity	*In vivo* activity	Advantages	Ref.
PEG^{5K}–CA_8	56	1 μM	IC_{50} = 4.3 ng mL^{-1} on SKOV3-luc-D3 ovarian cancer cells	Superior anti-tumor activity for PTX–PEG^{5k}–CA_8 as compared with Taxol after intravenous injection in subcutaneous SKOV3-luc tumor bearing mice	High drug loading level, nontoxic carrier, high drug loading capacity, relatively small sustained drug release profile, superior stability, preferential accumulation in tumors, superior anti-tumor activity as compared with Taxol	84, 90
PEG–poly (lysine-cysteine-Ebes)–CA	27	0.67 μM	Less cytotoxicity compared to Taxol on SKOV-3 cells, but higher cytotoxicity compared to Taxol with an enriched GSH level	Increased *in vivo* therapeutic efficacy compared to the equivalent dose of free drug in the subcutaneous SKOV-3 tumor bearing mice	Superior drug loading capacity, enhanced micellar stability, prolonged *in vivo* circulation time, preferential tumor targeting, and superior *in vivo* anti-tumor activity as compared with Taxol	80
[poly(β-benzyl-L-aspartate)]-polyester-PEG	90	10^{-8} M	Enhanced uptake of ligand-clustered micelles in ovarian tumor cells	Higher *in vivo* antitumor efficacy for the folate-bearing linear–dendritic micelles compared to free PTX in FR-expressing KB xenograft model in nude mice	Suitable circulation half-life, resistance to dilution effects and destabilization by *in vivo* conditions, increased targeting of the micelles to FR-expressing cells, increased accumulation	91
Semi-PAMAM-*b*-poly(D,L-lactic acid)	87.4	5.01 mg L^{-1}	IC_{50} = 2.23 ± 0.15 μg mL^{-1} on human breast cancer cell lines (MCF-7), equipotent anticancer efficacy as control Taxotere	1.53 fold higher half-life of DTX in micelles compared to Taxotere®	Biocompatibility, improved cellular uptake, facilitated anticancer drug release under acidic conditions	92

philic dendritic polyester-PEG block (Compound **3**),[91] after intravenous injection in BALB/c mice without tumors, distribution half-lives ($t_{1/2,\ \text{distribution}}$) of the encapsulated PTX (2.5 wt%) and free PTX (2.5 wt% equivalent) were 1.72 ± 0.2 hour, and 0.61 ± 0.4 hour, and their elimination half-lives ($t_{1/2,\ \text{elimination}}$) were 9.06 ± 2 hours, and 4.32 ± 3 hours, respectively, indicating a much higher bioavailability of the PTX-loaded LDP micelles compared to the free drug. This can be attributed to the low CMC of micelles, making the system more resistant to dilution effects and destabilization by *in vivo* conditions. Also 10–12% weight loss was revealed in mice receiving free-PTX and signs of hair loss were observed after six injections. No signs of toxicity were shown in mice receiving PTX-encapsulated injections. *In vivo* antitumor efficacy investigations, evaluated in the FR-expressing KB xenograft model in nude mice, showed that the folate-bearing linear–dendritic micelles (PTX dosage = 2.5 mg kg^{-1}) are as effective as a higher dose of free PTX (10 mg kg^{-1}). Comparison of the tumor killing effects between folate-targeted and untargeted micelles (PTX dosage = 2.5 mg kg^{-1}) determined the higher antitumor efficacy for the folate-targeted LDP system. This was attributed to more efficient entering of the folate targeted micelles into tumor cells from the extracellular space, through FR-mediated uptake, and subsequent intracellular release of the drug.[91] The measured circulation half-life of PTX encapsulated [poly(β-benzyl-L-aspartate)]-*block*-dendritic polyester-PEG was significantly higher than the values reported in preclinical trials for PTX loaded PEG-*block*-poly(D,L-lactide) linear block copolymers in the literature.[94] The longer stability, due to low micelle CMC, more resistance to dilution effects and destabilization by *in vivo* conditions, increased targeting of the micelles to FR-expressing cells, increased accumulation over a 5-day period, and the potency of the therapy with a low PTX dose of 2.5 mg kg^{-1} make this system promising for antitumor treatment. For achieving a relatively similar effect, this dosage regimen is much lighter in comparison to other studies involving folate-mediated therapy.[95–97] However, the data also suggest a gradual loss of PTX from the micelles at longer time points *via* slow leakage of the drug from the interior of the micelle, and future design of the system may be applied to further address this issue.[91]

Pharmacokinetic study in Sprague–Dawley (SD) rats illustrated that semi-polyamidoamine-*b*-poly(D,L-lactic acid) micelles (Compound **4**) prolonged DTX retention in blood circulation (1.737 h) in comparison to Taxotere® (commercial vehicle of DTX) (1.231 h), and the half-life of DTX in micelles was 1.53 fold higher than that of the Taxotere® control.[92] A plausible explanation was that ester-terminated hydrophilic dendrons and a dense micelle structure were capable of preventing the drug molecules from being easily eliminated from the physiological environment. Investigation of intracellular uptake capacity evaluated in MCF-7 cells demonstrated that fluorescent dye C6 labeled semi-polyamidoamine-*b*-poly(D,L-lactic acid) micelles had been internalized into the cytoplasm. Previous studies indicated that multivalent dendrimers enhanced membrane adhesion and disruption.[98] The multivalent dendritic surface of linear–dendritic semi-polyamidoamine-*b*-poly(D,L-lactic acid) might also increase binding sites with the membrane and facilitate micelle uptake. Further studies are needed to elucidate the uptake mechanisms of semi-polyamidoamine-*b*-poly(D,L-lactic acid) micelles. Generally, low CMC would be beneficial to semi-polyamidoamine-*b*-poly(D,L-lactic acid) micelles in order to avoid dilution in the blood circulation. Some other advantages such as biocompatibility, improved cellular uptake, and facilitated anticancer drug release under acidic conditions make linear–dendritic semi-polyamidoamine-*b*-poly(D,L-lactic acid) useful for anticancer drug delivery. However, its safety and efficacy in chemotherapy should be further studied.[92]

4.2. Paclitaxel-conjugated linear–dendritic block copolymers

4.2.1. Physicochemical properties. A linear–dendritic targeting system for PTX delivery has been reported by Clementi *et al.*,[8] employing alendronate (ALN), a bone-targeting agent used for the treatment of osteoporosis and bone metastases. A PEG–dendrimer–ALN structure has been designed using β-glutamic acid as a symmetric bicarboxylic branching unit and linking of ALN to carboxylic PEG–dendrimer groups. Coupling of PTX to PEG–dendrimer–ALN through ester linkage yielded the linear–dendritic ALN-mediated bone targeting prodrug (Compound **5**) (Fig. 12).

This design leads to an amphiphilic conjugate, with PTX being highly hydrophobic and ALN being hydrophilic. The spatial separation of these drugs, besides offering the possibility to form self-assembled micelles, will maintain all ALN molecules exposed to the water, promptly available for binding to the bone mineral HA.[8] The content of ALN and PTX in the PEG–(β-Glu) dendrimer was determined as 11% w/w and 4.7% w/w, respectively. The mean hydrodynamic diameter of PTX–PEG–(β-Glu) dendrimer–ALN conjugates was 200 nm. Investigation of drug release showed that the hydrolysis rate of the ester bond between PTX and the polymer was higher in both

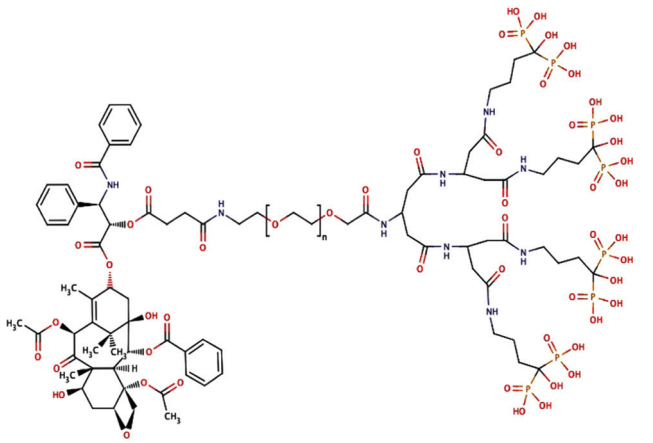

Fig. 12 Chemical structure of PTX conjugated PEG–(β-Glu) dendrimer–ALN (Compound **5**). Reprinted with permission from ref. 8. Copyright (2011) American Chemical Society.

Table 2 Paclitaxel-conjugated linear–dendritic block copolymers

Carrier name	Size	CMC	*In vitro* activity	*In vivo* activity	Advantages	Ref.
PEG–poly (β-glutamic acid)–ALN	200	n[a]	Similar IC_{50} for PTX–PEG–dendrimer–ALN and free PTX (25–60 nM) on PC3 human prostate cancer cells	n[a]	Nontoxic carrier building blocks, half-life prolongation of conjugates, targeting bone neoplasms, fast drug release in the surroundings of bone metastasis	8

[a] n: not reported.

plasma and buffer solution at physiological pH (7.4), compared to that in buffer solution at lysosomal pH (pH 5). This phenomenon indicated that PTX is released by a hydrolytically based mechanism without a significant contribution of esterases. The stability of PTX–PEG–(β-Glu) dendrimer–ALN was evaluated in buffer solutions at physiological pH (7.4), at lysosomal pH (5), and in mice plasma. At pH 7.4 and in plasma, about 50% of the PTX–PEG–ALN conjugate was degraded within the first 1 h; the remaining conjugate was degraded within 24 h. The stability of the conjugate micelles, monitored at 37 °C for 24 h by DLS, was in line with the kinetics of PTX release. The micelles of PTX–PEG–ALN conjugates preserved the same size for 24 h when incubated in buffer at pH 5, whereas at pH 7.4 the same micelles were stable for 3 h, then the PTX release from the conjugates destabilized the system.[8]

4.2.2. *In vitro* evaluations. ALN-mediated binding capacity of PEG–(β-Glu) dendrimer–ALN and PTX conjugated PEG–(β-Glu) dendrimer–ALN (Compound **5**) to bone mineral was evaluated *in vitro*, employing HA mineral mimicking bone tissue.[8] By fast protein liquid chromatography (FPLC) analysis, it was revealed that, following 5 min of incubation, 80% or 90% of PTX–PEG–dendrimer–ALN or PEG–ALN conjugates, respectively, were bound to HA and reached a plateau. On the other hand, non-targeting PEG could not bind to HA after 60 min of incubation, confirming the role of ALN in the bone targeting process.

Illustrated by *in vitro* rat red blood cell (RBC) hemolysis assay, PTX–PEG–(β-Glu) dendrimer–ALN showed no hemolytic activity at up to 5 mg mL^{-1}. Regarding significant hemolytic activity of the commercial solubilizing vehicle of PTX, PEG–(β-Glu) dendrimer–ALN can be suggested as a promising carrier for PTX. *In vitro* cytotoxicity assay on PC3 human prostate cancer cells exhibited similar IC_{50} for PTX–PEG–dendrimer–ALN and free PTX (25–60 nM).[8]

4.2.3. *In vivo* evaluations. The pharmacokinetic studies of PTX dissolved in 1 : 1 : 8 ethanol–Cremophor EL–saline and PTX–PEG–(β-Glu) dendrimer–ALN (Compound **5**) showed an improved Pharmacokinetic Profile in Mice.[8] After administration of free PTX, high levels of the drug were recorded, however at 5 min post-injection the PTX concentration decreased dramatically, and it was not detectable at 60 min. On the contrary, the conjugates showed a marked half-life prolongation, with detectable levels of PTX after 24 h for PTX–PEG–(β-Glu) dendrimer–ALN. In particular, elimination half-lives ($T_{1/2\beta}$) were 15.1 and 85.5 min for PTX and PTX–PEG–(β-Glu) dendrimer–ALN, respectively.[8]

PTX–PEG–(β-Glu) dendrimer–ALN conjugate was designed for strong bone tropism and fast drug release. Therefore, with PTX–PEG–(β-Glu) dendrimer–ALN conjugate, a cathepsin B-cleavable linker might not be suitable because the derivative *in vivo* will bind to the bone HA matrix. The high affinity to the bone originating from the presence of a bisphosphonate in the conjugate can affect the conjugate internalization into cancer cells and consequently slow the rate of PTX release, if a cathepsin B-cleavable linker is used. Cathepsin B is over-expressed in lysosomes of many types of tumor cells, but is also secreted to the extracellular matrix. In general, enzymatic cleavage is efficient when slow and controlled drug release is required. When a fast release is desired, a different mechanism, such as hydrolysis, is necessary. Therefore, a PTX–polymer hydrolysis at physiological conditions is preferred because it allows drug release in the surroundings of bone metastasis, where the conjugate will fast accumulate.

PTX was linked to PEG through an ester linkage exploiting a succinimidyl spacer, which releases the drug at physiological pH. The hydrolysis rate of the ester bond between the drug and the polymer was higher in buffer at pH 7.4 than in pH 5. Interestingly, the incubation in plasma showed a drug release comparable to that in buffer at pH 7.4, suggesting that PTX is released by a hydrolytically based mechanism without a significant contribution of esterases. Besides nontoxic building blocks, the derivative can target bone neoplasms by dual-targeting as follows: (1) through ALN (active mechanism), and (2) by exploiting the EPR effect (passive mechanism), which is due to the atypically leaky tumor blood vasculature, which enhances tumor accumulation of the conjugate thanks to its increased size with respect to the free drug (Table 2).[8]

5. Doxorubicin

Doxorubicin (DOX) is a widely used anticancer drug in the treatment of many types of cancer, including hematological malignancies, many types of carcinoma, and soft tissue sarcomas. DOX is known to interact with DNA by intercalation and to inhibit the biosynthesis of macromolecules.[67,99–101]

However, drawbacks such as poor water solubility, poor penetration *in vitro* and *in vivo*, and dose dependent side-effects such as cardiotoxicity, caused by lack of tumor selectivity, limit its application in chemotherapy.[101–103] Several techniques have been used to enhance tumor targeting and reduce the toxicity without sacrificing efficacy. The use of macromolecular drug carriers such as liposomes,[104] polymeric micelles,[105] dendrimers[106] and linear–dendritic copolymers[107] is the focus of research. One clinical example is DoxilVR, a polyethylene glycol (PEG) containing liposomal formulation of DOX that limits the cardiotoxicity while maintaining the same survivability as the free drug.[102]

5.1. Doxorubicin-encapsulated linear–dendritic block copolymers

5.1.1. Physicochemical properties. Gillies and Fréchet have reported DOX encapsulation in acid-sensitive linear–dendritic micelles. The linear–dendritic structure was composed of a PEO block and a G3 polyester dendrimer of 2,2-bis(hydroxymethyl) propanoic acid units bearing cyclic acetals of 2,4,6-trimethoxybenzaldehyde (Compound **6** in Fig. 13). DOX was loaded into micelles by an oil/water emulsion method in which chloroform was used as the organic phase, and 3 equiv NEt_3 was used relative to DOX, as the drug is known to partition most effectively into the chloroform phase and into the micelle upon deprotonation of the glycosidic amine. Release of the drug occurred through disruption of the micelle caused by hydrolysis of the cyclic acetals at acidic pH and change in micelle solubility.[107]

A drug loading of approximately 12 wt% was determined according to absorbance using UV-visible spectroscopy. The DOX-loaded micelles demonstrated the particle size of 35 nm and a small fraction of aggregates in the size range 200–400 nm was observed. Additionally, a CMC value of 40 mg L^{-1} was determined for this system. At pH 7.4, the micelles were stable over several days, with no significant changes in the size distribution over this time period. In contrast, over several hours at pH 5.0, the size of the DOX-loaded micelles increased and the fraction of aggregates in the population became greater. This aggregation probably occurred upon disruption of the micelles due to acetal hydrolysis and was facilitated by the tendency of DOX to form aggregates by π-stacking. Investigation of drug release at different pH values demonstrated a pH-dependent mode of release of DOX from copolymer 1. After 24 h, drug release of more than 80%, about 40% and about 30% was observed at pH values of 4.0, 5.0 and 6.0, respectively, while at pH 7.4 the system was very stable with less than 10% of the DOX being released over 72 h. These results indicated that the hydrolysis of the pH-sensitive acetals likely plays a role in the mode of drug release, leading to the selective release of DOX in mildly acidic physiological environments (such as tumor tissues). In addition, the increased stability of the pH-sensitive system at pH 7.4 is advantageous so that DOX will not be released during blood circulation, thus avoiding the undesirable organ accumulation and toxicity associated with the free drug.[107]

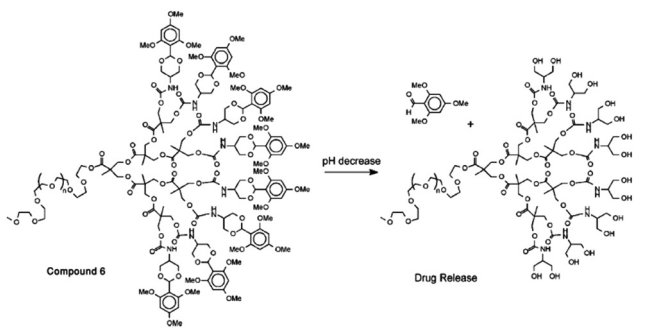

Fig. 13 Hydrolysis of acetals on the dendrimer periphery of the micelle-forming copolymer **6** leads to a solubility change designed to disrupt micelle formation and trigger the release of the drug. Reprinted with permission from ref. 107. Copyright (2005) American Chemical Society.

A newly developed telodendrimer platform, consisting of PEG as the linear block and cholic acid attached to the amine terminus of lysine as the dendritic block, has been employed to prepare DOX micellar formulations for the targeted delivery of DOX to lymphoma.[108] As mentioned before,[84] PEG^{5k}–CA_8 micellar NPs provided a suitable drug delivery system for PTX (a hydrophobic drug) in the treatment of cancer. In their study, Xiao *et al.* showed that the delivery of DOX using this nanocarrier is limited by the relatively low drug loading capacity and poor stability.[108] Using the dry-down method, PEG^{5K}–CA_8 telodendrimers can efficiently encapsulate hydrophobic drug DOX into the core of the micelles (Compound 7). PEG^{5k}–CA_8 telodendrimer, along with different amounts of neutralized DOX, were first dissolved in $CHCl_3$–MeOH, mixed, and evaporated on a rotavapor to obtain a homogeneous dry polymer film. The film was reconstituted in 1 mL phosphate buffered solution (PBS), followed by sonication for 30 min, allowing the sample film to disperse into the micelle solution.[108]

Based on their report, PEG^{5k}–CA_8 micelle was found to have a DOX loading capacity of 8.2% w/w. Another telodendrimer with a similar structure, PEG^{2k}–CA_4, was suggested to encapsulate DOX, which resulted in a higher drug loading capacity of 14.8% w/w. The particle sizes of DOX-loaded PEG^{5k}–CA_8 and PEG^{2k}–CA_4 micelles were in the range 12–17 nm in diameter. Drug release profiles illustrated biphasic patterns for both DOX-loaded PEG^{2k}–CA_4 and PEG^{5k}–CA_8 micellar formulations. It was indicated that 50% DOX cumulative release occurred from DOX–PEG^{5k}–CA_8 during the first 6 h. This value was 35% for DOX–PEG^{2k}–CA_4 over the same time. After the initial fast release, the slow linear release was observed for both systems over the next 7 days. However, the DOX release rate from DOX–PEG^{2k}–CA_4 micelles was significantly slower than that from DOX–PEG^{5k}–CA_8 micelles, reflecting the better stability and stronger interaction between the nanocarrier and the drug in DOX–PEG^{2k}–CA_4. Particle size monitoring confirmed the stability of DOX–PEG^{2k}–CA_4 in physiological conditions. As shown by DLS measurements (Fig. 14), DOX–PEG^{2k}–CA_4 micelles as

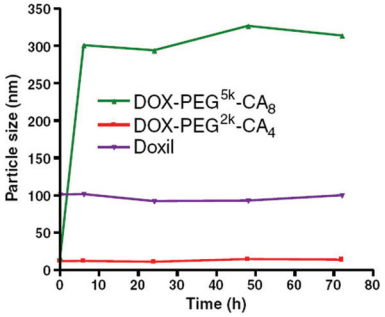

Fig. 14 DLS measurement of particle size change of DOX-loaded PEG^{5k}–CA_8 micelles, and Doxil® in 50% FBS over time at 37 °C. DOX loading level was 2 mg ml^{-1} DOX in 20 mg ml^{-1} telodendrimer, respectively. Reprinted with permission from ref. 108. Copyright (2011) Elsevier B.V.

well as Doxil® were able to maintain their initial particle sizes over 72 h incubation in the presence of 50% FBS. In contrast, DOX–PEG^{5k}–CA_8 micelles started to form bigger aggregates (around 300 nm) after a 6-hour incubation with 50% FBS.[108]

Wu *et al.* developed dendritic–linear block copolymer-modified magnetic iron oxide nanoparticles as a carrier for DOX, which displays thermosensitive drug release behaviors.[109] In their study, magnetic iron oxide (Fe_3O_4) nanoparticles were first prepared by organic solution-phase decomposition of the iron precursor at high temperature. The prepared magnetic iron oxide nanoparticle surfaces were capped by the propargyl focal point polyamidoamine (PAMAM)-type dendron, having four carboxyl acid end groups. Then, by a click reaction, the surface initiator was introduced onto the propargyl group, and using two-step surface-initiated ATRP, poly(2-dimethylaminoethyl methacrylate) (PDMAEMA) chains and poly(*N*-isopropylacrylamide) (PNIPAM) chains were sequentially introduced onto the magnetic nanoparticle surfaces resulting in PAMAM-*b*-PDMAEMA-*b*-PNIPAM block copolymer-modified magnetic iron oxide nanoparticles. At the final step, to increase stability of the nanoparticles and reverse aggregation, a cross-linking reaction between PDMAEMA block and 1,2-bis-(2-iodoethoxy)ethane (BIEE) was carried out (Fig. 15). After the crosslinking reaction, the magnetic nanoparticles were stabilized in water, forming a stable brown solution and no precipitation occurred for 4 months. However, non-crosslinked Fe_3O_4-PAMAM-*b*-PDMAEMA-*b*-PNIPAM nanoparticles could be only stabilized in water for 2 months. It was also verified that the cross-linking reaction could be helpful to stabilize magnetic iron oxide nanoparticles. DLS measurements of freshly cross-linked block copolymer-modified nanoparticles diluted in water provided an average hydrodynamic diameter of particles in solution equal to ~32 nm. DOX has been loaded into the PAMAM-*b*-PDMAEMA-*b*-PNIPAM shell of the modified nanoparticles with a loading efficiency of 22.7% (Compound **8**).[109]

Investigation of drug release behaviour of DOX-loaded nanoparticles demonstrated the cumulative release amounts of 26.8% and 13.7% at 25 °C and 37 °C, respectively (pH = 7.4,

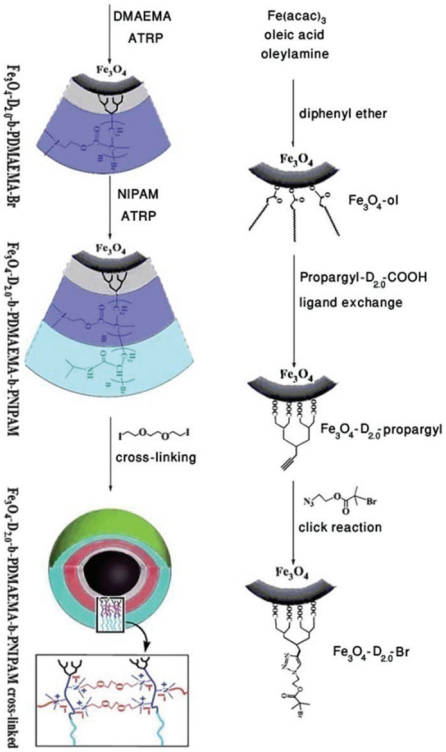

Fig. 15 Synthesis and surface modification of superparamagnetic Fe_3O_4 nanoparticles (Compound **8**). Reprinted with permission from ref. 109. Copyright (2011) The Royal Society of Chemistry.

5 h). This phenomenon was also observed after 24 h with the cumulative release amounts of 41% and 26% at 25 °C and 37 °C, respectively. It was noted that the cumulative release amount was higher at 25 °C than at 37 °C, confirming thermosensitive release caused by PNIPAM block chains in the collapsed and hydrophobic conformation at 37 °C above the LCST, which can retard drug release.[109]

Also, superparamagnetic iron oxide nanoparticles (SPIONs), grafted with a DOX-loaded water-soluble dendritic–linear-brush-like triblock copolymer, polyamidoamine-*b*-poly(2-(dimethylamino)ethyl methacrylate)-*b*-poly(poly(ethylene glycol) methyl ether methacrylate) (PAMAM-*b*-PDMAEMA-*b*-PPEGMA), have been reported as a pH-sensitive drug delivery system (Compound **9**).[110] Immobilization of an ATRP macroinitiator, containing PAMAM G2-typed dendron, on the surface of Fe_3O_4 nanoparticles has been carried out according to the reported procedure in the literature.[109] Then, water soluble dendritic–linear-brush-like triblock copolymer (PAMAM-*b*-PDMAEMA-*b*-PPEGMA)-grafted SPIONs have been prepared by gradual growing of PDMAEMA and PPEGMA from nanoparticle surfaces using the ATRP "grafting from" approach. After removal of the Fe_3O_4 cores with hydrochloric acid, M_n and PDI of the grafted copolymers PAMAM-*b*-PDMAEMA-Br were 3900 g mol^{-1} and 1.08, respectively. For the final grafted copolymers PAMAM-*b*-PDMAEMA-*b*-PPEGMA, M_n and PDI were 26 300 g mol^{-1} and 1.25, respectively. DLS measurement confirmed

that the obtained dendritic–linear-brush-like triblock copolymer-grafted SPIONs had a uniform hydrodynamic particle size of average diameter less than 30 nm. For drug loading, DOX–HCl (2.0 mg) was dissolved in methanol (4.0 mL), and triethylamine (25 μL) was then added into the solution to remove hydrochloride. Drug loading was done by drop-wise addition of the DOX solution with stirring to 3 mL Fe_3O_4-PAMAM-*b*-PDMAEMA-*b*-PPEGMA nanoparticles in methanol (concentration of 2.5 mg mL^{-1}). The mixture was shaken for 24 h in the dark at room temperature to allow the drug partition into the polymer shell. The modified Fe_3O_4-PAMAM-*b*-PDMAEMA-*b*-PPEGMA nanoparticles possessed the thicker shell of polymers, which is beneficial to enhance hydrophobic interactions and hydrogen binding with DOX and improve the loading capacity.[110] *In vitro* drug release experiments showed a pH-responsive drug release behavior for DOX-loaded nanoparticles. The cumulative release amounts of DOX within 48 h at pH 4.7, 7.4 and 11.0 are 83.1%, 64.7% and 8.3%, respectively. The higher release at pH 4.7 has been attributed to decreased hydrogen bond interaction between PDMAEMA and DOX due to the protonation of PDMAEMA chains and DOX at pH 4.7. On the other hand, PDMAEMA chains tend to swell due to the protonated tertiary amino groups at pH 4.7, which is beneficial to accelerate DOX release.[110]

The antitumor effect of doxorubicin encapsulated into amphiphilic linear–dendritic hybrids of PEG–G*n*–PCL (*n* = 0, 1, 2) (Compound **10**) has been evaluated in MDA-MB-231 and MDA-MB-468 breast adenocarcinomas.[102] The linear component of PEG has been employed as the hydrophilic block with a dendron branched poly(ε-caprolactone) (PCL) as the hydrophobic one. The dendrons have been prepared from the 2,2-bis(methylol)propionic acid (bisMPA) building block, bearing click chemistry moieties in the focal point to attach PEG (Fig. 16).

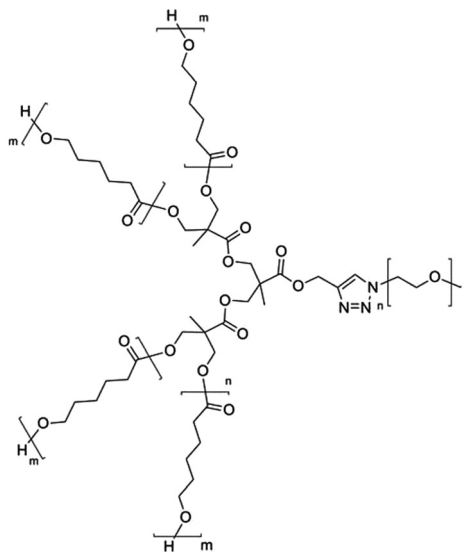

Fig. 16 Chemical structure of PEG–G2–PCL (Compound **10**). Reprinted with permission from ref. 102. Copyright (2011) Wiley Periodicals, Inc.

The amphiphilic PEG–G*n*–PCL structures were capable of forming self-assembled micelles with diameters of about 100 nm. Sequestering doxorubicin achieved a loading efficiency up to 22% for PEG2k–G1–PCL30. It has been demonstrated that the loading of DOX resulted in aggregation of the smaller particles into larger ones, suggesting that some PEG components used in these linear–dendritic hybrids are not sufficiently large to effectively shield the particle from particle–particle interactions. Also increasing the generation of the dendron to two resulted in a substantial loss of loading efficiency down to 8% (PEG5k–G2–PCL30).[102] This has been attributed to the effect of lower crystallinity, due to the effect of the dendritic branching, resulting in a less densely packed hydrophobic core. Also, the incorporation of DOX in a nanoscale confined crystalline core will reduce the crystallinity further. Drug release studies revealed that the mode of release was independent of block portion and dendrimer generation employed in the micelle construction, suggesting that the core material did not influence the diffusion path of the drug from the core. The release of about 60% at 6 h and more than 80% at 24 h has been shown for all evaluated systems.[102]

Recently carbon nanotubes have been introduced as promising materials for the delivery of drugs, RNA, DNA, peptides and other biologically active molecules into cells, because of the ability to cross cell membranes.[111–114] Despite the great potential of carbon nanotubes (CNTs) in anticancer drug delivery, concerns regarding their carcinogenicity, inefficient dispersion in aqueous solutions and biological activity *in vivo* still remain. One important and feasible route to overcome these problems is modification of CNTs with polymers, which are widely studied and play a vital role in biological and biomedical fields, especially in drug delivery.[115] Two methods are used to modify the CNTs by polymers based on either physical interactions or chemical bonding and are so called "noncovalent" or "covalent" approaches, respectively. The noncovalent approach is based on poor van der Waals interactions between CNTs and polymers and includes dispersion with the low molar mass polymers, polymer wrapping and polymer adsorption.[116–118] In the covalent approach, molecules or macromolecules are grafted onto the surface of CNTs through chemical linkages, raising the solubility of CNTs even with a low degree of functionalization. Covalent attachment of polymer chains to the surface of CNTs can be accomplished by either "grafting to" or "grafting from" methods.[114,115,119–124] We proved that polymers not only raise the functionality, biocompatibility and water solubility of CNT but also are able to change the CNT conformations dramatically. A drug carrier composed of polyglycerol–poly(ethylene glycol)–polyglycerol (PG–PEG–PG) ABA linear–dendritic copolymer and CNTs was designed and potential application of the obtained structure to load and transport the anticancer drug DOX was investigated (Compound **11**).[125] Fig. 17 illustrates the schematic structure of the used linear–dendritic copolymer. It has been observed that noncovalent interactions between (PG–PEG–PG) linear–dendritic copolymer and CNTs lead to the conformation alteration of CNTs from an extended toward a closed state due

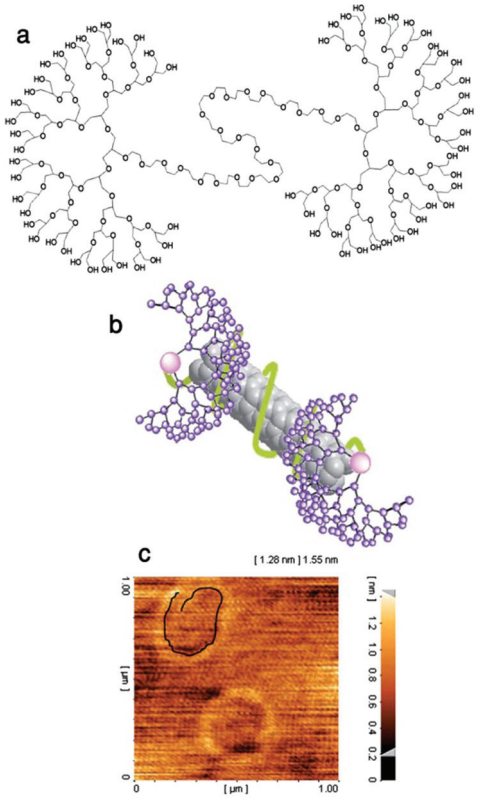

Fig. 17 (a) Schematic representation of PG–PEG–PG ABA type linear dendritic copolymer, (b) schematic representation of noncovalent interactions between linear–dendritic copolymers and the surface of CNTs that lead to new hybrid nanomaterials with improved properties, (c) AFM image of PG–PEG–PG/MWCNT liposome-like nanocapsules containing encapsulated DOX molecules. The highlighted object in the top-left part of image, by a black line, shows the MWCNTs (Compound **11**). Reprinted with permission from ref. 125. Copyright (2012) The Royal Society of Chemistry.

to liposome-like nanocapsule (LLNs) formation. The size of the PG–PEG–PG/MWCNT LLNs filled with DOX molecules was estimated to be 350 nm.

Loading capacities for the PG–PEG–PG/MWCNT LLNs were determined by HPLC as 2.2 grams to one gram of LLNs.[125]

Poor water solubility and low functionality are two critical factors that limit the biomedical applications of CNT/γ-Fe_2O_3NP hybrid nanomaterials. Non-covalent method for improving solubility is based on supramolecular interactions between CNTs and polymers and includes polymer wrapping or adsorption. In this method, the structure of CNTs is not damaged as much as in the covalent method, but its disadvantage is the low functionality of the final product. A new method to improve the functionality and water solubility of CNT/γ-Fe_2O_3NP hybrid nanomaterials without damaging their structure has been reported by using linear–dendritic copolymers.[126–128]

An example of non-covalent interactions between CNTs and linear–dendritic copolymers is hybrid nanostructure-based magnetic drug delivery systems (HNMDDSs), including carbon nanotubes, magnetic iron oxide nanoparticles, and linear–dendritic PAMAM–PEG–PAMAM copolymer.[32] PAMAM–PEG–PAMAM was employed to solubilize and functionalize carbon nanotubes through supramolecular interactions. The resulting Fe_3O_4-MWCNTs/PAMAM–PEG–PAMAM hybrid nanomaterials were utilized to encapsulate DOX (through π–π stacking) with a loading capacity of about 3.3% (Compound **12**). According to dynamic light scattering, the average diameter of DOX loaded Fe_3O_4-MWCNTs/PAMAM–PEG–PAMAM nanomaterials in water was 207 nm and aqueous solutions of hybrid nanomaterials were stable over several weeks at room temperature.[32]

Based on VSM curves, the saturation of magnetization of Fe_3O_4-MWCNTs/PAMAM–PEG–PAMAM and DOX/Fe_3O_4-MWCNTs/PAMAM–PEG–PAMAM were slightly smaller than that of Fe_3O_4-MWCNTs, but both had similar properties that were close to the superparamagnetic behavior, indicating that the magnetic properties of Fe_3O_4-MWCNTs did not lose by the non-covalent interaction of DOX and PAMAM–PEG–PAMAM on their surfaces. With this unique property, DOX/γ-Fe_3O_4-MWCNTs/PAMAM–PEG–PAMAM can be used as a promising material in many fields such as cancer diagnosis and therapy (Fig. 18).[32]

Using copper(I)-catalyzed azide–alkyne cycloaddition (CuAAC)-based click chemistry and "dendrone-first" method, Hed *et al.* synthesized a set of dendritic linear hybrid materials composed of linear PEG and dendritic aliphatic bis-MPA polyesters (G4).[129] To achieve amphiphilic structures, the bis-MPA layer also introduced hydrophobicity, using benzylidene-protected bis-MPA anhydride. Finally, the convergent coupling was carried out between monofunctional PEG5k-acetylene and azide functional dendrons azide-[G4]-$(Bz)_8$ by CuAAC click chemistry (Fig. 19).

Increased sizes of the micelles has been demonstrated after encapsulation of DOX into the amphiphilic PEG-[G4]-$(Bz)_8$ (diameters reported for the intensity average DLS data: 88 nm for PEG-[G4]-$(Bz)_8$, and 300 nm for DOX loaded PEG-[G4]-$(Bz)_8$

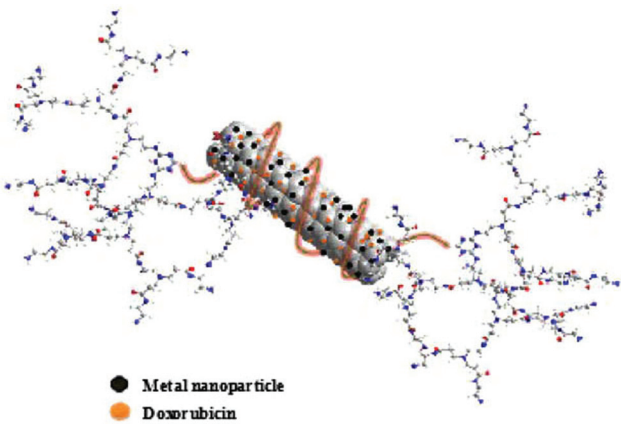

Fig. 18 The schematic representation of HNMDDSs including carbon nanotubes, magnetic iron oxide nanoparticles, and linear–dendritic PAMAM–PEG–PAMAM copolymer (Compound **12**). Reprinted with permission from ref. 32. Copyright (2013) Iranian Chemical society.

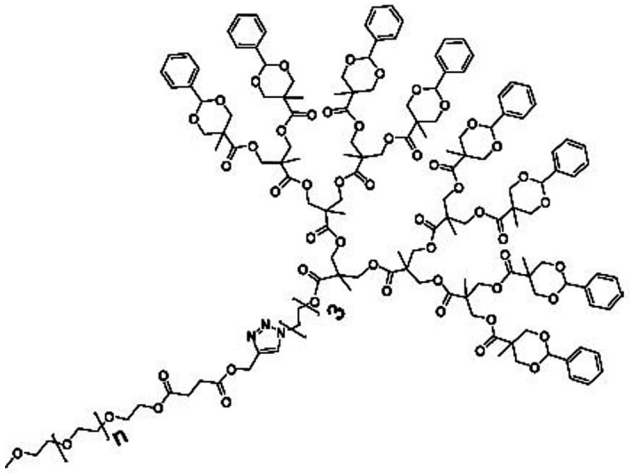

Fig. 19 Schematic structure of DL PEG-[G4]-$(Bz)_8$ (Compound **13**). Reprinted with permission from ref. 129. Copyright (2013) Wiley Periodicals, Inc.

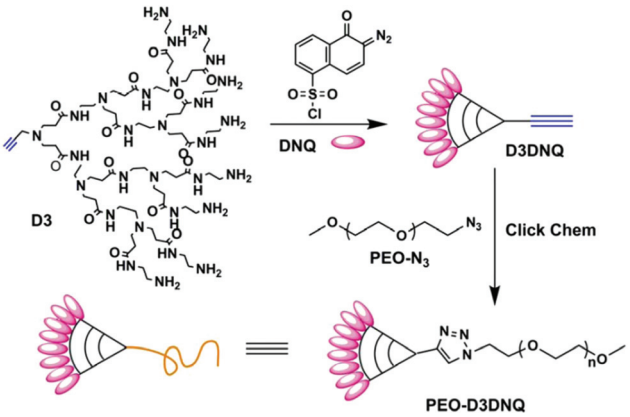

Fig. 20 Synthesis of linear–dendritic amphiphiles PEO–PAMAM (D3) DNQ by click chemistry (Compound **14**). Reprinted with permission from ref. 132. Copyright (2013) The Royal Society of Chemistry.

(Compound **13**)) indicating that the PEG length used for these materials is not sufficient to suppress aggregation. A loading efficiency of 51% has been found for DOX-loaded PEG-[G4]-$(Bz)_8$. Drug release studies exhibited a burst release during the first 12 h, under which at least 80% of the DOX was released, and around 90% of the content was released within 72 h. This phenomenon has been attributed to the low capacity of the hydrophobic domain to act as a diffusion barrier. It was suggested that increasing the PEG molecular weight should be noted to restrict aggregation and achieve better controlled release kinetics.[129]

Recently, the stimuli-responsive polymeric micelles and assemblies that are triggered by the light as external stimuli have been widely investigated for "on–off" drug delivery systems and "on-demand" nanomedicines, because of their assembly/disassembly switch. Compared with UV light, the near infrared (NIR) light between 750 and 1000 nm can penetrate up to a centimetre in depth of the tissues with less damage and scattering, which makes the NIR-sensitive nanomedicines promising as noninvasive and on-demand therapeutic candidates.[130,131]

Sun *et al.* have reported near-infrared (NIR) light-responsive linear–dendritic amphiphiles consisting of linear PEO and dendritic PAMAM (third-generation, D3) decorated with diazonaphthoquinone (DNQ) employed for NIR-triggered release of the anticancer drug doxorubicin (Compound **14**).[132] In their synthetic route, the reaction between the alkyne focal point PAMAM Dendron (D3: bearing eight primary amine groups) and DNQ sulfonyl chloride has been utilized to yield the clickable dendron D3DNQ (with eight DNQ groups), which has then been click conjugated with azide-terminated PEO (5 K) to produce the final linear–dendritic amphiphiles (Fig. 20). It has been demonstrated that under NIR (*e.g.* 808 nm) irradiation, the hydrophobic diazonaphthoquinone (DNQ) molecule transforms into the hydrophilic photoproduct 3-indenecarboxylic acid (pK_a = 4.5) *via* the Wolff rearrangement,[132] which would result in the disassembly and/or disruption of DNQ-containing micelles in PBS (*e.g.* pH 7.4).[133–135]

Besides having a common spherical morphology, PEO5K–D3DNQ micelles had a DLS-determined diameter of ~90 nm. In addition, the average size of the micelles slightly changed over 25 days in PBS (10 mM, pH 7.4) at 37 °C, suggesting that they were dynamically stable *in vitro*. A DOX-loading capacity of about 20 wt% has been determined for PEO5K–D3DNQ micelles. Determined by DLS, the DOX-loaded PEO5K–D3DNQ micelles increased from 90 nm (blank micelles) to 160 nm. These results also suggested that the hydrophobic DOX drug was indeed encapsulated into the hydrophobic core of the micelles. Similar to their blank counterparts, the DOX-loaded micelles presented a nearly spherical morphology. *In vitro* drug release studies demonstrated a NIR-triggered drug release profile for DOX-loaded PEO5K–D3DNQ micelles. The accelerated drug-release was exhibited after 10 min of 808 nm irradiation. It was found that 90% of DOX was released within about 210 h, compared with that without irradiation (about 420 h). Moreover, the apparent drug-release rate of DOX-loaded PEO5K–D3DNQ micelles accelerated nearly 8 times after 30 min of 808 nm irradiation compared to 10 min radiation, indicating NIR-responsive DOX release from the nanomedicines.[132]

5.1.2. *In vitro* evaluations. Based on *in vitro* cytotoxicity investigations evaluated on MDA-MB-231 breast cancer cells, IC_{50} of approximately 3 μg mL^{-1} and 0.8 μg mL^{-1} has been determined for DOX-loaded PEO-*block*-G3 polyester dendrimer of 2,2-bis(hydroxymethyl)propanoic acid units bearing cyclic acetals of 2,4,6-trimethoxybenzaldehyde micelles (Compound **6**) and free drug, respectively.[107] The somewhat lower toxicity of the micelle system may result from the gradual release of DOX within the cell and from differences in the released drug's cellular localization relative to the free drug. However, IC_{50} of 3 μg mL^{-1} for DOX-loaded micelles indicated the release of free and active DOX in the cells and indicated

encouraging therapeutic potential of the system. Drug localization in intracellular organelles has been proved for DOX-loaded micelles by Laser scanning confocal microscopy images, while free DOX was localized in the cell nucleus after 24 h (Fig. 21).[107] Drug localization in intracellular organelles has been proved for DOX loaded micelles by Laser scanning confocal microscopy images. As shown in Fig. 21a, MDAMB-231 cells exposed to free DOX show significant accumulation of DOX in the nucleus after 24 h. In contrast, cells exposed to DOX-loaded pH-sensitive micelles have a punctate fluorescence, which is concentrated in the cytoplasm after 24 h, as shown in Fig. 21b. These observations are important for several reasons. First, the absence of DOX fluorescence in the nucleus suggests that the micelles are stable in the presence of cells and serum-containing cell medium, as the rapid destabilization of the micelles in the extracellular environment and subsequent release of DOX outside the cell would be expected to result in an image similar to that observed for free DOX. In addition, the fluorescence in the cytoplasm suggests that the DOX-loaded micelles are indeed taken up by cells, and its punctate nature is consistent with the localization of the drug in subcellular organelles.[107] The increased stability of the pH-sensitive system at pH 7.4, and controlled release of therapeutics in mildly acidic physiological environments make the DOX-loaded PEO-*block*-G3 polyester (bis-MPA) dendrimer, bearing cyclic acetals of 2,4,6-trimethoxybenzaldehyde, promising for anticancer drug delivery. The somewhat lower toxicity of the micelle system was observed in comparison with free DOX. However, the potential for the selective accumulation of the micelle system in tumor tissue by the enhanced permeation and retention effect may enhance its overall therapeutic efficacy *in vivo* relative to free DOX.[107]

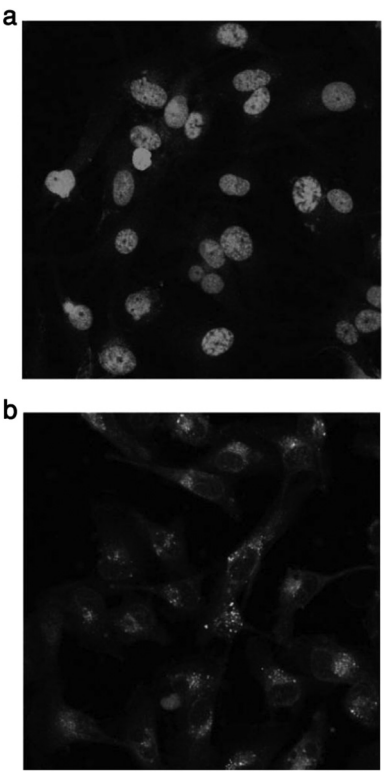

Fig. 21 Laser scanning confocal microscopy images of (a) DOX and (b) DOX-loaded pH-sensitive micelles (PEO-*block*-G3 polyester dendrimer of 2,2-bis(hydroxymethyl)propanoic acid units bearing cyclic acetals of 2,4,6-trimethoxybenzaldehyde) incubated with MDAMB-231 cells for 24 h. Reprinted with permission from ref. 107. Copyright (2005) American Chemical Society.

Cellular uptake evaluations on Raji lymphoma cells indicated that cells treated with DOX–PEG^{5k}–CA_8 (Compound **7**) and DOX–PEG^{2k}–CA_4 micelles showed MFI (median fluorescence intensity) 1.8-fold and 1.9-fold higher than free DOX, respectively, proving efficient internalizing of drug loaded micelles in the mentioned cells.[108] Similar *in vitro* cytotoxicities have been found for drug loaded micelles against T- and B-lymphoma cells as the free drug, exhibiting IC_{50} values of 20–50 ng ml^{-1} DOX. The higher value of the maximum tolerated dose (MTD) found for DOX–PEG^{2k}–CA_4 micelles (15 mg kg^{-1}) compared to free DOX (10 mg kg^{-1}) in non-tumor bearing BLAB/c mice has been attributed to the prolonged circulation time and the controlled drug release property.[108] In the case of DOX-loaded PAMAM-*b*-PDMAEMA-*b*-PNIPAM block copolymer-modified magnetic iron oxide nanoparticles (Compound **8**),[109] *in vitro* cytotoxicity studies revealed higher inhibition on Hela cells for free DOX (IC_{50} = 0.66 mg mL^{-1}), in comparison with the loaded DOX in the modified nanoparticles (IC_{50} = 1.49 mg mL^{-1}) at the same concentrations of DOX. This result has been explained by the slow release of the drug from the drug-loaded nanoparticles. At the same time, the result confirmed that the DOX-loaded nanoparticles were beneficial for decreasing the side effects of DOX on cells.[109] *In vitro* cytotoxicity of blank Fe_3O_4-dendritic–linear-brush-like copolymer PAMAM-*b*-PDMAEMA-*b*-PPEGMA nanoparticles on NIH 3T3 cells demonstrated cell viability of almost 100%.[110] Also an *in vitro* hemolysis assay with rabbit erythrocytes confirmed the high biocompatibility of the Fe_3O_4-modified nanoparticles. *In vitro* cytotoxicity investigations on HeLa cells showed IC_{50} values of 2.72 μg mL^{-1} and ~0.72 μg mL^{-1} for DOX loaded in the modified nanoparticles (Compound **9**) and free DOX, respectively. This result demonstrated that dendritic–linear-brush-like structures retard the toxic effect of DOX on the cells due to the slow release of the drug from the drug-loaded nanoparticles, indicating that the modified nanoparticles can delay drug release, in which a more compact brush structure would possibly result in a lower diffusion rate of drug molecules.[110] This system offers the preparation of water soluble and biocompatible modified Fe_3O_4 nanoparticles for the physical encapsulation of DOX. pH-sensitive and delayed drug release was reported, which can be beneficial to further facilitate potential biomedical applications of magnetic nanoparticles. Of course, biodistribution investigations and *in vivo* studies are necessary.[110] It has been shown that all drug loaded PEG–G*n*–PCL systems (Compound **10**) delivered an effective dose of DOX to the breast cancer cells, comparable to that of the free drug.[102] Determined by *in vitro* cytotoxicity

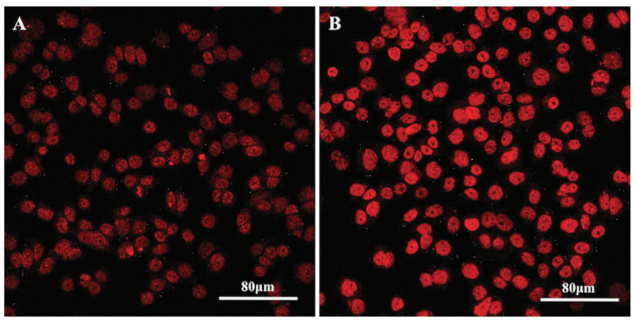

Fig. 22 Confocal microscopy of DOX in MDA-MB-468 cells. Cells were cultured in the medium with DOX-PEG5k-G1-PCL60 (containing 2 μg mL^{-1} DOX) for 4 h (A) and 24 h (B). Both images were captured with the same parameters on confocal microscopy and adjusted to the same contrast level and brightness. Reprinted with permission from ref. 102. Copyright (2011) Wiley Periodicals, Inc.

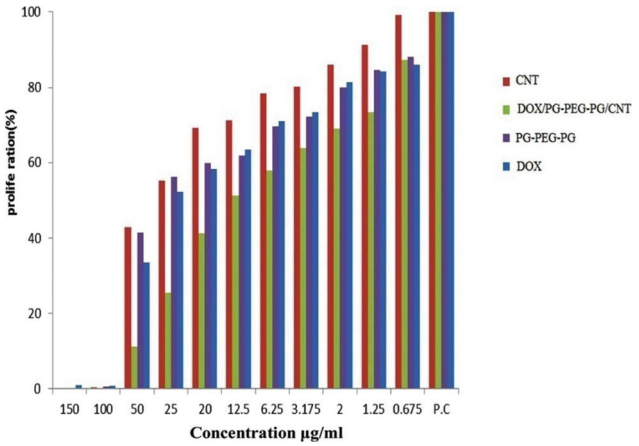

Fig. 23 The MTT assay results for opened MWCNT, PG–PEG–PG linear–dendritic copolymer, DOX/PG–PEG–PG/MWCNT drug delivery system and free DOX incubated with murine colon adenocarcinoma tumor C26 line. Reprinted with permission from ref. 125. Copyright (2012) The Royal Society of Chemistry.

studies, cell viability was decreased to 60–80% for MDA-MB-231 cells at 1 μg mL^{-1} concentration of loaded DOX, while at lower concentrations than 1 μg mL^{-1} the cell viability was 60% for MDA-MB-468 cells. The higher toxicity of free and loaded DOX on MDA-MB-468 cells contributes to the greater sensitivity of MDA-MB-468 cells to DOX. As proved by confocal imaging, the intensity of DOX fluorescence, released from DOX-loaded micelles, increased with time, and the fluorescence became more concentrated in the cell nuclei at the later time-point (Fig. 22).

According to flow cytometry investigations, in spite of the lower cellular uptake of DOX from the carrier-loaded DOX, the level of apoptosis of cells was comparable for free DOX and carrier-loaded DOX, confirming the PEG–G*n*–PCL system as a promising anticancer drug carrier.[102] Biocompatibility of empty micelles, good drug loading efficacy and efficient killing of the breast cancer cells, in spite of the lower cellular uptake, are significant advantages of the DOX loaded PEG–G*n*–PCL system. However, to reduce the release rates and potentially the observed aggregation of the drug-loaded micelles, a longer PEG component is most likely necessary. Pharmacokinetics and other *in vivo* investigations are also necessary.[102]

In vitro cytotoxicity assays on the murine colon adenocarcinoma tumor C26 line demonstrated higher anticancer effects for DOX/PG–PEG–PG/MWCNTs (Compound **11**), in comparison with free DOX in equal concentrations. With respect to this point that equal concentrations of free DOX and the DOX/PG–PEG–PG/MWCNT drug delivery system mean a much lower concentration of DOX in the latter case, the toxicity of DOX molecules loaded inside LLNs against cancer cells is much higher than those shown in Fig. 23.[125] Hydrophilic dendritic polymers not only raise the functionality, biocompatibility and water solubility of CNTs but also change their conformations from a linear to a packed state. Changes in the conformation of the CNTs upon noncovalent interactions with PG–PEG–PG ABA type linear–dendritic copolymer led to liposome-like nanocapsules (LLNs). Since one of the proposed reasons for the carcinogenicity of carbon nanotubes is their length and rigid structure, flexible liposome-like nanocapsules prepared by this strategy could be safer and far from the asbestos-like physicochemical properties of CNTs and therefore their potential health hazards. Avoiding these health hazards, it is possible to develop CNTs for biomedical applications.[125]

By *in vitro* cytotoxicity tests conducted on mouse tissue connective fibroblast adhesive cell line (L929), it was found that in low concentrations the toxicity of DOX-loaded Fe_3O_4-MWCNTs/PAMAM–PEG–PAMAM hybrid nanomaterials (Compound **12**) was much higher than other systems and even free DOX, indicating the critical role of the carbon nanotube in transferring hybrid nanomaterial drug delivery systems, and therefore loaded DOX, from the cell membrane.[32] Since PEG improves the processability, water solubility and long blood circulation of CNTs through non-covalent interactions, supramolecular interactions between linear–dendritic PAMAM–PEG–PAMAM copolymers and CNTs lead to water soluble and high functional hybrid nanomaterials. Additionally, high loading capacity, higher toxicity compared to free DOX, and good superparamagnetic behavior make DOX/γ-Fe_3O_4-MWCNTs/PAMAM–PEG–PAMAM a promising material for anticancer drug delivery.[32]

By *in vitro* cytotoxicity assays in the breast cancer cells (MDA-MB-231), the PEG-*block*-bis-MPA polyesters (G4)-$(Bz)_8$ have been found to be nontoxic.[94] Also a reduced cell viability of 55% has been determined for DOX–PEG-(G4)-$(Bz)_8$ (Compound **13**) containing 10 μg ml^{-1} DOX, in comparison with 73% cell viability obtained at the same concentration of free DOX, showing that DOX-loaded micelles delivered the therapeutic effect with high efficacy.[129] In summary, DOX encapsulated PEG-*block*-bis-MPA polyesters (G4)-$(Bz)_8$ showed some advantages, such as nontoxicity of the linear–dendritic carrier and the higher cytotoxic effect against MDA-MB-231 cancer

cells in comparison with free DOX. However, higher molecular weights of PEG are necessary to provide sufficient stealth or steric repulsion during DOX loading and to avoid aggregation. Additionally, strategies for achieving better controlled release kinetics should be noticed. Pharmacokinetics studies and *in vivo* tests can help this system develop for cancer therapy.[129]

By flow cytometry profiles it has been proved that the DOX-loaded PEO5K–PAMAM (D3)–diazonaphthoquinone (DNQ) micelles (Compound **14**) could quickly enter into HeLa cells in a time-independent manner compared with free DOX (Fig. 24).[132] This phenomenon has been attributed to the nanomedicines of <200 nm internalization by HeLa cells in an endocytosis process, compared with a diffusion process for the cellular uptake of free DOX.[135] *In vitro* cytotoxicity studies evaluated in HeLa cells at 6 μg mL^{-1} DOX dosage showed the cell viability of ~65% and ~18% for the DOX-loaded PEO5K–D3DNQ micelles and free DOX, respectively. This lower cytotoxicity of DOX-loaded micelles corresponds to their sustained drug-release behaviour. Interestingly, the cell viability for the DOX-loaded micelles decreased to ~35% after 30 min of 808 nm irradiation, exhibiting a NIR-triggered cytotoxicity.[132] Collectively, DOX-loaded PEO5K–PAMAM (D3)–diazonaphthoquinone (DNQ) micelles demonstrated some interesting advantages, including the stability of drug-free micelles in PBS at 37 °C and pH = 7.4, tuned release of DOX by NIR light irradiation, quick entrance into HeLa cells compared to free DOX, DOX release inside the cells, and then killing the cells in a NIR-triggered manner. Disrupting the micelles by 808 nm NIR irradiation may be a challenge for this system, however biodistribution studies and *in vivo* tests can develop this promising anticancer system.[132]

5.1.3. *In vivo* evaluations. Biodistribution studies showed 2.0-fold and 2.2-fold higher drug uptake for DOX–PEG^{5k}–CA_8 and DOX–PEG^{2k}–CA_4 micelles compared to that for free DOX in the tumor tissue of treated mice.[108] This enhanced accumulation corresponded to the prolonged circulation and the EPR effect in linear–dendritic micelle formulations (Compound 7). Compared to free DOX, significantly reduced drug distribution in the heart has been achieved by both DOX–PEG–CA formulations. However, relatively higher uptake in the liver and spleen has been exhibited for DOX-micellar systems caused by nonspecific elimination of micellar NPs *via* the reticulo-endothelial system (RES), such as macrophage in the liver and spleen. Better inhibition of tumor growth was shown for DOX–PEG^{2k}–CA_4 micelles because of their longer retention time and slower drug release rate. By day 28 post-injection, the relative tumor volume (RTV) of 7.7 and 6.8 was achieved for Raji lymphoma bearing mice treated with DOX–PEG^{5k}–CA_8 and DOX–PEG^{2k}–CA_4, respectively. This value was 9.9 for free DOX treated mice.[108] Besides stability under physiological conditions, DOX encapsulated PEG^{mk}–CA_n micelles offered some significant advantages in comparison to free DOX, such as higher *in vitro* cellular uptake, higher maximum tolerated dose, increased retention time in the blood, higher uptake in tumor tissue *in vivo*, higher antitumor efficacy *in vivo*, and reduced drug distribution in the heart. These all make PEG^{mk}–CA_n micelles attractive for cancer therapy (Table 3).[108]

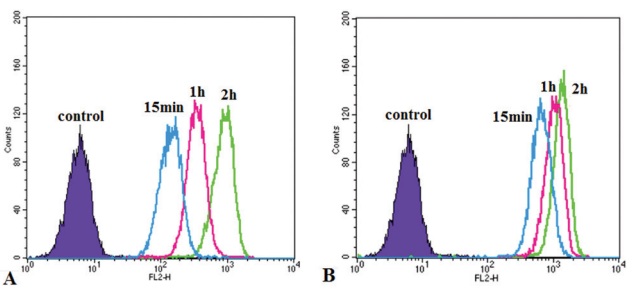

Fig. 24 Flow cytometry histogram profiles of HeLa cells incubated with free DOX (A) and DOX-loaded micelles of PEO5K–PAMAM (D3) DNQ (B) for different time intervals. Reprinted with permission from ref. 132. Copyright (2013) The Royal Society of Chemistry.

5.2. Doxorubicin-conjugated linear–dendritic block copolymers

5.2.1. Physicochemical properties. Padilla De Jesús *et al.*[136] have designed a soluble carrier for DOX consisting of a 3-arm poly(ethylene oxide) (PEO) and three [G-2] dendritic polyester with 2,2-bis(hydroxymethyl)propanoic acid monomer units (Compound **15**), providing the multivalency necessary for drug attachment (Fig. 25). DOX has been covalently linked to the linear–dendritic structure *via* an acid-labile hydrazone, which can remain stable under physiological conditions, and can be cleaved in the vicinity of a tumor prior to being internalized by the cancer cell because of the more acidic environment around the tumor tissue.[136]

Drug release studies indicated that a 100% release would be achieved after 10 min, 3 h, 26.5 h, and 10 days for pH 2.5, 4.5, 5.5, and 6.5, respectively. This confirms the suitability of the hydrazone linkage for a pH-dependent release that is compatible with conditions found in tumors.[136]

Gillies and Fréchet also reported interesting polyester dendrimer–PEO bow-tie hybrids consisting of 2,2-bis(hydroxymethyl) propionic acid based polyester dendrimers and PEO in which PEO was linked to the dendritic scaffold *via* carbamate bonds.[137,138]

Later, the [G-3]-$(PEO_{5k})_8$-[G-4]-$(OH)_{16}$ bow-tie structure (molecular mass ~45 kDa) was utilized to provide the dendrimer–DOX conjugates by coupling hydrazide linkers to the hydroxyl groups of the bow tie (Compound **16**), followed by hydrazone formation with DOX hydrochloride and subsequent chromatographic separation from free DOX. DOX loading was consistently found to be 8–10 wt% for different batches.[139,140] Notably, the bow-tie DOX conjugate was readily dissolved in water at DOX concentrations as high as 6 mg ml^{-1} (~60 mg ml^{-1} polymer), indicating that the PEO arms of the bow-tie dendrimer can shield the hydrophobic drug moieties at the core of the molecule, perhaps in a structure similar to that of a unimolecular micelle. A volume average hydrodynamic diameter of 8 nm for the conjugate was determined using dynamic light scattering, indicating that intermolecular

Table 3 Doxorubicin-encapsulated linear–dendritic block copolymers

Carrier name	Size (nm)	*In vitro* activity	*In vivo* activity	Advantages	Ref.
PEO–Poly(bis-MPA)–2,4,6-trimethoxybenzaldehyde	35 nm 200–400[a] (cmc = 40 mg L^{-1})	Lower cytotoxicity on MDA-MB-231 breast cancer cells for DOX-loaded carrier (IC_{50} = 3 μg mL^{-1}) compared to free DOX (IC_{50} = 0.8 μg mL^{-1})	n[b]	Stability at pH 7.4, controlled release of therapeutics in mildly acidic physiological environments, potential for the selective accumulation of the micelle system in tumor tissue by EPR effect	107
PEG^{5k}–CA_8	12–17	Similar *in vitro* cytotoxicities (IC_{50} = 20–50 ng ml^{-1}) of drug loaded micelles and free drug against T- and B-lymphoma cells	Higher antitumor activity compared to free drug on Raji lymphoma bearing mice	Stability under physiological conditions, higher *in vitro* cellular uptake, higher maximum tolerated dose, increased retention time in the blood, higher uptake in tumor tissue *in vivo*, higher antitumor efficacy *in vivo*	108
Fe_3O_4-PAMAM-*b*-PDMAEMA-*b*-PNIPAM cross linked	32	Lower cytotoxicity (IC_{50} = 1.49 mg mL^{-1}) on Hela cells compared to free DOX (IC_{50} = 0.66 mg mL^{-1})	n[b]	Stabilized magnetic iron oxide nanoparticles, thermosensitive release mode, decrease the side effects of DOX on cells	109
Fe_3O_4-PAMAM-*b*-PDMAEMA-*b*-PPEGMA	30	Less cytotoxicity on Hela cells (IC_{50} of 2.72 μg mL^{-1}) compared to free DOX (IC_{50} of 0.72 μg mL^{-1})	n[b]	Water soluble and biocompatible modified Fe_3O_4 nanoparticles as carrier, pH-sensitive and delayed drug release	110
PEG–G2 (bis-MPA)–PCL	865	Greater sensitivity of MDA-MB-468 cells to DOX released from micelles, comparable level of apoptosis of cells for free DOX and carrier-loaded DOX	n[b]	Biocompatibility of carrier micelles, good drug loading efficacy and efficient killing of the breast cancer	102
PG–PEG–PG/MWCNTs	350	Higher anticancer effects in comparison with free DOX on murine colon adenocarcinoma tumor C26 line	n[b]	Functionality, biocompatibility and water solubility of CNTs, higher anticancer effects compared to free DOX	125
Fe_3O_4-MWCNTs/PAMAM–PEG–PAMAM	207	Higher cytotoxicity than free DOX on mouse tissue connective fibroblast adhesive cell line (L929)	n[b]	Water solubility and high functionality of hybrid nanomaterials. high loading capacity, higher toxicity compared to free DOX, and good superparamagnetic behavior	32
PEG-poly(bis-MPA)-$(Bz)_8$	300	Higher cytotoxicity effects on MDA-MB-231 breast cancer cells compared to free DOX	n[b]	Nontoxicity of linear–dendritic carrier and higher cytotoxic effect in comparison with free DOX *in vitro*	129
PEO–PAMAM–DNQ	160 (cac = 0.0206 mg mL^{-1})	Lower cytotoxicity of DOX-loaded micelles in comparison with free drug in HeLa cells	n[b]	Stability in physiological conditions, tuned release of DOX by NIR light irradiation, quick entrance into HeLa cells compared to free DOX, DOX releasing inside the cells	132

[a] A small fraction of aggregates. [b] n: not reported.

aggregation did not occur.[139] The release of the drug from the DOX-conjugated bow-tie polymer at pH 5.0 and 7.4 buffers at 37 °C was monitored chromatographically. At pH 5, the drug was released from the dendrimer rapidly, and the concentration of free doxorubicin in solution increased steadily with $t_{1/2}$ = 6 ± 1 h, reaching 100% release within 48 h. Only a small amount (<10%) of the same compound was released after 48 h at pH 7.4 (Fig. 26).[139,140]

Huang *et al.*[141] have reported the liver-targeting potential of polymeric prodrug of doxorubicin bearing Galactose conjugated linear dendritic block copolymers. Galactose as the targeting ligand has been conjugated to linear PEG, and DOX has been coupled to the PAMAM dendritic section *via* an acid-labile hydrazone linker to produce the Gal-PEG-*b*-PAMAM-DOX_n drug delivery system (Compound **17**) (Fig. 27). It has been demonstrated that the galactosylated drug carrier could reach hepatocytes *via* receptor-mediated active targeting, due to the high affinity of asialo-glycoprotein (ASGP) receptor to galactosyl residues.[142]

Determined by ^{1}HNMR, the molar ratio of DOX to copolymer was 5.5 : 1, which was lower than the theoretical value (8 : 1), because of the steric hindrance that leads to the lower drug loading.

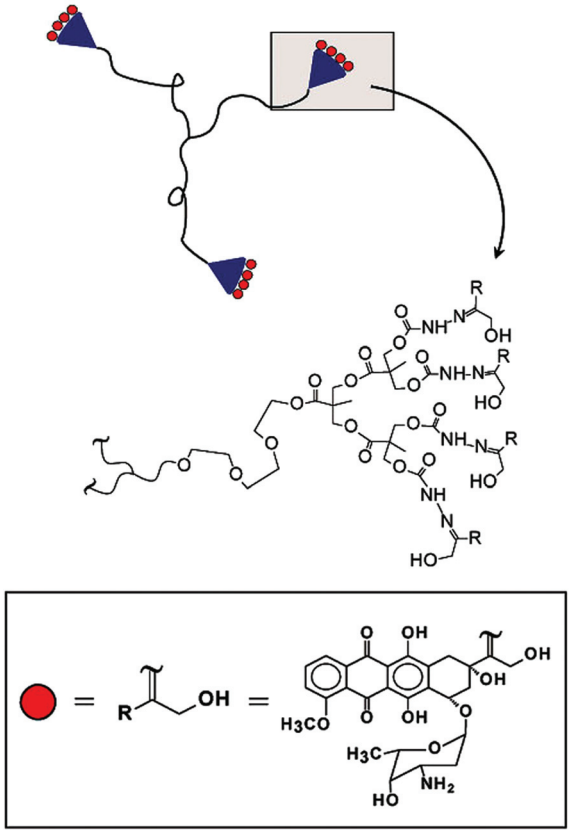

Fig. 25 Polymer drug conjugate consisting of 3-arm PEO-polyester dendrimer and doxorubicin using a hydrazone covalent bond as a linker (Compound **15**). Reprinted with permission from ref. 136. Copyright (2002) American Chemical Society.

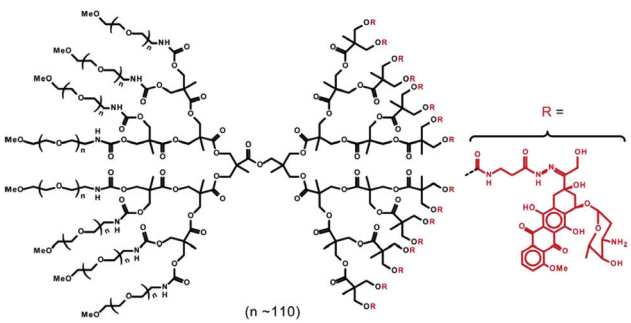

Fig. 26 [G-3]-$(PEO_{5k})_8$-[G-4]-$(OH)_{16}$-doxorubicin conjugates (Compound **16**). Reprinted with permission from ref. 140. Copyright (2006) American Chemical Society.

The acid-sensitive degradation of the hydrazone linker between DOX and the Gal-PEG-*b*-PAMAM carrier caused a pH-triggered drug release profile. It has been determined that 14 and 32% of DOX was released at pH of 8.0 and 7.4, respectively, in 30 h. On the other hand, at pH = 5.6, 97% of DOX release was observed after 15 h. This indicates the stable circulation of the polymeric drug in the bloodstream (pH = 7.4),

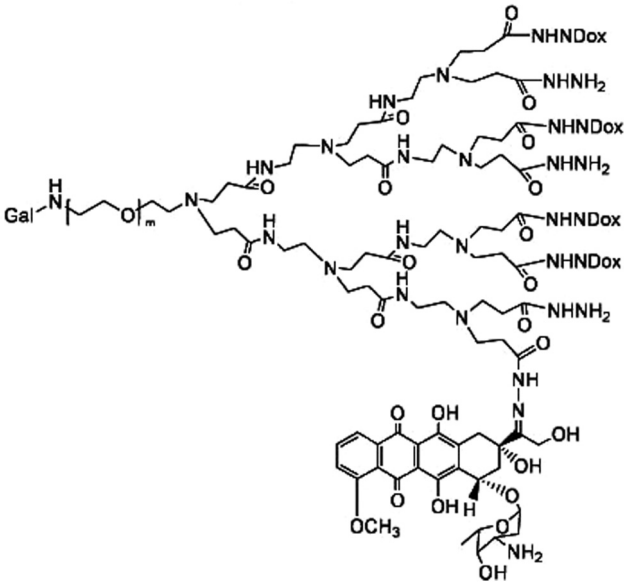

Fig. 27 Gal-PEG-*b*-PAMAM-DOX_n prodrug (Compound **17**). Reprinted with permission from ref. 141. Copyright (2010) Society of Chemical Industry.

and triggered drug release in endosomes and lysosomes (pH = 5.6–6.5) of cancer cells.[141]

In a recent study, She *et al.* have demonstrated the use of mPEGylated peptide Dendron–DOX conjugate (Compound **18**) as a pH-stimulated drug delivery system for breast tumor therapy.[143] In their study, the tail of the L-lysine dendron has been functionalized with two alkynyl groups. Then, mPEG (2 kDa) with an azido group at one end has been covalently linked to the peptide dendron by Cu^I-catalyzed azide–alkyne cycloaddition (CuAAC). DOX has been conjugated to the dendron through a pH-sensitive hydrazone bond, resulting in a compact nanoparticle, *via* self-assembly governed by Dendron–DOX itself, as shown in Fig. 28.

UV-vis spectrophotometry indicated the presence of 2 DOX molecules for each mPEGylated peptide Dendron-doxorubicin (14 wt%). The mPEGylated peptide Dendron–DOX conjugate

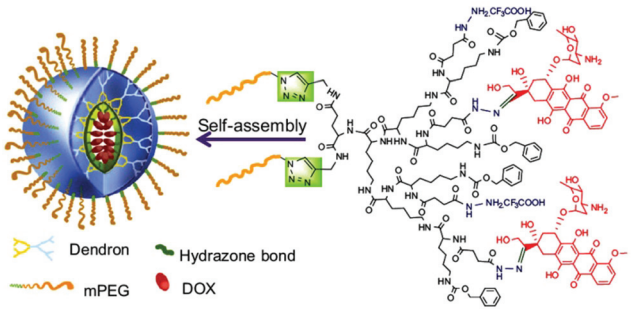

Fig. 28 Structures of mPEGylated peptide dendron, and the illustration of the dendron-DOX conjugate based nanoparticle (Compound **18**). Reprinted with permission from ref. 143. Copyright (2012) Elsevier Ltd.

aggregated to a nanosized particle in water (pH = 7.4), displaying average hydrodynamic sizes around 220 nm.[143] Generally, producing drive force segments is needed to introduce to the PEGylation and functionalization of the dendron for self-assembly.[144] For this designed dendron, the self-assembly behavior was mediated by the mPEGylated peptide Dendron–DOX itself. The primary driving force responsible for the self-assembly behavior is the minimization of the interfacial energy, governed by the balance between the hydrophilic interaction of the linear mPEG and the hydrophobic interaction of the Dendron–DOX block.[144] Secondly, the driving forces governing the self-assembly of the prepared mPEGylated peptide Dendron–DOX, such as π–π stacking, dipole interactions, H-bonding and the pre-organized branched architecture of the dendritic block, should also be considered, since the DOX is composed of multiple domains of different chemical compositions, *e.g.*, hydrophobic, aliphatic and aromatic.[145] At predetermined time points, higher release amounts (80%) at pH 5, in comparison with release amounts at pH 7.4 (20%), revealed the pH-sensitive mode of drug release for mPEGylated peptide Dendron-doxorubicin nanoparticles. This accelerated release has been attributed to the cleavage of hydrazone linkers at lower pH values.[143]

In another study She *et al.* have also used Cu^{I}-catalyzed azide–alkyne cycloaddition (CuAAC) click chemistry to covalently attaching the L-lysine peptide dendron to heparin, resulting in water-soluble dendronized heparin.[146] Then, DOX has been conjugated to the surface of the dendron through a pH-sensitive hydrazone bond, resulting in a compact nanoparticle *via* self-assembly in water (pH = 7.4), displaying average hydrodynamic sizes around 90 nm and PDI of 0.140 (DOX content 9 wt%) (Compound **19**) (Fig. 29).

Self-assembly behavior was mediated by the dendronized heparin-DOX conjugate itself. As mentioned before,[146] the primary driving force responsible for the self-assembly behavior is the minimization of the interfacial energy governed by the balance between the hydrophilic interaction of the linear polymer and the hydrophobic interaction of the dendronized heparin-DOX block. Secondly, the driving forces governing the self-assembly of prepared dendronized heparin-DOX, such as π–π stacking, dipole interactions, H-bonding and the preorganized branched architecture should also be considered, since the DOX is composed of multiple domains of different chemical compositions, *e.g.*, hydrophobic, aliphatic and aromatic. Based on drug release profiles, showing 20% DOX release at pH 7.4 after 56 h incubation, it was concluded that the dendronized heparin-DOX system was stable in the circulation system (pH 7.4). In contrast, cleavage of the acid-labile hydrazone bonds of DOX-conjugated nanoparticles accelerated the release of drug at pH 5.0 (>80%), indicating the ability of nanoparticles to release the DOX in the acidic endosomes and/or lysosomes with pH ranging from 4.0–6.0.[146]

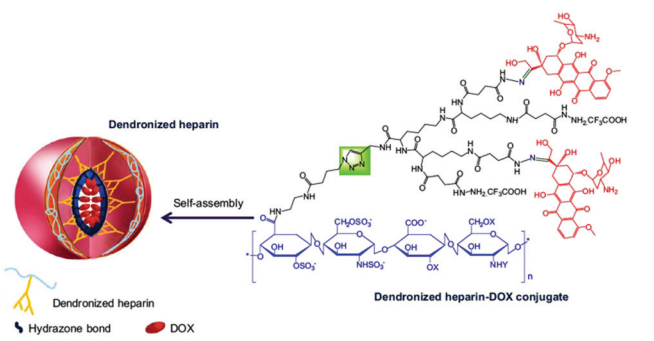

Fig. 29 Illustration of a dendronized heparin-DOX conjugate based nanoparticle (Compound **19**). Reprinted with permission from ref. 146. Copyright (2012) Elsevier Ltd.

In a research work reported by Zhang *et al.*,[147] a co-delivery strategy for anti-cancer treatment has been employed, utilizing 10-hydroxycamptothecin (HCPT) encapsulated MPEG-*b*-PAMAM-DOX amphiphilic linear–dendritic prodrug. In the preparation route, MPEG-*b*-PAMAM G2.5 has been hydrazinolysized to MPEG-*b*-PAMAM G3X by hydrazine hydrate. Then, DOX as the hydrophobic part of the amphiphilic copolymer has been conjugated to PAMAM *via* an acid-labile hydrazone linkage by reacting with the keto groups of DOX. UV absorbance studies gave a DOX content of 52.9 wt% for MPEG2000-*b*-PAMAM-DOX and 31.0 wt% for MPEG5000-*b*-PAMAM-DOX. HCPT loading into DOX-conjugated nanoparticles has been carried out by a solvent displacement method with pH adjusted to 6.5, in which the hydrazone bond was stable while HCPT could maintain its lactone form.[148,149] HCPT content has been determined to be 19.2 and 21.6 wt% for MPEG2000-*b*-PAMAM-DOX and MPEG5000-*b*-PAMAM-DOX (Compound **20**) nanoparticles, respectively. The nanoparticles were of uniform size and spherical shape. The radii of nanoparticles formed by MPEG2000-*b*-PAMAM-DOX and MPEG5000-*b*-PAMAM-DOX were about 50 and 60 nm, respectively. As a hydrophobic molecule, HCPT was wrapped in the core of the nanoparticles, which were formed by the self-assembly of MPEG-*b*-PAMAM-DOX prodrugs. The radii of the HCPT loaded nanoparticles formed by MPEG2000-*b*-PAMAM-DOX and MPEG5000-*b*-PAMAM-DOX were 88 nm and 122 nm, respectively. The increase in size of the nanoparticles after HCPT loading indicates the successful incorporation of HCPT in the hydrophobic core.[147] A pH-dependent release mode has been demonstrated for both drugs released from HCPT loaded MPEG-*b*-PAMAM-DOX. There has been no initial DOX burst release from DOX-conjugated nanoparticles because of the chemical combination of DOX to the copolymer. The release of DOX molecules was negligible at pH 7.4, indicating the stability of a hydrazone bond at this pH. Lowering the pH to 5.5 and 4.5 caused an increase in DOX release of about 30% and 60% in 48 h, respectively. Also faster release of HCPT has been demonstrated in pH 4.5 compared to pH 5.5, attributed to the faster cleavage of DOX and faster disassembly of the self-assembled nanoparticles at lower pH (Fig. 30).[147]

Another pH-responsive prodrug formulation based on linear–dendritic MPEG-*b*-PAMAM has been recently reported by Zhang *et al.*[78] Firstly, linear–dendritic MPEG-*b*-PAMAM was

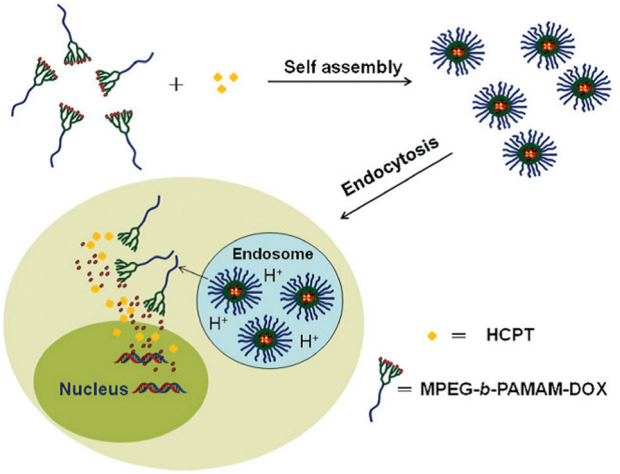

Fig. 30 Illustration of MPEG-*b*-PAMAM block copolymer conjugated with DOX and its self-assembled HCPT loaded nanoparticles for the pH-responsive intracellular release (Compound **20**). Reprinted with permission from ref. 147. Copyright (2013) Wiley-VCH Verlag GmbH & Co. KGaA, Weinheim.

modified with lipoic acid (LA) and then doxorubicin was conjugated to the modified structure by an acid-labile hydrazone bond, resulting in amphiphilic structures that could be self-assembled to the nanosized micelles (Compound **21**) (Fig. 31). Due to the significant glutathione (GSH) concentration difference between the extracellular milieu (2–20 mM) and the cytoplasm (2–10 mM), the reduction responsive cross-linked micelles are attracting more and more attention. Therefore, the obtained MPEG-*b*-PAMAM-LA/DOX micelles have been cross-linked by disulfide bonding through introducing 10 mol%

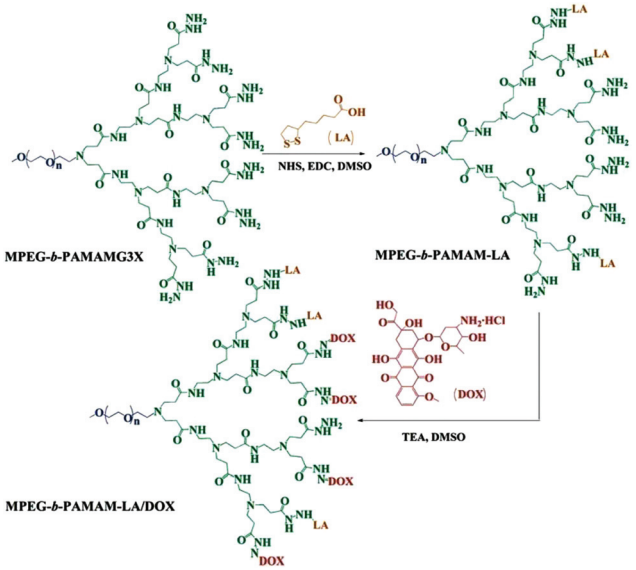

Fig. 31 Synthesis pathway of MPEG-*b*-PAMAM-LA/DOX (Compound **21**). Reprinted with permission from ref. 78. Copyright (2014) the Royal Society of Chemistry.

DTT relative to the lipoyl units in borate buffer (pH 8.5). With the MPEG segment as the hydrophilic moiety and LA and DOX as the hydrophobic moieties, the amphiphilic prodrug self-assembled into spherically shaped micelles. The particle size of the cross-linked prodrug particles was ~140 nm. The stability of the cross-linked MPEG-*b*-PAMAM-LA/DOX NPs was evaluated in 20 mM PB solution for different time intervals. After standing for 4 days, 8 days and 16 days, the particle size of the NPs only slightly changed from the original 144 nm to 161 nm after 16 days of incubation, also suggesting the good stability of the cross-linked NPs. The change in the particle size in response to 10 mM GSH was monitored over time in 20 mM PB solution, to investigate whether cross-linked NPs can be de-cross-linked in a reductive environment. It was shown that the addition of GSH led to a dramatic increase and wide distribution of the particle size, implying the cleavage of disulfide bonds by reduced GSH. The DOX loading content of cross-linked MPEG-*b*-PAMAM-LA/DOX micelles has been determined to be 25.6 wt%. The high drug loading content has been ascribed to the multiple amine groups on the PAMAM backbone.[78]

A pH-dependent release for DOX from core-cross-linked MPEG-*b*-PAMAM-LA/DOX nanoparticles has been demonstrated. At pH 7.4, only about 6% of the loaded DOX was released in 72 h, while about 35% of DOX was released at pH 5.5. These results indicate that the hydrazone bond is stable at the physiological pH of 7.4, but would be cleaved at the endosomal pH of 5.5. Also reduction-sensitive release behavior has been found for cross-linked MPEG-*b*-PAMAM-LA/DOX. At the same pH value, higher DOX release has been achieved with a higher GSH concentration. This has been attributed to the cleavage of the disulfide bonds by GSH, leading to de-cross-linking of the nanoparticles and the rapid release of DOX.[78]

5.2.2. *In vitro* evaluations. Based on *in vitro* cytotoxicity of the drug–polymer conjugate, evaluated on three cell lines B16F10, MDA-MB-435, and MDA-MB-231, the free drug was more potent than the DOX-conjugated 3-arm (PEO) star–three [G2] polyester dendritic block with bis-MPA units (Compound **15**); 6-fold in the B16F10 cells, 50-fold in the MDA-MB-231, and 9-fold in the MDA-MB-435 cells. Cell uptake of the polymer–drug conjugate (monitored *via* fluorescence confocal microscopy) proved the cell uptake of the conjugate by endocytosis, through fluorescence observation in the cytosol. On the other hand, both the cytoplasm and the nuclei were highly fluorescent after exposure to free doxorubicin.[136]

In spite of substantial intratumoral concentrations of polymer and drug, attempts at chemotherapy utilizing the doxorubicin functionalized 3-armed (PEO) star–three [G2] polyester bis-MPA dendrimer in murine tumor models (B16F10) were largely unsuccessful.[140] This was attributed to hydrazone carboxylate linkages, which were utilized in this system to attach a doxorubicin topolymeric structure (Fig. 25). Lee *et al.*[140] investigated the hydrolysis kinetics of hydrazone carboxylate linked doxorubicin and proposed intramolecular nucleophilic attack of the C-14 hydroxyl of doxorubicin on the carbonyl group of the hydrazone carboxylate linker (Fig. 32).

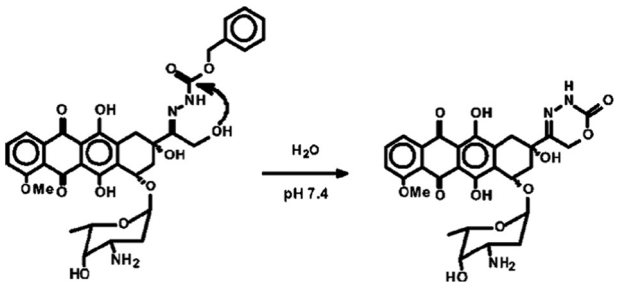

Fig. 32 Intramolecular cyclization in a hydrazone carboxylate linked doxorubicin system. Reprinted with permission from ref. 140. Copyright (2006) American Chemical Society.

The proposed intramolecular cyclization reaction involving the doxorubicin C-14 hydroxyl and the carboxylate-substituted hydrazone rationalizes the seemingly anomalous hydrolysis kinetics seen for hydrazone carboxylate linked doxorubicin, and provides a possible explanation for the poor antitumor activity exhibited by polymer–doxorubicin conjugates utilizing this specific type of linkage.[140]

In vitro cytotoxicity studies of polyester dendrimer–PEO bow-tie hybrids, with a range of MWs 20–100 KDa as well as low and high degrees of branching, on MDA-MB-231 cancer cells, showed no significant toxicity up to 10 mg mL^{-1}, the highest concentration evaluated, with cell viabilities exceeding 85% relative to controls at all concentrations.[138] The cytotoxic activity of DOX-conjugated bow-tie polyester dendrimer–PEO (Compound **16**) on C-26 cells was found to be considerably less than that for the free DOX on an equimolar basis (IC_{50}, DOX = 0.08 ± 0.02 μg ml^{-1}; IC_{50}, hydrazone bow-tie DOX = 1.4 ± 0.2 μg ml^{-1}). This result was attributed to the slower rate of cellular uptake for the dendrimers when compared with the free drug and to the gradual release of free drug from the polymers, due to hydrolysis of the linkers and the polyester dendrimer backbone.[139]

By *in vitro* cytotoxicity studies against Bel-7402 cells, the cell viability has been determined as 11%, 60% and 50% in cells treated with free DOX, non-targeting PEG-*b*-PAMAM-DOX_m, and targeting Gal-PEG-*b*-PAMAM-DOX_n (Compound **17**), respectively, at DOX concentration of 40 μg mL^{-1}.[141] Compared to free DOX, decreased cytotoxicity of the polymeric prodrugs has been attributed to their gradual drug release profiles. Also higher cytotoxicity of galactose conjugated prodrug in comparison with the non-targeting one has been explained by the receptor-mediated higher cell uptake of Gal-PEG-*b*-PAMAM-DOX_n. ASGP receptors in Bel-7402 and galactosyl residue in the prodrug are responsible for the increased intracellular drug concentration.[141]

Lower *in vitro* cytotoxicity, evaluated on mouse breast cancer cell line (4T1), was seen for mPEGylated peptide Dendron–DOX conjugate nanoparticles (Compound **18**) (IC_{50} = 151 ng mL^{-1}) compared with free DOX (IC_{50} = 25.9 ng mL^{-1}).[143] This has been explained by the amphipathic properties of DOX and the higher ability of small molecules to cross the cell membrane. Cell viability of 95% for non-drug conjugated nanoparticles indicated that the mPEGylated peptide dendron was nontoxic and DOX released from the DOX-conjugated nanoparticle in the acidic environment of endosomes was responsible for cytotoxicity.[143]

Dendronized heparin–DOX (Compound **19**) showed IC_{50} of 300 ng mL^{-1} against the mouse breast cancer cell line (4T1), approximately 11-fold of free DOX with IC_{50} of 27 ng mL^{-1}.[146] This lower cytotoxicity of dendronized heparin–DOX was due to the amphipathic properties of free DOX and its ability to easily cross the cell membrane. More than 90% of 4T1 cells have still been alive after the treatment with drug-free dendronized heparin, showing non-cytotoxicity of the dendronized heparin nanoparticle. So it is clear that the cytotoxicity of the nanoparticle with the drug would not be due to the dendronized heparin block, but the drug DOX, proving the release of DOX from the nanoparticle in the acidic environment of endosomes.[146]

Flow cytometric analysis demonstrated that HCPT loaded MPEG-*b*-PAMAM-DOX nanoparticles (Compound **20**) could be effectively taken up by MCF-7 cells.[147] After 10 h incubation with MCF-7 cells, about 80% HCPT has been internalized by MCF-7 cells from both HCPT loaded MPEG-*b*-PAMAM-DOX nanoparticles, much higher than the internalization content of free HCPT, indicating that DOX conjugated nanoparticles increased the solubility of free HCPT and delivered HCPT efficiently to MCF-7 cells. Higher *in vitro* cytotoxicity has been determined for HCPT loaded MPEG-*b*-PAMAM-DOX nanoparticles compared to free DOX and free HCPT in MCF-7 and HepG2 cell lines. Moreover, the HCPT loaded MPEG-*b*-PAMAM-DOX exhibited better cytotoxicities than the physical mixtures of MPEG-*b*-PAMAM-DOX and HCPT.[147] This confirmed that the DOX conjugated prodrugs could effectively encapsulate HCPT and subsequently release it in the cell, leading to enhanced drug activity and better *in vitro* antitumor effect for the co-delivery system. Enhanced cell apoptosis has been demonstrated for the co-delivery system. Evaluated by flow cytometry in MCF-7 cells, HCPT loaded MPEG2000-*b*-PAMAM-DOX and MPEG5000-*b*-PAMAM-DOX caused 13.3 and 13.4% late apoptotic cells and 81.7 and 81.3% normal cells, respectively. Both HCPT loaded nanoparticles resulted in more apoptotic cells than the blank MPEG-*b*-PAMAM-DOX nanoparticles (4.7% late apoptotic cells and 89.2% normal cells for MPEG2000-*b*-PAMAM-DOX, 4.9% late apoptotic cells and 88.6% normal cells for MPEG5000-*b*-PAMAM-DOX) and free HCPT (6.1% late apoptotic cells and 88.8% normal cells) with a concentration of 1 μg mL^{-1}.[147] The advantages of co-delivery of two anticancer drugs (DOX and HCPT), high drug loading content, pH-dependent drug release, higher cellular uptake compared to free HCPT, and higher *in vitro* cytotoxicity compared to free HCPT and free DOX, make HCPT loaded MPEG-*b*-PAMAM-DOX nanoparticles attractive for drug delivery. More investigations, especially pharmacokinetic studies and *in vivo* antitumor efficacy, can help this system develop for cancer therapy applications.[147]

By comparison of the CLSM results in HeLa cells, after 3 and 16 h incubation with cross-linked MPEG-*b*-PAMAM-LA/

DOX micelles (Compound **21**) (Fig. 33), it has been determined that the effective cellular uptake of the nanoparticles and efficient DOX release had taken place after a longer period of incubation.[78] In fact, after cellular uptake, the acidic environment and the relatively higher GSH concentration in both endosomes and the cytoplasmic matrix triggered the cleavage of the hydrazone bonds and disulfide bonds of cross-linked MPEG-*b*-PAMAM-LA/DOX, causing the slow release of DOX. Also the weaker DOX fluorescence observed for the cells treated with cross-linked MPEG-*b*-PAMAM-LA/DOX nanoparticles in comparison with that of free DOX has been explained by slower internalization and the self-quenching effect of DOX in the nanoparticles.[78]

By *in vitro* cytotoxicity studies it has been found that cross-linked nanoparticles have been more effective after a longer period of incubation. The IC_{50} value of the cross-linked nanoparticles decreased from 18.9 μg mL^{-1} to 2.5 μg mL^{-1} for HeLa cells, with increasing incubation time from 24 to 72 h. The decrease of IC_{50} has also been shown for A549 cells from more than 20 μg mL^{-1} to 6.3 μg mL^{-1} under the same incubation conditions. Enhanced inhibition of the cell proliferation has been demonstrated for cross-linked nanoparticles incubated with GSH pretreated HeLa and A549 cells. This higher cytotoxicity has been attributed to the cleavage of disulfide cross-linking by GSH and faster release of DOX.[78] Because of the high drug loading content, pH and reduction-sensitive DOX release behavior (regarding the acidic environment and the relatively higher GSH concentration in both endosomes and the cytoplasmic matrix), higher *in vitro* cytotoxic effect with the increase in incubation time, the core cross-linked MPEG-*b*-PAMAM-LA/DOX NPs showed bright prospects for anti-cancer therapy. However, investigations of *in vivo* efficacy, tolerable doses, and biodistribution studies are needed to complete the cross-linked MPEG-*b*-PAMAM-LA/DOX system.[78]

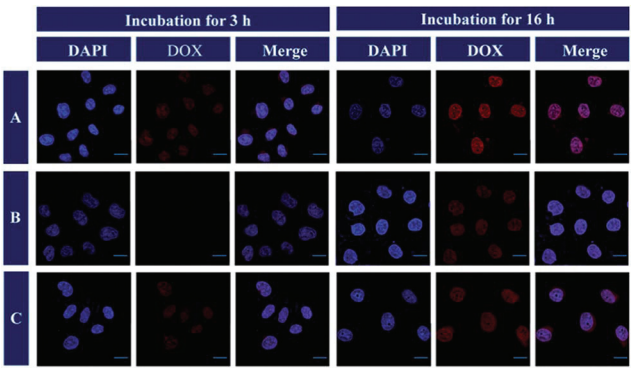

Fig. 33 Confocal laser scanning microscopy of HeLa cells (1.0×10^5 cells per well) after incubation with (A) free DOX, (B) cross-linked MPEG-*b*-PAMAM-LA/DOXNPs (the cells were not pretreated) and (C) cross-linked MPEG-*b*-PAMAM-LA/DOXNPs (the cells were pretreated with 10 mM GSH) for 3 h and 16 h at 37 °C (DOX equivalent concentration: 0.5 μg mL^{-1} for all formulations). The scale bars represent 20 μm. Reprinted with permission from ref. 78. Copyright (2014) The Royal Society of Chemistry.

5.2.3. *In vivo* evaluation. Biodistribution Studies of the DOX-conjugated 3-arm (PEO) star–three [G2] polyester dendritic blocks with bis-MPA units (Compound **15**) performed on CD-1 female mice demonstrated no significant accumulation in any vital organ, including the liver, heart, and lungs (Fig. 34).[136] This is a preferred distribution pattern compared with the free drug, which partitions into a variety of organs such as the liver and heart. Also the polymer–DOX conjugate exhibited a longer circulatory half-life (72 min), as compared to the half-life of the free drug (8 min), demonstrating the influence of the 3-arm PEO–polyester dendritic system in the pharmacokinetics and the distribution of the drug.[136]

According to the reported results, it is concluded that DOX-conjugated 3-arm (PEO) star–three [G2] polyester dendritic block with bis-MPA units (Compound **16**) shows advantages including biocompatibility of the carrier, pH-dependent release, which is compatible with conditions found in tumors, no significant accumulation in vital organs, and a longer circulatory half-life than the free drug. But its lower cytotoxicity in comparison with the free drug arises from hydrazone carboxylate linkages, which lead to the intramolecular cyclization reaction and subsequent poor antitumor activity.[136,140]

According to biodistribution studies of bow-tie polyester dendrimer–PEO[138] on CD-1 female mice at a dose of approximately 40 mg kg^{-1}, no specific organ accumulation was observed for these bow-tie polymers, with a significant portion of the dose (35–46%) found in the carcass after 48 h. Less than 4% of the dose was found in the urine for each of these polymers, indicating that their effective sizes are above the threshold for renal filtration. After 48 h, 6–16% of the dose was excreted in the feces. Therefore, the primary route for elimination of these molecules was *via* intestinal excretion, believed to be the primary route by which large molecules that cannot be excreted through the kidney can escape the body.[138]

Biodistribution experiments of DOX-conjugated bow-tie polyester dendrimer–PEO performed in BALB/c mice bearing

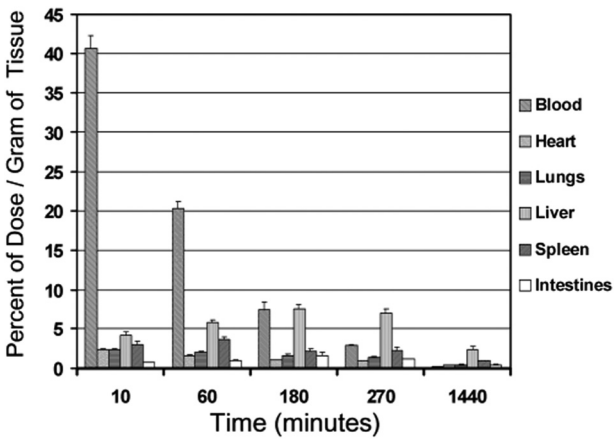

Fig. 34 Biodistribution of 3-arm PEO–polyester dendrimer/DOX conjugate. Reprinted with permission from ref. 136. Copyright (2002) American Chemical Society.

s.c. C-26 tumors showed an elimination half-life of 16 ± 1 h for the hydrazone-linked bow-tie DOX conjugate.[139] In previous studies, a blood elimination half-life of 31 ± 2 h was observed for a drug-free bow-tie PEO–polyester dendrimer.[138] The long circulation half-life of the conjugates contrasts with the short half-life of the free drug, which is <10 min. The tumor concentrations of DOX measured 48 h after administration of either DOX-conjugated bow-tie polyester dendrimer–PEO (20 mg kg^{-1} DOX) or free DOX (6 mg kg^{-1}) were approximately nine times higher for mice treated with DOX-conjugated bow-tie polyester dendrimer–PEO by percentage injected dose per gram of tumor. The enhanced tumor uptake of the dendrimer bound drug is a reflection of its longer circulation half-life, which exploits passive targeting by means of the EPR effect.[139] Animal serum analysis determined a significant increase in the serum creatine kinase, lactic dehydrogenase, and serum transaminase values in animals that received the 40 and 60 mg kg^{-1} doses of DOX-conjugated bow-tie polyester dendrimer–PEO, compared with animals that received saline or the 20 mg kg^{-1} dose, indicating the presence of damage to muscle tissue and to the liver at these dose levels. So it was concluded that the maximum tolerated single dose is between 20 and 40 mg kg^{-1} DOX equivalents or between ~200 and 500 mg kg^{-1} DOX-conjugated bow-tie polyester dendrimer–PEO in healthy BALB/c mice.[139] To determine the optimal dosing schedule for antitumor therapy, BALB/c mice bearing s.c. C-26 tumors were administered a single dose of DOX-conjugated bow-tie polyester dendrimer–PEO (10 mg kg^{-1} DOX) on various days after tumor inoculation. Five different groups of mice were treated with a single i.v. injection of polymer on day 2, 4, 8, 12, or 16 after their tumors were implanted. The dosing schedule experiment showed that mice treated on day 8 responded the most favorably to treatment, a result that was statistically different from the mice treated on days 4, 12, and 16. A dose–response experiment was performed by monitoring the tumor growth and survival of BALB/c mice treated with a single dose of DOX-conjugated bow-tie polyester dendrimer–PEO, 8 days after implantation of a s.c. C-26 tumor. Remarkably, at the highest dose administered (20 mg kg^{-1} DOX equivalents), complete tumor regression was observed, resulting in 100% survival of mice in this treatment group over the 60-day experiment. In contrast, none of the free DOX (6 mg kg^{-1}) administered mice were still alive on day 25. The activity of the DOX-conjugated bow-tie polyester dendrimer–PEO *in vivo*, despite its reduced *in vitro* toxicity relative to free DOX, is convincing evidence of the dendrimer's ability to modulate the pharmacokinetic profiles of attached anticancer drugs.[139]

Collectively, the DOX conjugated [G-3]-$(PEO_{5k})_8$-[G-4]-$(OH)_{16}$ bow-tie structure showed some significant advantages, for example water solubility even at DOX concentrations of 6 mg mL^{-1}, pH-dependent release, no significant toxicity of the carrier, long circulation half-life of the conjugates, and enhanced tumor uptake. In spite of reduced *in vitro* toxicity, the DOX-conjugated bow-tie polyester dendrimer–PEO showed higher antitumor activity *in vivo*. These results introduce DOX-conjugated bow-tie polyester dendrimer–PEO as a promising anticancer system.[138,139]

The liver-targeting potential of galactose conjugated PEG-*b*-PAMAM-DOX_n prodrug (Compound **17**) has been confirmed using contrast-enhanced MRI carried out on Female ICR mice.[141] Comparison of signal enhancement in liver for Gal-PEG-*b*-PAMAM-Gd and mPEG-*b*-PAMAM-Gd complexes showed the maximum liver ENH of both agents after 6 h of injection. Then, a rapid decrease of ENH has been observed for mPEG-*b*-PAMAM-Gd. In contrast, Gal-PEG-*b*-PAMAM-Gd showed a gradual decrease in ENH due to the high affinity of the ASGP receptor at the liver surface to galactosyl residues in Gal-PEG-*b*-PAMAM-Gd, proving its active liver-targeting potential. *In vivo* antitumor evaluations indicated inhibition of tumor growth after Gal-PEG-*b*-PAMAM-DOX_n administration (Fig. 35). Gal-PEG-*b*-PAMAM-DOX_n showed better *in vivo* antitumor efficacy than free DOX, suggesting its great potential as a polymeric antitumor prodrug. In mice treated with free DOX, an increase in tumor size was found after ten days. These data offer Gal-PEG-*b*-PAMAM-DOX_n as a useful targeting anticancer agent.[141] Properties reported for Gal-PEG-*b*-PAMAM-DOX_n, including stability in pH 7.4, triggered drug release in pH 5.6–6.5 and sensitivity of the drug vehicle to lower pH of tumor cells, receptor mediated liver targeting, higher *in vivo* antitumor efficacy in spite of lower *in vitro* activity compared to the free drug make this system interesting for anticancer investigations. Additionally, biodistribution and pharmacokinetics studies can develop this system.[141]

Determined by *in vivo* experiments, the tumor weights in mice treated with mPEGylated L-lysine Dendron–DOX conjugate nanoparticle (Compound **18**) were obviously lower compared with the tumors from the free drug DOX treatment group.[143] The high antitumor activity of the DOX-conjugated nanoparticle has been attributed to the neutral charged surface, longer blood circulation, potential higher accumulation in tumors *via* the EPR effect and the accelerated release of DOX from endosomes. Also a smaller shift in body weight

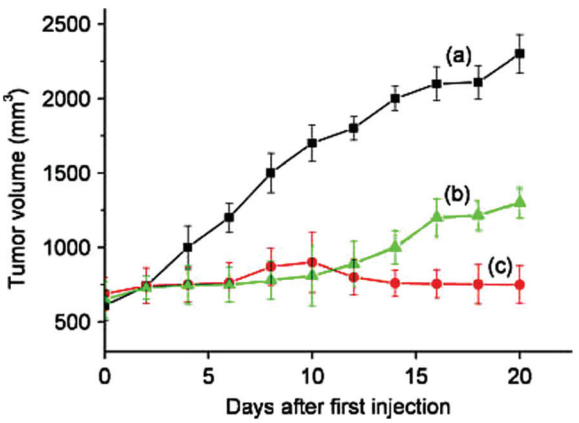

Fig. 35 *In vivo* antitumor efficacy of (a) PBS, (b) DOX and (c) Gal-PEG-*b*-PAMAM-DOX_n (mean ± SD, n = 8). Reprinted with permission from ref. 141. Copyright (2010) Society of Chemical Industry.

shift has been observed for the group administrated DOX-conjugated nanoparticles compared to the free DOX treated ones, indicating better drug tolerance. As shown in Fig. 36, histologically, for mice administrated free drug DOX, heart toxicity induced by DOX was observed due to necrosis (grade 1), acute infiltration of inflammatory cells at the epicardium and cardiac myocyte under the epicardium. In contrast, the mice administrated with drug-free peptide dendron and peptide Dendron–DOX conjugate based nanoparticles were normal and no visible difference was observed compared to the control.[143]

According to *in vivo* experiments, higher antitumor activity has been obtained for DOX-conjugated mPEGylated L-lysine Dendron nanoparticles.[143] Lower tumor weights have been observed in mice administrated with DOX-conjugated nanoparticles in comparison with the tumors from the free drug DOX treatment group. This result is caused by the neutral charged surface, longer blood circulation, potential higher accumulation in the tumor *via* the EPR effect and the accelerated release of DOX from endosomes.[150] Also less body weight loss has been observed for the group administrated DOX-conjugated nanoparticle compared to the free DOX treated ones, indicating better drug tolerability. Histological analysis on normal mice demonstrated the heart toxicity for mice administrated free drug DOX.[143] The toxicity has been attributed to the necrosis (grade 1) with acute infiltration of inflammatory cells at the epicardium and cardiac myocyte under the epicardium (Fig. 36). In contrast, no toxicity has been observed in mice administrated with drug-free nanoparticles and peptide Dendron–DOX nanoparticles. The low molecular weight of the mPEG-peptide dendron and its biodegradability, high accumulation of DOX-conjugated nanoparticles in tumor tissue but lower accumulation in normal tissue *via* EPR effects, and the

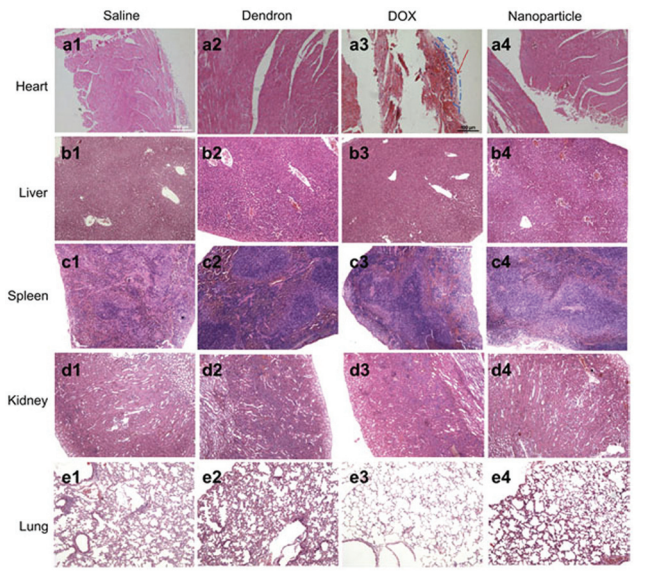

Fig. 36 Histological analysis for different organs of normal mice administrated control (Saline), drug-free peptide dendron (Dendron), free drug DOX (DOX) and mPEGylated peptide dendron-DOX conjugate based nanoparticle (Nanoparticle) (heart: ×200, other tissues: ×100). The analysis showed that the free drug DOX resulted in heart toxicity due to the observed necrosis (grade 1) with infiltration of acute inflammatory cells in the epicardium and cardiac myocyte under the epicardium (a3). In contrast, organs of mice administrated saline, drug-free mPEGylated peptide dendron and mPEGylated peptide dendron–DOX conjugate based nanoparticle did not exhibit signs of toxicity. Reprinted with permission from ref. 143. Copyright (2012) Elsevier Ltd.

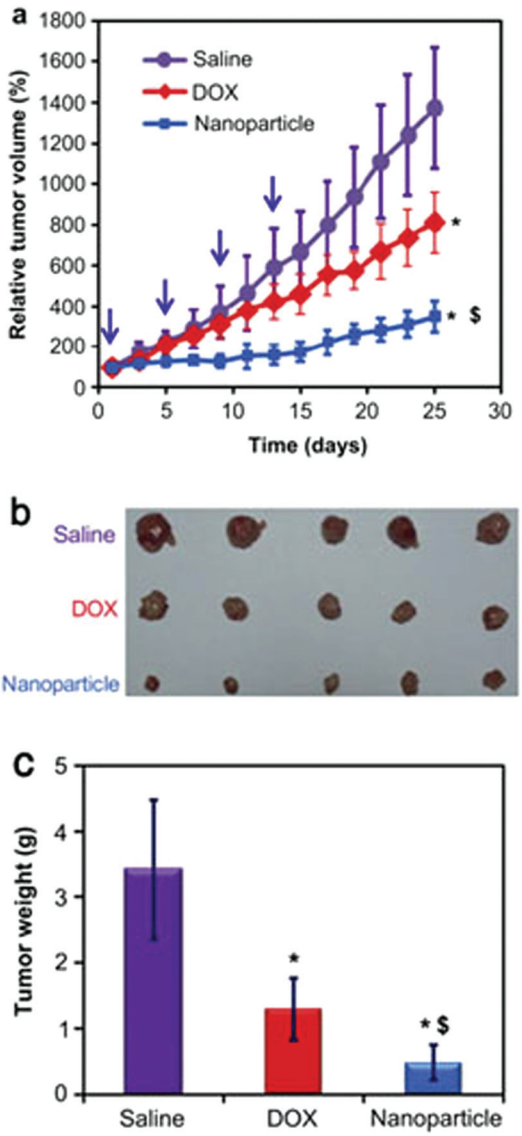

Fig. 37 *In vivo* tumor growth inhibition by nanoparticles. Comparison of the tumor inhibition effect of the dendronized heparin–DOX conjugate based nanoparticle with drug (Nanoparticle) *versus* free drug DOX (DOX) and saline in the breast tumor model (n = 5). The nanoparticle demonstrated significant tumor inhibition (*p < 0.001, compared to Saline; $^{\$}p$ < 0.001, compared to the free drug DOX) (a). At the end of this experiment, tumor tissues were collected from each sacrificed animal after 25 days treatment, photographed (b) and weighed (*p < 0.01, compared to saline; $^{\$}p$ < 0.05, compared to the free drug DOX) (c). Reprinted with permission from ref. 146. Copyright (2012) Elsevier Ltd.

sensitivity of the drug vehicle to the lower pH of tumor cells promote clearance from the organism and thereby enhance the *in vivo* biocompatibility.[143] The overall structural design of mPEGylated L-lysine Dendron–DOX conjugate and its properties, such as nontoxicity of the vehicle, pH-sensitive drug release, enhanced tumor inhibition *in vivo* in spite of lower *in vitro* cytotoxicity in comparison with free DOX, better drug tolerability, enhanced *in vivo* biocompatibility, and reduced side effects make this prodrug a safe and efficient anticancer drug delivery system.[143] From *in vivo* studies on mice bearing the 4T1 breast tumor model, She *et al.* showed that the tumors treated with dendronized heparin–DOX nanoparticle (Compound **19**) exhibited a significantly stronger response than the tumors treated with saline only or free drug DOX.[146] In particular, after 25 days of therapy, a statistically significant improvement was obtained for mice treated with nanoparticles, compared to the control and DOX treated groups, seen by the much smaller tumor volume, as shown in the tumor growth curves (Fig. 37a, $p < 0.001$). The tumor sizes from mice administrated dendronized heparin–DOX conjugate based nanoparticles were obviously smaller than those from the free drug DOX treatment group and controls. (Fig. 37b), which was proportional to the observed relative tumor volume results (Fig. 37a). Simultaneously, the tumor weights in mice treated with nanoparticles were noticeably lower compared with the tumors from the free drug DOX treatment group ($p < 0.05$) and control ($p < 0.001$) (Fig. 37c).[146] The high antitumor activity of the nanoparticle was attributed to the negatively charged surface, longer blood circulation, potential higher accumulation in the tumor *via* the EPR effect and the accelerated release of DOX from the endosomes.[151] Regarding the advantages of the non-toxicity of the carrier, pH-sensitive drug release, and higher antitumor activity *in vivo*, dendronized heparin–DOX may therefore be a potential nanoscale drug delivery vehicle for breast cancer therapy. Certainly, pharmacokinetics studies make this system more helpful for cancer therapy purposes.[146]

Although these DOX-conjugated linear–dendritic polymer systems demonstrated low *in vitro* cytotoxicities in comparison with the free drug,[136,141,143,146] the larger accumulation in tumor tissue *in vivo* could counter balance the low *in vitro* toxicity. High molecular weight polymers preferentially accumulate in solid tumor tissue due to a combination of the leaky character of tumor blood vessels formed during neo-angiogenesis

Table 4 Doxorubicin-conjugated linear–dendritic block copolymers

Carrier name	Size (nm)	*In vitro* activity	*In vivo* activity	Advantages	Ref.
3-Arm PEO-(bis-MPA) dendrimer	n[a]	Less cytotoxicity compared to the free drug on B16F10, MDA-MB-435, and MDA-MB-231 cell line	No significant accumulation in any vital organ, including the liver, heart, and lungs evaluated on CD-1 female mice	Biocompatibility of carrier, pH-dependent release, no significant accumulation in vital organs, and longer circulatory half-life than the free drug	136
	8	Lower cytotoxic activity (IC_{50} = 1.4 ± 0.2 μg ml^{-1}) compared to free DOX (IC_{50} = 0.08 ± 0.02 μg ml^{-1}) on MDA-MB-231 cancer cells	Higher antitumor effects compared to free DOX on BALB/c mice bearing s.c. C-26 tumors	Water solubility even at DOX concentrations of 6 mg mL^{-1}, pH-dependent release, no significant toxicity of carrier, long circulation half-life of conjugates, and enhanced tumor uptake and higher antitumor activity *in vivo*	138, 139
Gal-PEG-*b*-PAMAM	n[a]	Reduced cytotoxic activity compared to free drug against Bel-7402 cells	Better *in vivo* antitumor efficacy than free DOX on female ICR mice	Stability in pH 7.4, triggered drug release in acidic pH, receptor mediated liver targeting, higher *in vivo* antitumor efficacy	141
mPEGylated poly(L-lysine) dendron	220	Lower cytotoxicity (IC_{50} = 151 ng mL^{-1}) compared with free DOX (IC_{50} = 25.9 ng mL^{-1}) on mouse breast cancer cell line (4T1)	Higher antitumor activity in comparison with free DOX	Nontoxicity of vehicle, pH-sensitive drug release, enhanced tumor inhibition *in vivo*, reduced side effects	143
Heparin-poly(L-lysine)	90	Lower cytotoxicity (IC_{50} of 300 ng mL^{-1}) compared with free DOX (IC_{50} of 27 ng mL^{-1}) against mouse breast cancer cell line (4T1)	Higher antitumor activity on mice bearing 4T1 breast tumor model compare to free drug	Non-toxicity of carrier, pH-sensitive drug release, and higher antitumor activity *in vivo*	146
MPEG-*b*-PAMAM	60	Higher *in vitro* cytotoxicity for nanoparticles compared to free DOX and free HCPT in MCF-7 and HepG2 cell lines	n[a]	Co-delivery of two anticancer drugs (DOX and HCPT), high drug loading content, pH-dependent drug release, higher cellular uptake compared to free HCPT, higher *in vitro* cytotoxicity	147
MPEG-*b*-PAMAM-LA	140 (CMC = 13.30 μg mL^{-1})	Being more effective after a longer period of incubation on HeLa cells and A549 cells	n[a]	High drug loading content, pH and reduction-sensitive DOX release behavior, higher *in vitro* cytotoxic effect with the elongation of the incubating time	78

[a] n: not reported.

and to limited lymphatic drainage. The combination of these two factors is responsible for the enhanced permeability and retention effect (EPR) observed with tumor tissue, which leads to a passive targeting of drugs to tumors. In addition, the larger hydrodynamic volume of polymers contributes to the increased plasma half-life of the drug–polymer conjugates, increasing the probability of accumulation of the therapeutic agent in the tumor tissue by means of the EPR effect. Drugs have also been conjugated to polymers to improve their water solubility properties, to decrease their toxicity due to local accumulation of the drug prior to reaching the target tissue, and to protect them from possible enzymatic degradation or hydrolysis. So these DOX-conjugated linear–dendritic systems are promising because they allow slow elution of doxorubicin into the tumor after administration, since the nanoparticle has much longer blood circulation time and higher accumulation in tumor tissue due to the EPR effect (Table 4).[136,141,143,146]

6. Cisplatin

Cisplatin (cis-dichlorodiammine platinum(II)) (CDDP) is one of the most potent anticancer agents available today and is widely used in the treatment of many malignancies, including testicular, ovarian, bladder, head and neck, small cell and non-small cell lung cancers because of its potent activity in cross-linking DNA upon entering the cells. It preferentially binds to the N7 atoms of guanine bases in DNA double-helix strands, thereby preventing the strands from uncoiling and separating. This prohibits the division of the cells and ultimately results in cellular apoptosis.[152–156] However, its clinical use is limited due to its significant toxic side effects, such as acute nephrotoxicity and chronic neurotoxicity. CDDP shows a rapid distribution over the whole body and high glomerular clearance within 15 min after intravenous injection. A total of 90% of the cisplatin is bound to plasma proteins in the blood and, thus, does not enter the cells; leading to lower therapeutic efficacy. Therefore, much effort has been devoted to developing a drug delivery system aimed at increasing the blood circulation period and accumulation in solid tumors.[157–159]

6.1. Cisplatin-conjugated linear–dendritic block copolymers

6.1.1. Physicochemical properties. Using linear–dendritic polycitric acid–polyethylene glycol–polycitric acid (PCA–PEG–PCA) copolymers (M_w ~2000 Da), Haririan *et al.* prepared conjugates of PCA–PEG–PCA–CDDP (Compound **22**) in an aqueous medium.[160] Drug loading of about 6 wt% platinum was achieved for the conjugates. By *in vitro* platinum release tests, it was found that the release rate in the acidic pH (5.4) was slightly greater and faster than the neutral pH (7.4), attributed to the catalytic effect of the acidic conditions on the ease of displacement of water molecules with chloride or carboxylate ions inside the cisplatin cavity.[160] It was observed that when the conjugates were formed from the dendrimers, an increase in the particle size was seen in the conjugates (141 nm), as contrasted with the dendrimers (85 nm). This phenomenon can result from the crosslinking of the dendrimers with cisplatin, which intercalates between two of the dendrimer molecules.[160]

In our previous study, we used polycitric acid–polyethylene glycol–polycitric acid (PCA–PEG–PCA) linear–dendritic copolymers to solubilize and functionalize multi-walled carbon nanotubes (MWCNTs) by noncovalent interactions.[161] We showed that a potential anticancer drug cisplatin can be conjugated to the carboxyl functional groups of the dendritic blocks of PCA–PEG–PCA linear–dendritic copolymers and then the prodrugs interacted with the MWCNTs noncovalently, leading to formation of MWCNT/PCA–PEG–PCA–CDDP hybrid nanomaterial-based drug delivery systems (HNDDSs) (Compound **23**). Based on our previous investigations, the cavity of the polymer-functionalized carbon nanotubes is able to host nanoparticles of up to 15 nm in diameter, due to their high solubility and opened cavity. Since the size of an individual PCA–PEG–PCA linear–dendritic copolymer is less than 10 nm,[162,163] they can transfer conjugated CDDP molecules to the cavity of MWCNT/PCA–PEG–PCA hybrid nanomaterials (Fig. 37b). As shown in the TEM images, the synthesized hybrid nanomaterials "transfer" CDDP molecules, not only by conjugation to the linear–dendritic copolymers on their surface but also in their cavity. Drug release studies at 37 °C and pH 7.4 showed a slow release rate, with cumulative release percentage around 40% after 168 h (Fig. 38).[161]

In another study, we reported the conjugation of CDDP with PCA–PEG–PCA/CNT/γ-Fe_2O_3NP hybrid nanomaterials (Compound **23**).[164] Deposition of γ-Fe_2O_3 nanoparticles onto the surface of CNTs led to magnetic CNT/γ-Fe_2O_3NP, and then non-covalent interactions between PCA–PEG–PCA and CNT/γ-Fe_2O_3NP resulted in PCA–PEG–PCA/CNT/γ-Fe_2O_3NP hybrid nanomaterials with improved water solubility, functionality, and potential application to target anticancer drugs. According to TGA analysis, the weight percent of PCA–PEG–PCA linear–dendritic copolymers absorbed onto the surface of CNTs is around 45%. While the molecular weight of CNTs is much more than that of linear–dendritic copolymers, it can be found that a large number of linear–dendritic copolymers are attached onto the surface of a CNT.[164] Based on TGA thermal

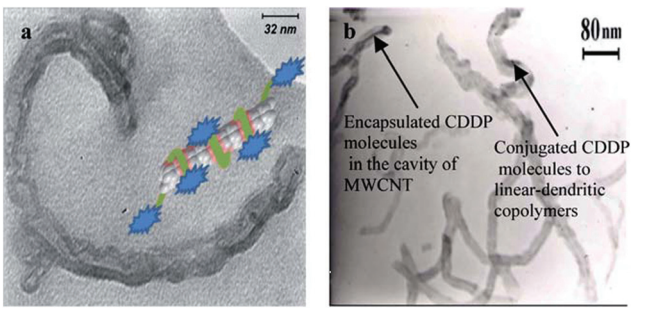

Fig. 38 TEM images of (a) MWCNT/PCA–PEG–PCA and (b) MWCNT/PCA–PEG–PCA–CDDP. Reprinted with permission from ref. 161. Copyright (2011) The Royal Society of Chemistry.

analysis, the weight percent of CDDP in the CDDP/PCA–PEG–PCA/CNT/γ-Fe_2O_3NP drug delivery system is around 7%. DLS experiments show that the average diameter of CNT/γ-Fe_2O_3NP hybrid nanomaterials in water changes from 977 to 190 nm upon interaction with PCA–PEG–PCA linear–dendritic copolymers, confirming that the conformation of CNTs converts from the linear to the globular form. This is of great importance, because the shape and size of nanomaterial- and especially CNT-based drug delivery systems affect their toxicity significantly, such that the carcinogenicity of CNTs is sometimes ascribed to their length, and has been compared to asbestos fibers. It should be kept in mind that another reason for the decrease in size of CNT/γ-Fe_2O_3NP hybrid nanomaterials could be the separation of their bundles toward individual objects, due to the noncovalent interactions with linear–dendritic copolymers. The CDDP/PCA–PEG–PCA/CNT/γ-Fe_2O_3NP drug delivery system in water is 11 nm bigger than the PCA–PEG–PCA/CNT/γ-Fe_2O_3NP hybrid nanomaterial, proving that the interaction of the CDDP/PCA–PEG–PCA anticancer prodrug with the surface of CNT/γ-Fe_2O_3NP is weaker than that of the PCA–PEG–PCA linear–dendritic copolymer. This result confirms that CDDP molecules are conjugated with the carboxyl functional groups of PCA blocks and limit interactions between linear–dendritic copolymers and hydroxyl functional groups of iron oxide nanoparticles anchored onto the surface of CNTs.[164] VSM curves showed that the saturation of magnetization of PCA–PEG–PCA/CNT/γ-Fe_2O_3NP hybrid nanomaterials was smaller than that of CNT/γ-Fe_2O_3NP, but both had similar properties (Fig. 39). This proved that the magnetic properties of CNT/γ-Fe_2O_3NP were not influenced by the self-assembly of PCA–PEG–PCA linear–dendritic copolymers on their surfaces, indicating that the PCA–PEG–PCA/CNT/γ-Fe_2O_3NP hybrid nanomaterial can be used as a promising material in cancer diagnosis and therapy.[164]

6.1.2. *In vitro* evaluations. *In vitro* cytotoxicity assay evaluated in CT26 cells (24 h incubation) demonstrated an IC_{50} of 0.8252 μg mL^{-1} for PCA–PEG–PCA (G2)–CDDP conjugates (Compound **22**), which was 9 fold lower than that of free cisplatin. IC_{50} determined for PCA–PEG–PCA(G2)–CDDP conjugates in HT1080 cell lines (48 h incubation) was 0.973 μg mL^{-1}, which was 8.4 fold lower than that determined for free cisplatin.[160] These significantly higher toxicities were explained by two factors: (1) higher uptake of the conjugates as contrasted with the free cisplatin, due to the citric acid content of the conjugates, together with the greater demands of cancer cells for such energy sources during the time of incubation. (2) Increased liberation of the drug, attributed to lysosomal enzymes existing inside the cell, which gradually break down the bond between cisplatin and the dendrimers.[160]

Regarding the nontoxicity of PCA–PEG–PCA and the *in vitro* results gained for the conjugates of cisplatin–PCA–PEG–PCA, including greater and faster drug release rate in acidic pH, and greater cytotoxicity compared to free cisplatin, it is hoped that these conjugates would be able to maintain the observed potency *in vivo* and retain the parent drug conjugated at the surface of the dendrimers in physiological plasma conditions. Future *in vivo* studies will be able to clarify the potentiality of these entities in the cure of both sensitive and resistant cancerous cells.[160]

In vitro cytotoxicity studies on murine colon adenocarcinoma tumor C26 cancer cells demonstrated higher cytoxicity for MWCNT/PCA–PEG–PCA–CDDP HNDDSs (Compound **23**) in comparison with the free drug.[161] This was attributed to the complementary roles of carbon nanotubes and PCA–PEG–PCA linear–dendritic copolymers. MWCNTs raise the rate of "transferring" of the linear–dendritic copolymers from the cell membrane. On the other hand, PCA–PEG–PCA linear–dendritic copolymers improve the water solubility of the MWCNTs and, due to their citric acid backbone PCA–PEG–PCA, can probably be used as the source of energy by the cells that cause to insert MWCNTs in the cell metabolism.[161] In summary, the results from this study showed a slow rate of cisplatin release at physiological conditions and a higher cytotoxicity for MWCNT/PCA–PEG–PCA–CDDP in comparison with the free drug, which make this system useful for anticancer drug delivery. More studies in pharmacokinetics and the antitumor effect *in vivo* are required for developing this system in cancer therapy.[161]

In vitro cytotoxicity tests conducted on the mouse tissue connective fibroblast adhesive cell line (L929) demonstrated that a 100 μg ml^{-1} concentration of CDDP/PCA–PEG–PCA/CNT/γ-Fe_2O_3NP (Compound **24**) killed more than 95% of cancer cells (Fig. 40).[164] This high toxicity was explained by fast transfer through the cell membrane caused by CNT, and high water solubility and ability to insert into the cell metabolism caused by PCA–PEG–PCA.[164]

Noncovalent interactions between carbon nanotubes and linear–dendritic copolymers lead to hybrid nanomaterials having a hybrid of properties such as fast transfer through the cell membrane, high functionality, water solubility, biocompatibility, and ability to target drugs to tumors (Fig. 41). Sufficient *in vitro* cytotoxicity makes this system attractive for future *in vivo* studies (Table 5).[164]

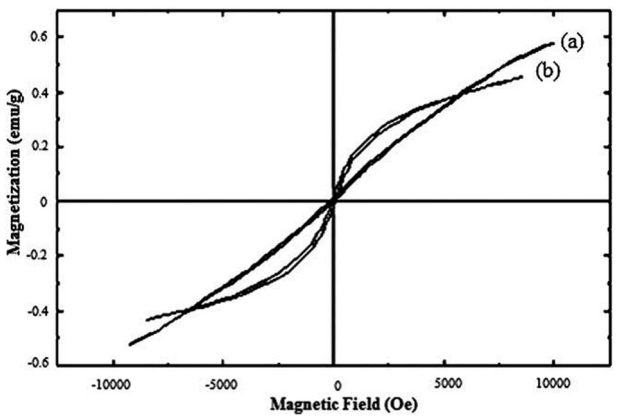

Fig. 39 Hysteresis loop by VSM of: (a) CNT/γ-Fe_2O_3NP and (b) PCA–PEG–PCA/CNT/γ-Fe_2O_3NP. Reprinted with permission from ref. 164. Copyright (2011) The Royal Society of Chemistry.

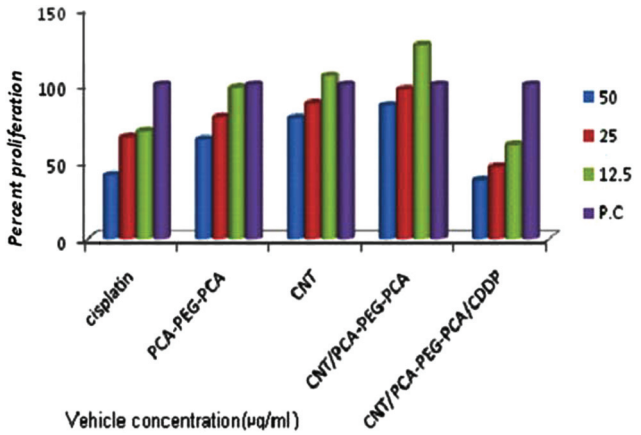

Fig. 40 Percentage survival of C26 cancer cells, assessed by the MTT assay, after exposure to free CDDP, opened MWCNT, PCA–PEG–PCA, MWCNT/PCA–PEG–PCA and MWCNT/PCA–PEG–PCA–CDDP at 12.5, 25 and 50 μg mL^{-1}(n = 3). P.C. is the positive control. Reprinted with permission from ref. 161. Copyright (2011) The Royal Society of Chemistry.

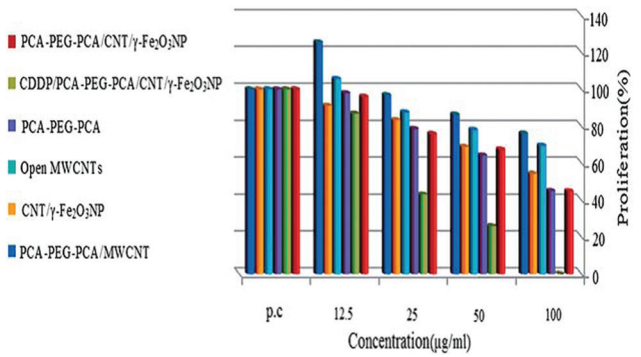

Fig. 41 The MTT assay results for opened MWCNT, CNT/γ-Fe_2O_3NP, PCA–PEG–PCA, PCA–PEG–PCA/CNT, PCA–PEG–PCA/CNT/γ-Fe_2O_3NP and CDDP/PCA–PEG–PCA/CNT/γ-Fe_2O_3NP hybrid nanomaterials. Reprinted with permission from ref. 164. Copyright (2011) The Royal Society of chemistry.

7. Camptothecin

Camptothecin (CPT), a natural plant alkaloid extracted from Camptotheca acuminate, is a promising antitumor agent that acts by stabilizing a topoisomerase I-induced single strand break in the phosphodiester backbone of DNA, thereby preventing religation. This causes the destruction of DNA strands during DNA replication in the cell cycle, which leads to cell death if the broken DNA is not repaired.[165–167] The drug is a pentacyclic indole alkaloid, with the terminal ring converting readily between the lactone in acidic environments (pH <5) to the carboxylate (pH >8) form. In order for CPT to be active, the lactone form must dominate. The opening of the lactone ring at physiological pH and above, which produces the less active and highly toxic carboxylate form, prevents the clinical application of CPT in cancer therapy. Moreover, poor solubility in water and in physiologically acceptable organic solvents restricts practical use of the active lactone form of CPT.[168–170] Attempts to overcome these limitations have involved the conjugation of camptothecin to biocompatible polymers (prodrug approach),[171] and encapsulation into liposomes,[172] polymeric micelles,[173] dendrimers,[174] and nanoparticles.[175]

7.1. Camptothecin-conjugated linear–dendritic block copolymers

7.1.1. Physicochemical properties. Camptothecin has been conjugated to PEG-*block*-dendritic polylysine to tailor the hydrophobicity of amphiphilic linear–dendritic PEG–polylysine–CPT conjugates (Compound **25**).[79] By CPT content-controlled self-assembly, nanostructures – nanospheres or nanorods of different diameters and lengths, have been obtained. As shown in Fig. 42, CPT–PDP containing a disulfide bond and an NHS active ester group has been reacted with PEG-*block*-dendritic polylysine (PEG_{45}–DPLL–G_2) of different generations. The CPT contents of PEG–polylysine G_0–CPT, PEG–polylysine G_1–DiCPT, PEG–polylysine G_2–TetraCPT and PEG–polylysine G_3–OctaCPT were 13.4%, 21.4%, 30.6%, and 38.9% by weight, respectively.

Table 5 Cisplatin-conjugated linear–dendritic block copolymers

Carrier name	Size (nm)	*In vitro* activity	*In vivo* activity	Advantages	Ref.
PCA–PEG–PCA	141	Significantly higher cytotoxicity in CT26 cells (IC_{50} of 0.8252 μg mL^{-1} for conjugates, 9 fold lower than free cisplatin) and in HT1080 cell lines (IC_{50} of 0.973 μg mL^{-1} for conjugates, 8.4 fold lower than free cisplatin)	n[a]	Nontoxicity of carrier, greater and faster drug release rate in acidic pH, and greater cytotoxicity compared to free cisplatin	160
MWCNT/PCA–PEG–PCA	371	Higher cytotoxicity for HNDDSs in comparison with the free drug on murine colon adenocarcinoma tumor C26 cancer cells	n[a]	Slow rate of cisplatin release at physiological conditions and higher cytotoxicity compared to the free drug	161
PCA–PEG–PCA/CNT/γ-Fe_2O_3	200	Higher cytotoxicity against the mouse tissue connective fibroblast adhesive cell line (L929)	n[a]	Fast transfer through the cell membrane, high functionality, water solubility, biocompatibility, sufficient *in vitro* cytotoxicity	164

[a] n: not reported.

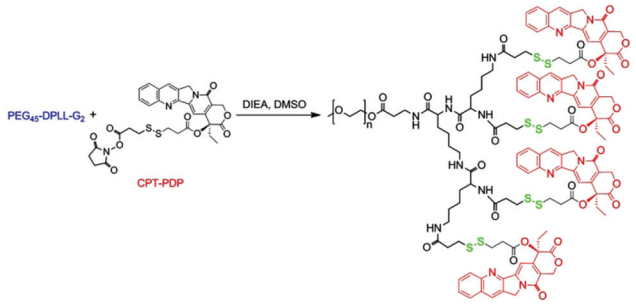

Fig. 42 Schematic illustration of PEG-dendritic polylysine (G2)–camptothecin conjunction reaction (Compound **25**). Reprinted with permission from ref. 79. Copyright (2013) Elsevier Ltd.

PEG–polylysine G_0–CPT and PEG–polylysine G_1–DiCPT formed uniform ~100 nm nanospheres. Interestingly, PEG45–TetraCPT and PEG45–OctaCPT formed unusual nanorods. The nanorods of PEG–polylysine G_2–TetraCPT were about 60 nm in diameter and 500 nm long, and those of PEG–polylysine G_3–OctaCPT were about 100 nm in diameter and about 1 mm long. The stability of the nanostructures was studied in PBS at 37 °C by DLS. PEG45–DiCPT nanospheres and PEG45–TetraCPT nanorods were stable for over five days and their sizes did not change over time, whereas PEG45–OctaCPT nanorods aggregated slightly. None of these nanostructures released any CPT under these conditions. *In vitro* drug release studies showed no CPT release from PEG–polylysine–CPT formulations due to the conjugation of CPT molecules by disulfide bonds, which can be cleaved intracellularly by GSH, indicating stability of formulations at physiological conditions but quickly releasing the drug CPT once in the cytosol. GSH-mediated release was evidenced by the addition of DTT, a strong reducing agent similar to GSH, which caused the immediate release of CPT-thioester (CPT-SH).[79]

7.1.2. *In vitro* evaluations. MTT assay on MCF-7 cells determined the IC_{50} value 0.138 μg mL^{-1} for PEG45–polylysine G_1–DiCPT, 0.073 μg mL^{-1} for PEG45–polylysine G_2–TetraCPT and 0.070 μg mL^{-1} for PEG45–polylysine G_3–OctaCPT, which are higher than that of free CPT (0.008 μg mL^{-1}).[79]

7.1.3. *In vivo* evaluations. Pharmacokinetics in BALB/c mice determined elimination half-life times ($t_{1/2}$) of 5.82 h for PEG–polylysine G_2–TetraCPT, which was significantly greater than those of PEG–polylysine G_1–DiCPT (1.61 h) and PEG–polylysine G_3–OctaCPT (1.70 h).[79] The prolonged circulation time of the PEG–polylysine G_2–TetraCPT nanorods has been attributed to their elongated shape, which might align or tumble in the flow to reduce clearance by the liver or spleen. Biodistribution studies after 4 h i.v. administration to BALB/c mice demonstrated the presence of nanostructures in the spleen. Also accumulation of some PEG–polylysine G_1–DiCPT in the liver (15.75 ± 3.85% ID per g tissue), and a significant amount of PEG–polylysine G_3–OctaCPT in the lung (64.89 ± 2.63%) was observed.[79] PEG–polylysine G_2–TetraCPT had lower concentrations in the liver and spleen than PEG–polylysine

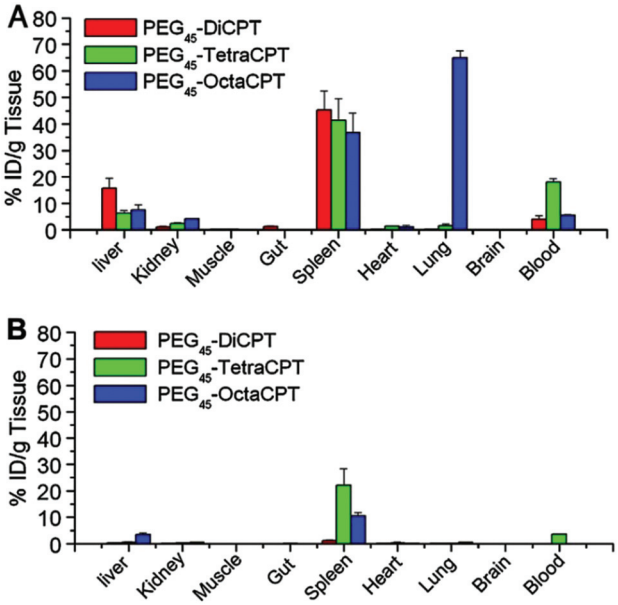

Fig. 43 The biodistribution at 4 h (A) or 24 h (B) post i.v. administration of the PEG–*x*CPT nanostructures. Dose, 10 mg CPT-eq. kg^{-1}, n = 4. - Reprinted with permission from ref. 79. Copyright (2013) Elsevier Ltd.

G_1–DiCPT. After 24 h, PEG–polylysine G_1–DiCPT almost disappeared from all the organs. The level of PEG–polylysine G_3–OctaCPT in the lung was also greatly reduced and little remained in the spleen (10.53 ± 1.31% ID per g of tissue) and liver (3.55 ± 0.57% ID per g tissue). PEG–polylysine G_2–TetraCPT was still found in the spleen (22.05 ± 6.33% ID per g tissue) and blood (3.59 ± 0.29% ID per g blood).[79] Collectively, high drug content, stability of formulations under physiological conditions, and a reduction-sensitive drug release profile, which leads to fast release in cytosol, made this system suitable for drug delivery. It was demonstrated that PEG–polylysine G_2–TetraCPT conjugate nanorods with proper lengths can unite the two opposites in cancer-drug delivery: long blood circulation *versus* fast cellular uptake and drug retention in circulation *versus* intracellular drug release, ideal for efficient tumor-drug delivery (Fig. 43).[79]

8. Conclusion

In summary, linear–dendritic block copolymers show great potential in anticancer drug delivery applications. The high architectural control and the option to tailor the properties of the linear–dendritic copolymers to the specific requirements of cancer therapy, including prolonged circulation times, increased drug solubility, reduced drug toxicity, selective delivery to tumors by active targeting with covalently bonded tumor-targeting agents, or passive targeting, resulting from the enhanced permeability and retention (EPR) effect, make these nanostructures promising carriers for a variety of anticancer drugs. The reported data demonstrate that in most

Table 6 Camptothecin-conjugated linear–dendritic block copolymers

Carrier name	Size (nm)	CMC	*In vitro* activity	*In vivo* activity	Advantages	Ref.
PEG–polylysine	100	PEG45–polylysine G1–DiCPT = 0.114 mg mL^{-1}, PEG45–polylysine G2-TetraCPT = 0.074 mg mL^{-1}, PEG45–polylysine G3–OctaCPT = 0.025 mg mL^{-1}	Lower cytotoxicity against MCF-7 cells, IC_{50} = 0.138 μg mL^{-1} for PEG45–polylysine G1–DiCPT, 0.073 μg mL^{-1} for PEG45–polylysine G2–TetraCPT and 0.070 μg mL^{-1} for PEG45–polylysine G3–OctaCPT, and 0.008 μg mL^{-1} for free CPT	After 24 h i.v. administration to BALB/c mice, greatly reduced level of PEG–polylysine G_3–OctaCPT in the lung, spleen, and liver. But the remaining PEG–polylysine G_2–TetraCPT was in the spleen and blood	High drug content, stability of formulations under physiological conditions, and reduction-sensitive drug release	79

studies PEG has been utilized as a linear segment of linear–dendritic anticancer carriers, because of its biocompatibility and hydrophilic properties. The chemotherapeutic agents can be loaded either as conjugated to the functional groups on the dendritic blocks or encapsulated by the hydrophobic interior of the dendritic segments of block copolymers. Several strategies have been employed for the delivery of loaded chemotherapeutic agents by different modes, such as pH-, enzyme-, light-, and glutathione-dependent. In many cases, slow drug release in physiological conditions, improved selectivity and higher drug accumulation in tumor tissues, and reduced drug toxicities were observed for drug loaded linear–dendritic copolymers, indicating these nanostructures as promising vehicles for anticancer agents. Although a large number of studies, investigating the *in vitro* and *in vivo* antitumor efficacy of anticancer drugs loaded by linear–dendritic copolymers are available, more research focusing on the biodistribution, pharmacokinetic studies, toxicity problems and side effects is needed. Clearly, more studies lead to better knowledge in the design of linear–dendritic based anticancer drug delivery systems, in order to achieve better targeting properties and higher antitumor effects, and to avoid the uptake in vital organs and side effects that can be used to assist in the optimization of clinical protocols (Table 6).

Abbreviations

CMC	Critical micelle concentration
PEG	Poly(ethylene glycol)
TEM	Transmission electron microscopy
DLS	Dynamic light scattering
PBS	Phosphate buffered saline
LDP	Linear–dendritic copolymers
PTX	Paclitaxel
DTX	Docetaxel
DOX	Doxorubicin
Cispt	Cisplatin
CPT	Camptothecin
HCPT	Hydroxycamptothecin
PAMAM	Polyamidoamine
CA	Cholic acid
ALN	Alendronate
bis-MPA	2,2-Bis(hydroxymethyl) propanoic acid
MWCNTs	Multi-walled carbon nanotubes
PG	Polyglycerol
Bz	Benzylidene
DNQ	Diazonaphthoquinone
NIR	Near-infrared light-responsive
PDMAEMA	Poly(2-dimethylaminoethyl methacrylate)
PNIPAM	Poly(*N*-isopropylacrylamide)
PDMAEMA	Poly(2-(dimethylamino)ethyl methacrylate)
PPEGMA	Poly(poly(ethylene glycol) methyl ether methacrylate)
PCL	Poly(ε-caprolactone)
LA	Lipoic acid
PCA	Polycitric acid
ENH	Enhanced value
ASGP	Asialo-glycoprotein receptor
FR	Folate receptor
GSH	Glutathione
LA	Lipoic acid
HNDDSs	Hybrid nanomaterial-based drug delivery systems
PDI	Polydispersity index
NIRF	Near infrared fluorescence imaging
EPR	Enhanced permission and retention effect
MTD	Most tolerated dosage
RES	Reticuloendothelial system

Acknowledgements

Authors would like to thank Iran Nano Council to support this work financially.

Notes and references

1 Y. Y. Diao, H. Y. Li, Y. H. Fu, M. Han, Y. L. Hu, H. L. Jiang, Y. Tsutsumi, Q. C. Wei, D. W. Chen and J. Q. Gao, *Int. J. Nanomed.*, 2011, **6**, 1955.
2 C. Oerlemans, W. Bult, M. Bos, G. Storm, J. F. Nijsen and W. E. Hennink, *Pharm. Res.*, 2010, **27**, 2569.
3 M. López-Gómez, E. Malmierca, M. de Górgolas and E. Casado, *Crit. Rev. Oncol./Hematol.*, 2013, **88**, 117.

4 L. Brannon-Peppas and O. J. Blanchette, *Adv. Drug Delivery Rev.*, 2004, **56**, 1649.
5 S. S. Feng and S. Chien, *Chem. Eng. Sci.*, 2003, **58**, 4087.
6 X. Zeng, R. Morgenstern and A. M. Nyström, *Biomaterials*, 2014, **35**, 1227.
7 L. Nobs, F. Buchegger, R. Gurny and E. Allémann, *Bioconjugate Chem.*, 2006, **17**, 139.
8 C. Clementi, K. Miller, A. Mero, R. Satchi-Fainaro and G. Pasut, *Mol. Pharm.*, 2011, **8**, 1063.
9 D. Brambilla, P. Lucianni and J.-C. Leroux, *J. Controlled Release*, 2014, **190**, 9.
10 M. Adeli, R. S. Sarabi, R. Y. Farsi, M. Mahmoudi and M. Kalantari, *J. Mater. Chem.*, 2011, **21**, 18686.
11 S. Lu, K. G. Neoh, C. Huang, Z. Shi and E. T. Kang, *J. Colloid Interface Sci.*, 2013, **412**, 46.
12 A. Krais, L. Wortmann, L. Hermanns, M. Feliu, M. Vahter, S. Stucky, M. Mathur and B. Fadeel, *Nanomed.: Nanotechnol. Biol. Med.*, 2014, **10**, 1421.
13 R. Jin, B. Lin, D. Li and H. Ai, *Curr. Opin. Pharm.*, 2014, **18**, 18.
14 M. Su, H. Liu, L. Ge, Y. Wang, S. Ge, J. Yu and M. Yan, *Electrochim. Acta*, 2014, **146**, 262.
15 X. Wang, X. Sun, J. Lao, H. He, T. Cheng, M. Wang, S. Wang and F. Huang, *Colloids Surf., B*, 2014, **122**, 638.
16 X. Cao, L. Tao, S. Wen, W. Hou and X. Shi, *Carbohydr. Res.*, 2014, **405**, 70.
17 M. Adeli, S. Beyranvand and R. Kabiri, *Polym. Chem.*, 2013, **4**, 669.
18 A. Batigelli, C. Ménard-Moyou and A. Bianco, *J. Mater. Chem. B*, 2014, **2**, 6144.
19 X. Y. Ke, V. W. L. Ng, S. J. Gao, Y. W. Tong, J. L. Hedrick and Y. Y. Yang, *Biomaterials*, 2014, **35**, 1096.
20 A. Pourjavadi, M. Adeli and M. Yazdi, *New J. Chem.*, 2013, **37**, 295.
21 C. Y. Ang, S. Y. Tan and Y. Zhao, *Org. Biomol. Chem.*, 2014, **12**, 4776.
22 B. K. Chegeni, A. Kakanejadifard, F. Abedi, R. Kabiri, F. Daneshnia and M. Adeli, *Colloid Polym. Sci.*, 2014, **292**, 3337.
23 S. Sunoqrot, J. Bugno, D. Lantvit, J. E. Burdette and S. Hong, *J. Controlled Release*, 2014, **191**, 115.
24 S. J. Guillaudeu, M. E. Fox, Y. M. Haidar, E. E. Dy, F. C. Szoka and J. M. Fréchet, *Bioconjugate Chem.*, 2008, **19**, 461.
25 A. Grotzky, E. Altamura, J. Adamcik, P. Carrara, P. Stano, F. Mavelli, T. Nauser, R. Mezzenga, A. D. Schlüter and P. Walde, *Langmuir*, 2013, **29**, 10831.
26 X. Zhang, S. Guo, R. Fan, M. Yu, F. Li, C. Zhu and Y. Gan, *Biomaterials*, 2012, **33**, 7103.
27 H. Maeda, *J. Controlled Release*, 2012, **164**, 138.
28 J. Fang, H. Nakamura and H. Maeda, *Adv. Drug Delivery Rev.*, 2011, **63**, 136.
29 H. S. Oberoi, F. C. Laquer, L. A. Marky, A. V. Kabanov and T. K. Bronich, *J. Controlled Release*, 2011, **153**, 64.
30 Y. Liu, H. Miyoshi and M. Nakamura, *Int. J. Cancer*, 2007, **120**, 2527.
31 F. Hosseini, A. Panahifar, M. Adeli, H. Amiri, A. Lascialfari, F. Orsini, M. R. Doschak and M. Mahmoudi, *Colloids Surf., B*, 2013, **103**, 652.
32 M. Adeli, M. Ashiri, B. K. Chegeni and P. Sasanpour, *J. Iran. Chem. Soc.*, 2013, **10**, 701.
33 A. Jhavery, P. Deshpande and V. Torchilin, *J. Controlled Release*, 2014, **190**, 352.
34 M. Ferrari, *Nat. Rev. Cancer*, 2005, **5**, 161.
35 M. E. Davis, Z. Chen and D. M. Shin, *Nat. Rev. Drug Discovery*, 2008, **7**, 771.
36 I. Gitsov, I. V. Berlinova and N. G. Vladimirov, *J. Polym. Sci., Part A: Polym. Chem.*, 2015, **53**, 178.
37 T. Gillich, C. Acikgöz, L. Isa, A. D. Schlüter, N. D. Spencer and M. Textor, *ACS Nano*, 2013, **7**, 316.
38 I. Gitsov, K. L. Wooley, C. J. Hawker and J. M. Fréchet, *J. Polym. Prep.*, 1991, **32**, 631.
39 I. Gitsov, K. L. Wooley and J. M. J. Fréchet, *Angew. Chem., Int. Ed. Engl.*, 1992, **31**, 1200.
40 A. Carlmark, E. Malmström and M. Malkoch, *Chem. Soc. Rev.*, 2013, **42**, 5858.
41 I. J. Gitsov, *Polym. Sci., Part A: Polym. Chem.*, 2008, **46**, 5295.
42 K. R. Lambrych and I. Gitsov, *Macromolecules*, 2003, **36**, 1068.
43 C. M. Dong and G. Liu, *Polym. Chem.*, 2013, **4**, 46.
44 B. K. Nanjwade, H. M. Bechra, G. K. Derkar, F. V. Manvi and V. K. Nanjwade, *Eur. J. Pharm. Sci.*, 2009, **38**, 185.
45 S. Mignani, S. El Kazzouli, M. Bousmina and J. P. Majoral, *Adv. Drug Delivery Rev.*, 2013, **65**, 1316.
46 V. Gajbhiye, V. K. Palanirajan, R. Tekade and N. K. Jain, *J. Pharm. Pharmacol.*, 2009, **61**, 989.
47 M. Adeli, A. K. Fard, F. Abedi, B. K. Chegeni and F. Bani, *Nanomed.: Nanotechnol. Biol. Med.*, 2013, **9**, 1203.
48 M. Adeli, Z. Zarnegar, A. Dadkhah, R. Hossieni, F. Salimi and A. Kanani, *J. Appl. Polym. Sci.*, 2007, **104**, 267.
49 M. W. P. L. Baars, R. Kleppinger, M. H. J. Koch and E. W. Meijer, *Angew. Chem., Int. Ed.*, 2000, **39**, 1285.
50 S. E. Stiriba, H. Kautz and H. Frey, *J. Am. Chem. Soc.*, 2002, **124**, 9698.
51 M. Krämer, J. F. Stumbé, H. Türk, S. Krause, A. Komp, L. Delineau, S. Prokhorova, H. Kautz and R. Haag, *Angew. Chem., Int. Ed.*, 2002, **114**, 4426.
52 Y. Chang, C. Park, K. T. Kim and C. Kim, *Langmuir*, 2005, **21**, 4334.
53 C. Zhu, C. Hard, C. Lin and I. Gitsov, *J. Polym. Sci., Part A: Polym. Chem.*, 2005, **43**, 4017.
54 I. Gitsov, in *Advances in Dendritic Macromolecules*, ed. G. R. Newkome, Elsevier Science, Amsterdam, 2002, vol. 5, p. 45.
55 T. M. Chapman, G. L. Hillyer, E. J. Mahan and K. A. Shaffer, *J. Am. Chem. Soc.*, 1994, **116**, 11195.
56 I. Gitsov, P. T. Ivanova and J. M. J. Fréchet, *Macromol. Rapid Commun.*, 1994, **15**, 387.
57 E. Blasco, M. Pinol and L. Oriol, *Macromol. Rapid Commun.*, 2014, **35**, 1090.
58 F. Wurm and H. Frey, *Prog. Polym. Sci.*, 2011, **36**, 1.

59 P. M. Nguyen and P. T. Hammond, *Langmuir*, 2006, **22**, 7825.
60 J. Zhua and X. Shi, *J. Mater. Chem. B*, 2013, **1**, 4199.
61 S. Mignani and J. P. Majoral, *New J. Chem.*, 2013, **37**, 3337.
62 Z. Zhou, A. D'Emanuele, K. Lennon and D. Attwood, *Macromolecules*, 2009, **42**, 7936.
63 C. Kojima, T. Suehiro, K. Watanabe, M. Ogawa, A. Fukuhara, E. Nishisaka, A. Harada, K. Kono, T. Inui and Y. Magata, *Acta Biomater.*, 2013, **9**, 5673.
64 A. R. Menjoge, M. Rangaramanujam, R. M. Kannan and D. A. Tomalia, *Drug Discovery Today*, 2010, **15**, 171.
65 P. Singh, U. Gupta, A. Asthana and N. K. Jain, *Bioconjugate Chem.*, 2008, **19**, 2239.
66 M. H. Li, S. K. Choi, T. P. Thomas, A. Desai, K. H. Lee, A. Kotlyar, M. M. B. Holl and J. R. Baker Jr., *Eur. J. Med. Chem.*, 2012, **47**, 560.
67 Y. Chang, X. Meng, Y. Zhao, K. Li, B. Zhao, M. Zhu, Y. Li, X. Chen and J. Wang, *J. Colloid Interface Sci.*, 2011, **363**, 403.
68 W. Yang, Y. Cheng, T. Xu, X. Wang and L. P. Wen, *Eur. J. Med. Chem.*, 2009, **44**, 862.
69 A. Sousa-Herves, R. Riguera and E. Fernandez-Megia, *New J. Chem.*, 2012, **36**, 205.
70 G. Whitton and E. R. Gillies, *J. Polym. Sci., Part A: Polym. Chem.*, 2015, **53**, 148.
71 T. P. Thomas, A. K. Patri, A. Myc, M. T. Myaing, J. Y. Ye, T. B. Norris and J. R. Baker Jr., *Biomacromolecules*, 2004, **5**, 2269.
72 M. F. Neerman, H. T. Chen, A. R. Parrish and E. E. Simanek, *Mol. Pharm.*, 2004, **1**, 390.
73 V. Torchilin, *Adv. Drug Delivery Rev.*, 2011, **63**, 131.
74 A. Buczkowski, S. Sekowski, A. Grala, D. Palecz, K. Milowska, P. Urbaniak, T. Gabryelak, H. Piekarski and B. Palecz, *Int. J. Pharm.*, 2011, **408**, 266.
75 Y. Wang, R. Guo, X. Cao, M. Shen and X. Shi, *Biomaterials*, 2011, **32**, 3322.
76 H. Namazi and S. Jafarirad, *Int. J. Pharm.*, 2011, **407**, 167.
77 T. C. Stover, Y. S. Kim, T. L. Lowe and M. Kester, *Biomaterials*, 2008, **29**, 359.
78 Y. Zhang, C. Xiao, M. Li, J. Ding, C. He, X. Zhuang and X. Chen, *Polym. Chem.*, 2014, **5**, 2801.
79 Z. Zhou, X. Ma, E. Jin, J. Tang, M. Sui, Y. Shen, E. A. Van Kirk, W. J. Murdoch and M. Radosz, *Biomaterials*, 2013, **34**, 5722.
80 Y. Li, K. Xiao, J. Luo, W. Xiao, J. S. Lee, A. M. Gonik, J. Kato, T. A. Dong and K. S. Lam, *Biomaterials*, 2011, **32**, 6633.
81 K. Kono, C. Kojima, N. Hayashi, E. Nishisaka, K. Kiura, S. Watarai and A. Harada, *Biomaterials*, 2008, **29**, 1664.
82 E. R. Gillies and J. M. J. Fréchet, *Pure Appl. Chem.*, 2004, **76**, 1295.
83 J. Lim and E. E. Simanek, *Adv. Drug Delivery Rev.*, 2012, **64**, 826.
84 K. Xiao, J. Luo, W. L. Fowler, Y. Li, J. S. Lee, L. Xing, R. H. Cheng, L. Wang and K. S. Lam, *Biomaterials*, 2009, **30**, 6006.
85 T. Negishi, F. Koizumi, H. Uchino, J. Kuroda, T. Kawaguchi, S. Naito and Y. Matsumura, *Br. J. Cancer*, 2006, **95**, 601.
86 F. Nederberg, E. Appel, J. P. K. Tan, S. H. Kim, K. Fukushima, J. Sly, R. D. Miller, R. M. Waymouth, Y. Y. Yang and J. L. Hedrick, *Biomacromolecules*, 2009, **10**, 1460.
87 J. Lim, S. T. Lo, S. Hill, G. M. Pavan, X. Sun and E. E. Simanek, *Mol. Pharm.*, 2012, **9**, 404.
88 G. Gaucher, R. H. Marchessault and J. C. Leroux, *J. Controlled Release*, 2010, **143**, 2.
89 I. J. Majoros, A. Myc, T. Thomas, C. B. Mehta and J. R. Baker Jr., *Biomacromolecules*, 2006, **7**, 572.
90 J. Luo, K. Xiao, Y. Li, J. S. Lee, L. Shi, Y. H. Tan, L. Xing, R. H. Cheng, G. Y. Liu and K. S. Lam, *Bioconjugate Chem.*, 2010, **21**, 1216.
91 Z. Poon, J. A. Lee, S. Huang, R. J. Prevost and P. T. Hammond, *Nanomed.: Nanotechnol. Biol. Med.*, 2011, **7**, 201.
92 H. Qiao, J. Li, Y. Wang, Q. Ping, G. Wang and X. Gu, *Int. J. Pharm.*, 2013, **452**, 363.
93 S. Unezaki, K. Maruyama, J. Hosoda and I. Nagai, *Int. J. Pharm.*, 1996, **144**, 11.
94 S. C. Kim, D. W. Kim, Y. H. Shim, J. S. Bang, H. S. Oh, S. Wan Kim, *et al.*, *J. Controlled Release*, 2001, **72**, 191.
95 P. J. Stevens, M. Sekido and R. J. A. Lee, *Pharm. Res.*, 2004, **21**, 2153.
96 H. S. Yoo and T. G. Park, *J. Controlled Release*, 2004, **96**, 273.
97 J. F. Kukowska-Latallo, K. A. Candido, Z. Cao, S. S. Nigavekar, I. J. Majoros, T. P. Thomas, *et al.*, *Cancer Res.*, 2005, **65**, 5317.
98 C. Chamorro, M. A. Boerman, C. J. Arnusch, E. Breukink and R. J. Pieters, *Biochim. Biophys. Acta, Biomembr.*, 2012, **1818**, 2171.
99 S. Aryal, J. J. Grailer, S. P. D. A. Steeberband and S. Gong, *J. Mater. Chem.*, 2009, **19**, 7879.
100 J. Chen, M. M. Q. Xing and W. Zhong, *Polymer*, 2011, **52**, 933.
101 K. T. Al-Jamal, W. T. Al-Jamal, J. T. W. Wang, N. Rubio, J. Buddle, D. Gathercole, M. Zloh and K. Kostarelos, *ACS Nano*, 2013, **7**, 1905.
102 Z. Wu, X. Zeng, Y. Zhang, N. Feliu, P. Lundberg, B. Fadeel, M. Malkoch and A. M. Nyström, *J. Polym. Sci., Part A: Polym. Chem.*, 2012, **50**, 217.
103 G. Minotti, P. Menna, E. Salvatorelli, G. Cairo and L. Gianni, *Pharmacol. Rev.*, 2004, **56**, 185.
104 Z. Deng, F. Yan, Q. Jin, F. Li, J. Wu, X. Liu and H. Zheng, *J. Controlled Release*, 2014, **174**, 109.
105 G. Y. Li, S. Song, L. Guo and S. M. Ma, *J. Polym. Sci., Part A: Polym. Chem.*, 2008, **46**, 5028.
106 Y. Wang, X. Cao, R. Guo, M. Shen, M. Zhang, M. Zhu and X. Shi, *Polym. Chem.*, 2011, **2**, 1754.
107 E. R. Gillies and J. M. J. Fréchet, *Bioconjugate Chem.*, 2005, **16**, 361.
108 K. Xiao, J. Luo, Y. Li, J. S. Lee, G. Fung and K. S. Lam, *J. Controlled Release*, 2011, **155**, 272.

109 X. Wu, X. He, L. Zhong, S. Lin, D. Wang, X. Zhu and D. Yan, *J. Mater. Chem.*, 2011, **21**, 13611.
110 X. He, X. Wu, X. Cai, S. Lin, M. Xie, X. Zhu and D. Yan, *Langmuir*, 2012, **28**, 11929.
111 M. Adeli, N. Mirab, M. S. Alavidjeh, Z. Sobhani and F. Atyabi, *Polymer*, 2009, **50**, 3528.
112 N. W. S. Kam, Z. Liu and H. Dai, *J. Am. Chem. Soc.*, 2005, **127**, 12492.
113 M. Maleki, M. Adeli, A. Kakanejadifard, S. Movahedi and F. Bani, *Polymer*, 2013, **54**, 4802.
114 D. A. Yarotski, S. V. Kilina, A. A. Talin, S. Tretiak, O. V. Prezhdo, A. V. Balatsky, *et al.*, *Nano Lett.*, 2009, **9**, 12.
115 M. Adeli, R. Soleyman, Z. Beiranvand and F. Madani, *Chem. Soc. Rev.*, 2013, **42**, 5231.
116 M. Yuksel, D. G. Colak, M. Akin, *et al.*, *Biomacromolecules*, 2012, **13**, 2680.
117 H. Durmaz, A. Dag, U. Tunca and G. Hizal, *J. Polym. Sci., Part A: Polym. Chem.*, 2012, **50**, 2406.
118 G. J. Bahun and A. Adronov, *J. Polym. Sci., Part A: Polym. Chem.*, 2010, **48**, 1016.
119 P. Liu, *Eur. Polym. J.*, 2005, **41**, 2693.
120 A. B. Dalton, C. Stephan, J. N. Coleman, B. McCarthy, P. M. Ajayan and S. Lefrant, *J. Phys. Chem. B*, 2000, **104**, 10012.
121 J. Chen, H. Liu, W. A. Weimer, M. D. Halls, D. H. Waldeck and G. C. Walker, *J. Am. Chem. Soc.*, 2002, **124**, 9034.
122 M. Adeli, N. Mirab and F. Zabihi, *Nanotechnology*, 2009, **20**, 485603.
123 C.-C. Liu, S. Sadhasivam, S. Savitha and F.-H. Lin, *Talanta*, 2014, **122**, 195.
124 J. J. Khandare, A. Jalota-Badhwar, S. D. Satavalekar, *et al.*, *Nanoscale*, 2012, **4**, 837.
125 M. Adeli, S. Beyranvand and M. Hamid, *J. Mater. Chem.*, 2012, **22**, 6947.
126 A. Simonyan and I. Gitsov, *Langmuir*, 2008, **24**, 11431.
127 I. Gitsov, K. R. Lambrych, V. A. Remnant and R. Pracitto, *J. Polym. Sci., Part A: Polym. Chem.*, 2000, **38**, 2711.
128 M. Adeli and R. Haag, *J. Polym. Sci., Part A: Polym. Chem.*, 2006, **44**, 5740.
129 Y. Hed, Y. Zhang, O. C. J. Andrén, X. Zeng, A. M. Nyström and M. Malkoch, *J. Polym. Sci., Part A: Polym. Chem.*, 2013, **51**, 3992.
130 N. Fomina, J. Sankaranarayanan and A. Almutairi, *Adv. Drug Delivery Rev.*, 2012, **64**, 1005.
131 G. Liu, W. Liu and C. M. Dong, *Polym. Chem.*, 2013, **4**, 3431.
132 L. Sun, B. Zhu, Y. Su and C. M. Dong, *Polym. Chem.*, 2014, **5**, 1605.
133 G. Liu, W. Liu and C. M. Dong, *Polym. Chem.*, 2013, **4**, 3431.
134 N. Fomina, J. Sankaranarayanan and A. Almutairi, *Adv. Drug Delivery Rev.*, 2012, **64**, 1005.
135 L. Sun, X. Ma, C. M. Dong, B. Zhu and X. Zhu, *Biomacromolecules*, 2012, **13**, 3581.
136 O. L. P. De Jesús, H. R. Ihre, L. Gagne, J. M. J. Fréchet and F. C. Szoka Jr., *Bioconjugate Chem.*, 2002, **13**, 453.
137 E. R. Gillies and J. M. J. Fréchet, *J. Am. Chem. Soc.*, 2002, **124**, 14137.
138 E. R. Gillies, E. Dy, J. M. J. Fréchet and F. C. Szoka, *Mol. Pharm.*, 2005, **2**, 129.
139 C. Lee, E. R. Gillies, E. Dy, M. E. Fox, A. T. Cramer, J. M. J. Fréchet, E. E. Dy and F. C. Szoka, *Proc. Natl. Acad. Sci. U. S. A.*, 2006, **45**, 16649.
140 C. C. Lee, A. T. Cramer, F. C. Szoka and J. M. J. Fréchet, *Bioconjugate Chem.*, 2006, **17**, 1364.
141 J. Huang, F. Gao, X. Tang, J. Yu, D. Wang, S. Liu and Y. Li, *Polym. Int.*, 2010, **59**, 1390.
142 M. Spiess, *Biochemistry*, 1990, **29**, 10009.
143 W. She, K. Luo, C. Zhang, G. Wang, Y. Geng, L. Li, B. He and Z. Gu, *Biomaterials*, 2013, **34**, 1613.
144 J. del Barrio, L. Oriol, C. Sanchez, J. L. Serrano, A. Di Cicco, P. Keller, *et al.*, *J. Am. Chem. Soc.*, 2010, **132**, 3762.
145 J. A. MacKay, M. Chen, J. R. McDaniel, W. Liu, A. J. Simnick and A. Chilkoti, *Nat. Mater.*, 2009, **8**, 993.
146 W. She, N. Li, K. Luo, C. Guo, G. Wang, Y. Geng and Z. Gu, *Biomaterials*, 2013, **34**, 2252.
147 Y. Zhang, C. Xiao, M. Li, J. Chen, J. Ding, C. He, X. Zhuang and X. Chen, *Macromol. Biosci.*, 2013, **13**, 584.
148 Y. Bae, N. Nishiyama, S. Fukushima, H. Koyama, M. Yasuhiro and K. Kataoka, *Bioconjugate Chem.*, 2005, **16**, 122.
149 A. Shenderova, T. G. Burke and S. P. Schwendeman, *Pharm. Res.*, 1999, **12**, 241.
150 M. E. Davis, *Nat. Rev. Drug Discovery*, 2008, **7**, 771.
151 S. Zhu, M. Hong, G. Tang, L. Qian, J. Lin, Y. Jiang and Y. Pei, *Biomaterials*, 2010, **31**, 1360.
152 G. Mattheolabakis, E. Taoufik, S. Haralambous, M. L. Roberts and K. Avgoustakis, *Eur. J. Pharm. Biopharm.*, 2009, **71**, 190.
153 T. Boulikas and M. Vougiouka, *Oncol. Rep.*, 2004, **11**, 559.
154 S. Aryal, C. M. J. Hu and L. Zhang, *ACS Nano*, 2010, **4**, 251.
155 D. Wang and S. J. Lippard, *Nat. Rev. Drug Discovery*, 2005, **4**, 307.
156 M. Galanski, V. B. Arion, M. A. Jakupec and B. K. Keppler, *Curr. Pharm. Des.*, 2003, **9**, 2078.
157 K. Osada, R. J. Christie and K. Kataoka, *J. R. Soc. Interface*, 2009, **6**, S325.
158 M. Casolaro, R. Cini, B. Del Bello, M. Ferrali and E. Maellaro, *Biomacromolecules*, 2009, **10**, 944.
159 E. Gianasi, M. Wasil, E. G. Evagorou, A. Keddle, G. Wilson and R. Duncan, *Eur. J. Cancer*, 1999, **35**, 994.
160 I. Haririan, M. S. Alavidjeh, M. R. Khorramizadeh, M. S. Ardestani, Z. Z. Ghane and H. Namazi, *Int. J. Nanomed.*, 2010, **5**, 63.
161 M. Adeli, F. Hakimpoor, M. Ashiri, R. Kabiri and M. Bavadi, *Soft Matter*, 2011, **7**, 4062.
162 A. T. Naeini, M. Adeli and M. Vossoughi, *Nanomed.: Nanotechnol. Biol. Med.*, 2010, **6**, 556.
163 A. T. Naeini, M. Adeli and M. Vossoughi, *Eur. Polym. J.*, 2010, **46**, 165.
164 E. Mehdipoor, M. Adeli, M. Bavadi, P. Sasanpour and B. Rashidian, *J. Mater. Chem.*, 2011, **21**, 15456.

165 S. Kusari, S. Zühlke and M. Spiteller, *J. Nat. Prod.*, 2009, **72**, 2.
166 M. Berrada, A. Serreqi, F. Dabbarh, A. Owusu, A. Gupta and S. Lehnert, *Biomaterials*, 2005, **26**, 2115.
167 Y. Cheng, M. Li and T. Xu, *Eur. J. Med. Chem.*, 2008, **43**, 1791.
168 K. M. Tyner, S. R. Schiffman and E. P. Giannelis, *J. Controlled Release*, 2004, **95**, 501.
169 L. Zhang, Y. Hu, X. Jiang, C. Yang, W. Lu and Y. H. Yang, *J. Controlled Release*, 2004, **96**, 135.
170 K. H. Min, K. Park, Y. S. Kim, S. M. Bae, S. Lee, H. G. Jo, R. W. Park, I. S. Kim, S. Y. Jeong, K. Kim and I. C. Kwon, *J. Controlled Release*, 2008, **127**, 208.
171 T. Schluep, J. Cheng, K. T. Khin and M. E. Davis, *Cancer Chemother. Pharmacol.*, 2006, **57**, 654.
172 S. Modi, T. X. Xiang and B. D. Anderson, *J. Controlled Release*, 2012, **162**, 330.
173 K. Kawano, M. Watanabe, T. Yamamoto, M. Yokoyama, P. Opanasopit, T. Okano and Y. Maitani, *J. Controlled Release*, 2006, **112**, 329.
174 S. Sadekar, G. Thiagarajan, K. Bartlett, D. Hubbard, A. Ray, L. D. McGill and H. Ghandehari, *Int. J. Pharm.*, 2013, **456**, 175.
175 S. M. Martins, B. Sarmento, C. Nunes, M. Lúcio, S. Reis and D. C. Ferreira, *Eur. J. Pharm. Biopharm.*, 2013, **85**, 488.